Purely Peptidic Amphiphiles: Understanding and Controlling their Self-Assembled Structures

Inauguraldissertation

zur

Erlangung der Würde eines Doktors der Philosophie

vorgelegt der

Philosophische-Naturwissenschaftlichen Fakultät

der Universität Basel

von

Thomas Bernhard Schuster

aus Moosburg a. d. Isar

Deutschland

Göttingen 2011

Genehmigt von der Philosophisch-Naturwissenschaftlichen Fakultät der Universität Basel auf Antrag von

Prof. Dr. Wolfgang Meier und

Prof. Dr. Corinne Vebert (Universität Genf)

Basel, den 22. Februar 2011

Prof. Dr. Martin Spiess

Dekan

To Sieglinde

Content

Impact of the work

Articles

Biomedical application of self-assembled peptide nanoparticles

de Bruyn Ouboter, D., Schuster, T., & Meier, W., **2011**, manuscript in preparation

Highly ordered gold nanoparticles – peptide composites

de Bruyn Ouboter, D., Schuster, T., & Meier, W., **2011**, manuscript in preparation

Hierarchical organization of purely peptidic amphiphiles into peptide beads

de Bruyn Ouboter, D., Schuster, T., Alexandre Mantion & Meier, W., J. of Phys. Chem. C, **2011**, accepted

Exploiting dimerization of purely peptidic amphiphiles to form vesicles

Schuster, T., de Bruyn Ouboter, D., Bruns, N. & Meier, W. *Small* **2011**

DOI: 10.1002/smll.201100701

From fibers to micelles using point mutated amphiphilic peptides

Schuster, T., de Bruyn Ouboter, D., Palivan, C. & Meier, W., *Langmuir* **2011**, 27, 4578

Reversible peptide particle formation using a mini amino acid sequence

Schuster, T., de Bruyn Ouboter, D., Bordignon, E., Jeschke, G. & Meier, W. Soft Matter **2010**, 6, 5596.

Oral presentation

From fibers to micelles using point mutated amphiphilic peptides

T. Schuster, D. de Bruyn Ouboter, W. Meier, SCS Fall Meeting, ETH Zürich, Switzerland, **2010**

Reversible peptide particle formation of a mini amino acid sequence

T. Schuster, D. de Bruyn Ouboter, E. Bordignon, C. Dittrich, G. Jeschke and W. Meier, EUPOC - HIERARCHICALLY STRUCTURED POLYMERS, Gargnano, Italy, **2010**

Posters

Vesicular structures from short amphiphilic peptides

T. Schuster, D. de Bruyn Ouboter, W. Meier, 3rd International NanoBio Conference, ETH Zürich, Switzerland, **2010**

Reversible peptide particle formation of a mini amino acid sequence

T. Schuster, D. de Bruyn Ouboter, W. Meier, SPS Annual Meeting, Basel, Switzerland, **2010**

Applications for self-assembled peptide beads

D. de Bruyn Ouboter, T. Schuster, Ch. Dittrich, W. Meier, NCCR Nanoscience Annual Meeting, Basel, Switzerland, **2010**

Insights in the self-assembly of helical peptides

T. Schuster, D. de Bruyn Ouboter, Ch. Dittrich, W. Meier, 40th CUSO Summer School, Villars, Switzerland, **2009**

Suitable applications of self-assembled peptide beads

D. de Bruyn Ouboter, T. Schuster, Ch. Dittrich, W. Meier, 40th CUSO Summer School, Villars, Switzerland, **2009**

Controlling the assembly of short helical D, L - peptides

T. Schuster, D. de Bruyn Ouboter, Ch. Dittrich, W. Meier, Swiss Chemical Society, Swiss Federal Institute of Technology Zürich, Switzerland, **2009**

Controlling the assembly of short helical D, L - peptides

T. Schuster, D. de Bruyn Ouboter, Ch. Dittrich, W. Meier, Swiss Chemical Society, Workshop on Nanoscience and the NCCR Nanoscience Annual Meeting, Basel, Switzerland, **2009**

Short helical D, L - peptides in solution and on surfaces

T. Schuster, Ch. Dittrich, D. de Bruyn Ouboter, W. Meier, Polymers in Life Science, Basel, Switzerland, **2008**

Solid supported membranes based on short helical peptides

T. Schuster, Ch. Dittrich, D. de Bruyn Ouboter, W. Meier, 11th European Conference on Organized Films, Potsdam, Germany, **2008**

Solid supported membranes based on amphiphilic gramicidin derivatives

T. Schuster, Ch. Dittrich, D. de Bruyn Ouboter, W. Meier, Biosurf VII, Zürich, Switzerland, **2007**

Summary of the thesis

Part 1. Introduction

This first chapter will provide a brief overview of the self-organization of amphiphilic molecules into supramolecular aggregates. The latter exist in as many sizes and morphologies as there are factors to influence them. Especially defined amino acid sequences offer numerous functionalities and are able to respond to environmental stimuli. Furthermore they consist of biodegradable material and, therefore, accumulation in the human body might be avoided in potential medical applications. Additionally, advantages and drawbacks among different synthesis methods, *e.g.* polymerization, bioengineering techniques or solid-phase peptide synthesis, are discussed.

Part 2. Reversible peptide particle formation using a mini amino acid sequence

The self-assembly of amphiphilic peptides with a specific amino acid sequence into micelles and spherical peptide nanoparticles has been investigated. The undecamer peptide that was used features a repetitive L-tryptophan and D-leucine [LW-DL] motif representing the hydrophobic block – which is a truncated version of gramicidin A (gA), named gT. The N-terminally attached hydrophilic section was either lysine (K) or acetylated lysine (X) and was optionally terminated with cysteine for post-functionalization of the thiol group. Aggregation into micelles and a minor fraction of peptide particles was observed for peptides containing charged lysine. Charge shielding with anionic counter ions followed the trends in the Hofmeister series and shifted the equilibrium towards the larger peptide aggregates.

Similarly, it was demonstrated that the corresponding uncharged peptide assembled into micelles and subsequently into peptide particles, termed 'peptide beads'. Furthermore formation of the peptide beads was studied as a function of temperature and solvent composition. We hypothesized that the peptide beads consisted of micelles – a structure described as multicompartment micelles (MCM).

Part 3. Highly ordered composite peptide – gold nanoparticles (Au-NP)

Peptide beads using AcC-X_3-gT and its analogues – including Ac-X_3-gT-C, a new peptide with the cysteine residue at the C instead of the N-terminus – have been further studied. Ac-X_3-gT-C peptide beads within the formation process were imaged by scanning electron microscopy (SEM), which demonstrated the aggregated micelles within the beads and agrees with the multi-compartment micelles (MCM) as hypothesized. Furthermore, we succeeded in creating highly ordered Ac-X_3-gT-C – Au-NP composites, which allowed us to visualize the inner structure of the nanoparticles. The presented composite materials are expected to exhibit exceptional electronic and optical properties.

Part 4. Molecular thin films produced by short amphiphilic peptides

The amphiphilic peptides – K_3-gT, C-K_3-gT and AcC-X_3-gT – have been studied with regard to the interaction within a lipid monolayer but also in pure peptide layers at the air-water interface. Experiments on the Langmuir trough allow the separate investigation of different parameters such as the choice of buffer subphase or its concentration. Thus, the intrinsic parameters for a peptide as well as the environmental conditions necessary to form a stable film have been determined. Results indicate the formation of a unimolecular flat film. Peptide layers have been successfully transferred onto a solid support or self-

assembled peptide monolayers (SAMs) have been created equally well via immersion and spin-coating. Preliminary mineralization experiments confirmed the successful creation of calcium phosphate crystals. Therefore, the created homogenous monomolecular interfaces are potentially useful for mineralization.

Part 5. From fibers to micelles using point mutated amphiphilic peptides

A peptide library has been synthesized to correlate the primary sequence, its secondary structure and the resulting self-assembly. The peptide design includes three parts: (a) a charged lysine part, (b) an acetylated lysine part and (c) a constant hydrophobic rod-like helix, based on gramicidin A. By stepwise replacement of free lysine (K) with acetylated lysine (X) we generated a library of a total of ten peptides Ac-X_8-gA and K_mX_{8-m}-gA (m ranging from 0 to 8). By using point mutations, we adjusted the degree of acetylation (DA) and thus the overall amphiphilicity of the peptides, which led to a change in the secondary structure in the aqueous environment from a β-sheet to an α-helix. This transition generated a significant change in the morphology of the self-assembled structures from fibers to micelles. Two different regions where observed with the conformation of the hydrophilic part of the peptide: one region, a β-sheet-like secondary structure, inducing fiber formation (high DA), the other an α-helical-like secondary structure generating micelle formation (moderate and low DA). The micellar structures depended on the degree of acetylation, which influenced their critical micelle concentration (cmc). In conclusion, our results demonstrate the control of self-assembled morphologies by point mutation of a peptide's primary sequence. This study is precisely important because it presents a first step towards molecular switches based on acetylation of a peptide inspired by the example of

phosphorylation of proteins or enzymes, to convert them into the active or inactive state by structural changes.

Part 6. Exploiting dimerization of amphiphilic peptides to form vesicles

This chapter focuses on essential parameters to successfully manage membrane formation from a purely peptidic system. Literature already provides fundamental rules for supramolecular aggregation such as amphiphilic design or a hydrophilic to hydrophobic ratio of about 1:3. However, smaller molecules of a defined nature need additional interaction to create stable vesicular structures. A crucial step in the formation of peptide membranes appears to be dimerization which originates from the introduction of intermolecular interactions, such as H-bonds or $\pi-\pi$ stacking of aromatic rings. The formation of a stabilized membrane subunit, *i.e.* dimers in the lateral or perpendicular directions (relative to the membrane) produced stable, purely peptidic vesicles and may well apply to other peptidic systems. These novel peptidic systems offer hydrophilic and hydrophobic compartments to encapsulate and integrate different drugs or payloads and could be used for gene delivery, since the design includes charged moieties.

Part 7. General conclusions and outlook

In this last chapter the achievements of the presented work are discussed and summarized. Furthermore, lines of research are suggested, *e.g.* the development of medical applications and the mimicking of lipid membranes, which, from the present point of view, appear to be the most promising and should be the focus of subsequent experiments.

1. Introduction

1.1. Self-assembled structures

Perhaps you recently had an encounter with a new skin care product at the supermarket while thinking about which skin cream to buy. This new product on the shelf was highlighted 'with liposomes'. The next day, on Wikipedia, you discovered what liposomes really are. They are formed of small, amphiphilic molecules that arrange themselves into a bilayer that closes back on itself to form a hollow, spherical structure in which the interaqueous compartment is isolated from the surroundings. Thus, active components can be protected within this aqueous cavity until their use. But this is just one of many solvophobic structures assembled from amphiphiles in a bottom-up approach. The simplest of such are probably micelles – spherical objects with a hydrophobic core and a hydrophilic shell. However, the micellar structure can change, *e.g.* with concentration, and become more elongated, to form cylindrical micelles. At even higher concentration, planar bilayers can be created within a lamellar phase without any curvature. Such structures can grow in the bilayer plane without limit and usually curve back onto themselves to minimize exposure of the hydrophobic part at the edges of the bilayer to the water and therefore form vesicles. These structures exhibit slight curvature, as do bicontinuous phases, in which the two radii of curvature are equal but of opposite sign. At even higher concentrations, a reversed micelle begins to encapsulate a decreased concentration of water with the hydrophilic part of the molecule forming the core. Some of these structures are illustrated in Fig. 1.1.[1] This is fascinating, but the challenge is to understand how these structures can be made in a

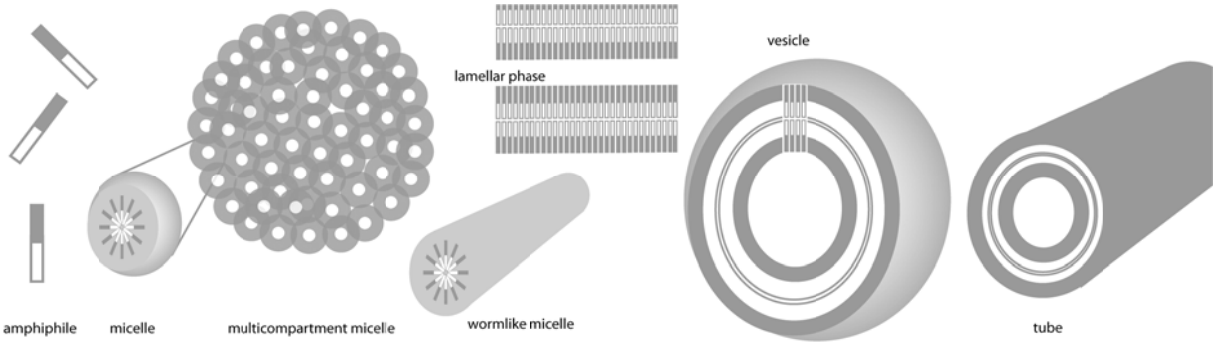

Fig. 1.1 Lyotropic structures as the concentration increases.

precise fashion, controlled, adjusted to specific requirements and applied in useful products. However, it is your choice whether the skin cream should contain 'liposomes'.

1.2. Hierarchical organization

Hierarchical organization is achieved when predefined subunits arrange themselves on an increasingly higher level of organization. Examples are liquid crystals such as the already mentioned lamellar phase, but also hexagonal, cubic, nematic gel or intermediate phases, which all exhibit long-range order. Based on micellar structure, the hierarchical organization includes large complex micelles (LCM) and multicompartment micelles (MCM). Eisenberg *et al.*[2] reported LCM, later also called 'large compound micelles', that consist of aggregated, inverted micelles, surrounded by a final layer of amphiphiles, forming a hydrophilic shell.[3] Diblock copolymers - forming micelles - can further aggregate into LCM, which themselves represent a transition state to form vesicles.[4] The more generalized terminology 'multicompartment micelles',[5] first proposed by Ringsdorf,[6] describes supramolecular aggregates with a hydrophilic shell and segregated hydrophobic cores. MCM from triblock copolymers contain at least two segregated domains within a collective structure.[5a, b, 5d, 7]

Nature also exploits a hierarchical approach to build-up, *e.g.* functional enzymes (*cf.* section 1.4.). Furthermore, spiders use hierarchical assemblies in combination with salt and shear stress to produce spider silk.[8] Artificial fibers in a hierarchical organization can be produced, *e.g.* by β-sheet-forming oligopeptides and hydrophobic, flexible and amorphous synthetic polymers,[9] or by combining block copolypeptides containing an α-helical poly(benzglutamate) (PBLG) block and a poly(lysine) block complexed with 2-deoxyguanosine 5-monophosphate (dBMP).[10]

1.3. Folding and self-assembly of amphiphilic molecules

Amphiphilic molecules spontaneously self-assemble into a variety of structures in solution. Amphiphilic indicates that one part of the molecule is attracted to the solvent, while the other is not. Thus the interactions between solute-solvent and solute-solute – a delicate interplay – determine the organization. Understanding the self-assembly means understanding those interactions and their driving forces.[1]

In aqueous solution the amphiphile aggregation is driven by the low solubility of the hydrophobic part. In the case of a micelle, three terms influence the free energy of

an amphiphile self-assembly in dilute solution: (i) a hydrophobic contribution, due to the hydrophobic part, gathered together within the interior of the aggregates, (ii) a surface term reflecting the opposing tendencies of the hydrophilic part to crowd close together to minimize the hydrophobic moieties (water contact) and spread apart from each other as a result of electrostatic repulsion, hydration and steric hindrance and (iii) a packing term. Surface and packing terms are usually expressed as the surfactant parameter N_S, which is defined as ν/la_0, where ν is the volume of the hydrophobic portion of the amphiphile, l its length and a_0 the effective area per head group. The surfactant parameter also correlates with the curvature of the assemblies and can be assigned to spherical micelles ($N_S = 0.33$), infinite cylinders ($N_S = 0.5$), planar bilayers and vesicles ($N_S = 1$), bicontinuous structures ($N_S \geq 1$) and inverted micelles ($N_S > 1$). The hydrophilic to hydrophobic ratio, calculated from the quantities of the corresponding parts, is another way to define their amphiphilicity and useful for comparisons of different systems.

The introduction of an insoluble molecule to water is equivalent to the introduction of a weak-interacting species into a liquid of high cohesive energy. The Gordon parameter - defined as $\gamma/V_m^{1/3}$, where γ is the surface tension and V_m the molar volume - is used to characterize the cohesive energy of solvents. As a consequence of decreasing cohesive energy densities, the driving force for aggregation decreases and therefore the critical micelle concentration (cmc) increases and become less well-defined. No aggregation has been found for Gordon parameters below 1.3 J m^{-3}.[1]

Hydrophobic interactions refer to the attractive forces between two or more apolar solutes in water and aggregation is associated with the liberation of water molecules structured around a single apolar solute (hydrophobic hydration), which increases the entropy of the system. The hydrophobic effect combines these phenomena.

Self-assembly is a physicochemical process, *i.e.* the amphiphilic molecules are associated physically. Therefore they can change the size or shape of their microstructures in response to small changes in concentration (*cf.* section 1.1), temperature, ionic strength, and choice of buffer, temperature, pH and pressure. These parameters are powerful, as shown by Rao *et al.*[11], who managed thermo- and pH-responsive micellization of poly(N-isopropylacrylamide) -*b*- poly(L-glutamic acid) (PNIPAM-b-PLGA). PNIPAM is known to dissolve in cold and dilute aqueous solution but

to precipitate above ~ 32 °C due to its lower critical solution temperature (LCST) phase behavior. In contrast PLGA exhibits a 2.5_1-helix if charged but adopts an α-helical conformation in the protonated state. Depending on the environmental conditions, PNIPAM formed the micelle core and PLGA the corona once (pH 2, T = 25°C) and, once vice versa (pH 10, T = 45°C). This example is just one of many,[12] but it demonstrates that the effect of environmental changes can cause conformational changes within the polymer, leading to redefined solute-solvent interaction. Consequently a new equilibrium state will be established. Also, ions and their concentrations are important parameters for assembly. Ions are ordered according to their properties at interfaces, *e.g.* between polymer and solvent as in the so-called Hofmeister series. They are categorized into chaotropic, or those that decrease surface tension and protein stability, and cosmotropic, those that have the opposite effect. Zhang *et al.*[13] demonstrated the impact of particular anions in the ability to lower the LCST of PNIPAM – following the Hofmeister series. They were able to sufficiently explain the effect of different ions by the polarization of water molecules, the hydrophobic hydration and direct ion-polymer interactions. On the other hand, the Hofmeister series – known for decades – is still an active field of research.

1.4. Understanding how nature builds-up hierarchically organized structures

1.4.1. Primary and secondary structure – from the 1D to the 3D world

Nature's machinery mainly consists of proteins and peptides that work as catalyst and transport systems, bind and release molecules such as oxygen, guarantee immunity, accomplish mobility, control growth, etc. Surprisingly, this variety of application contrasts with the fact that most proteins are linear biopolymers based on only 20 chiral amino acids (AAs). Nevertheless these AAs exhibits a plethora of functionalities such as acids, bases, alcohols, thiols, indols, etc. They also feature differing hydrophilicities, a few being even fluorescent and they are responsible for responses to environmental changes. The one dimensional code – the primary sequence, which contains all necessary information – is translated into three-dimensional working machinery. However, this contrasts our experiences in everyday life and our thinking, *e.g.* if we consider an

automobile factory assembly-line. Car parts are continuously put together, but not in a linear fashion with the expectation of final self-assembly.

Along the linear peptide backbone, rotation occurs along the N-C_α-bond and the C_α-C-bond, the relative angle of rotation is denoted as Φ and Ψ, respectively. Due to steric hindrance only ~ 25% of all combinations are possible. In natural L-peptides, three different periodic repetitive motifs, *i.e.* secondary structures known as α-helix, β-sheet and β-turn, are formed. Less frequently, *e.g.* in the gramicidin family, a 'rolled-up' β-sheet called a β-helix is found, which is caused by the alternating D, L configuration of the AA sequence and forces all hydrophobic side chains to project outward from the helix.

1.4.2. Alternating D, L - amino acid sequences

Nature concentrates on L-AAs for the construction of its machinery. In contrast, D-AAs occur rarely but provide access to a variety of structures that would not be possible with any L-configuration alone, which was pointed out by Durani,[14] illustrating the tremendous increase in stereoisomers for a 30-AA polypeptide form 1 (= 1^{30}) up to one billion (2^{30}). However, nature implemented some D-AAs, as for example in D, L- alternating sequences, one of which is present in the gramicidin family. The sequence for gramicidin is

Formyl-LV-G-LA-DL-LA-DV-LV-DV-LW-DL-LY-DL-LW-DL-LW-*ethanolamine*

with Y either tryptophan, phenylalanine or tyrosine corresponding to gramicidin A, B and C, respectively. Their mixture (80:5:15) is referred to as gramicidin D.[15] Gramicidin adopts a series of dimerization states: double helical, helical dimer in antiparallel and in differently-staggered parallel configurations, and is known for its antibiotic effect on gram-positive bacteria due to its monovalent ion conducting channel. Dimerization and its degree depend on the polarity of the environment and can be shifted by binding divalent ions. Besides the linear, a cyclic gramicidin S also exhibits the potential to form ion channels, by staggering and thus achieving a trans-membrane channel.

Gramicidin represents a key element in creating a defined hydrophobic moiety in an amphiphilic peptide because of its unique structure, which leads to a stable, completely hydrophobic exterior.

1.4.3. Tertiary, quaternary and hierarchical structures in nature

Ternary structure represents a completely folded primary sequence. The arrangement of several subunits within one functional protein is termed quaternary structure and is often stabilized by thiol-bridges.

One example of hierarchical organization is the thermosome, a chaperonin from the thermophilic organism *Thermoplasma acidophilum*, which is a spherical, hexadecameric complex, assisting protein folding. It consists of two stacked, eight-membered rings, each of which is built-up by alternating α and β subunits, forming one of two half-spheres.[16] Various processes are based on hierarchical proteinogenic structures ranging from the cytoskeleton of a cell, geckos using a distinct arrangement of keratin-like filaments on their toes, or spider silk, which is known for its outstanding mechanical properties. A recent review from Heim *et al.* provides a good overview.[17]

Furthermore, viruses causing a wide variety of diseases consist of a genetic material which is enclosed in a protective proteinaceous capsid. The latter displays a high level of self-assembly of – in theory - 60T, with T = 1, 3, 4, 7, etc. asymmetric protein subunits.[18]

To reproduce, control and use nature made materials on the basis of hierarchical organization we need to understand their principles of formation and to learn their code.

1.5. Synthetic approach to environmentally-responsive materials based on amino acids

The advantages of AAs have already been highlighted; however, there are a variety of methods to create biopolymers from AAs.

1.5.1. Polymerization

Polymerization is a powerful tool to create homopolymers. Polypeptides – their blocks consists of AAs – are synthesized by ring-opening polymerization of α-amino acid-N-carboxyanhydride (NCA) monomers in good yield and without racemization of chiral centers (*cf.* Fig. 1.2), but are affected by chain-breaking transfer and termination reactions, preventing block copolymer formation.[19] In addition to others, Deming *et al.* improved polymerization by using organo-nickel initiators[20] which leads to a low

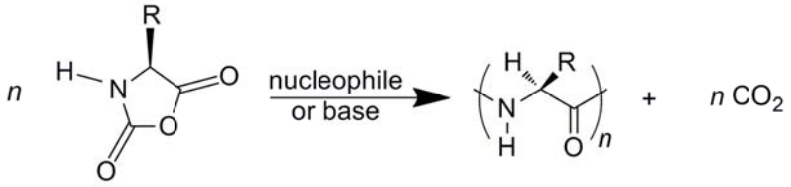

Fig. 1.2 Ring opening polymerization of α- amino acid-N-carboxyanhydrides.

polydispersity index (PD.I). However, it is in the nature of synthetic polymerization to result in a molecular weight distribution that can differ from batch to batch. Furthermore, polymerization techniques as described produce block copolymers but fail in the synthesis of a controlled and defined sequence of different amino acids. Therefore other methods are available.

1.5.2. Solid-phase peptide synthesis (SPPS) – control of the primary sequence

SPPS allows the synthesis of a defined AA sequence by linking a single AA to a functionalized resin, followed by elongation steps until the cleavage of the peptide, which can be up to 50 AAs long. The initial Boc-protection group strategy, which requires HF cleavage from the resin, is almost completely replaced by the cheaper and less dangerous Fmoc-protection strategy; here, TFA can be used. The solid support facilitates the intermediate purification steps by simple filtration and washing, and is similarly used in a variety of chemical reactions.[21] However, by-products from incomplete reaction or impure reagents accumulating on the resin during the elongation steps will necessitate post-purification steps to guarantee high peptide purity, generally performed by reversed-phase high pressure/performance liquid chromatography (RP-HPLC).

Resins are numerous, the most applied are Merrifield resin, Wang, Sasrin, and Rink amide resin, which vary in their cleavage conditions and definition of the peptide's C-terminus. Their load capacity ranges from 0.1 to 1.5 mmol g^{-1}, which avoids reactions between the groups and ensures enough space for the peptide to grow. Resins are insoluble but are able to swell in organic solvents due to their cross-linked polymer (usually polystyrene) nature.

Attachment, *i.e.* coupling of the first AA to the resin is very important since the efficiency of this reaction will determine the yield of the final product and may result in

by-products. The applied conditions often identical to the following reactions (*cf.* Fig. 1.3)

Elongation of the peptide chain starts with the deprotection of the Fmoc group by the weak base, piperidine. This step is followed by the addition of the protected AA, activated by HCTU and DIPEA/NMP. Finally, unreacted, free N-termini are acetylated with acetic anhydrate (Ac_2O) solution to prevent their further elongation, which will facilitate the separation from undesired sequences.

Cleavage of the peptide from the resin is performed with 95% TFA / 5% H_2O. Due to reactive carbo-cations, causing side reactions with AAs, the addition of scavengers is required, consisting generally of 2.5% triisopropylsilane, triethylsilane, or ethandithiol. Filtration from the resin is followed by precipitation in volatile solvents, therefore often *tert.* buthylmethylether, diisopropylether or diethylether are used.

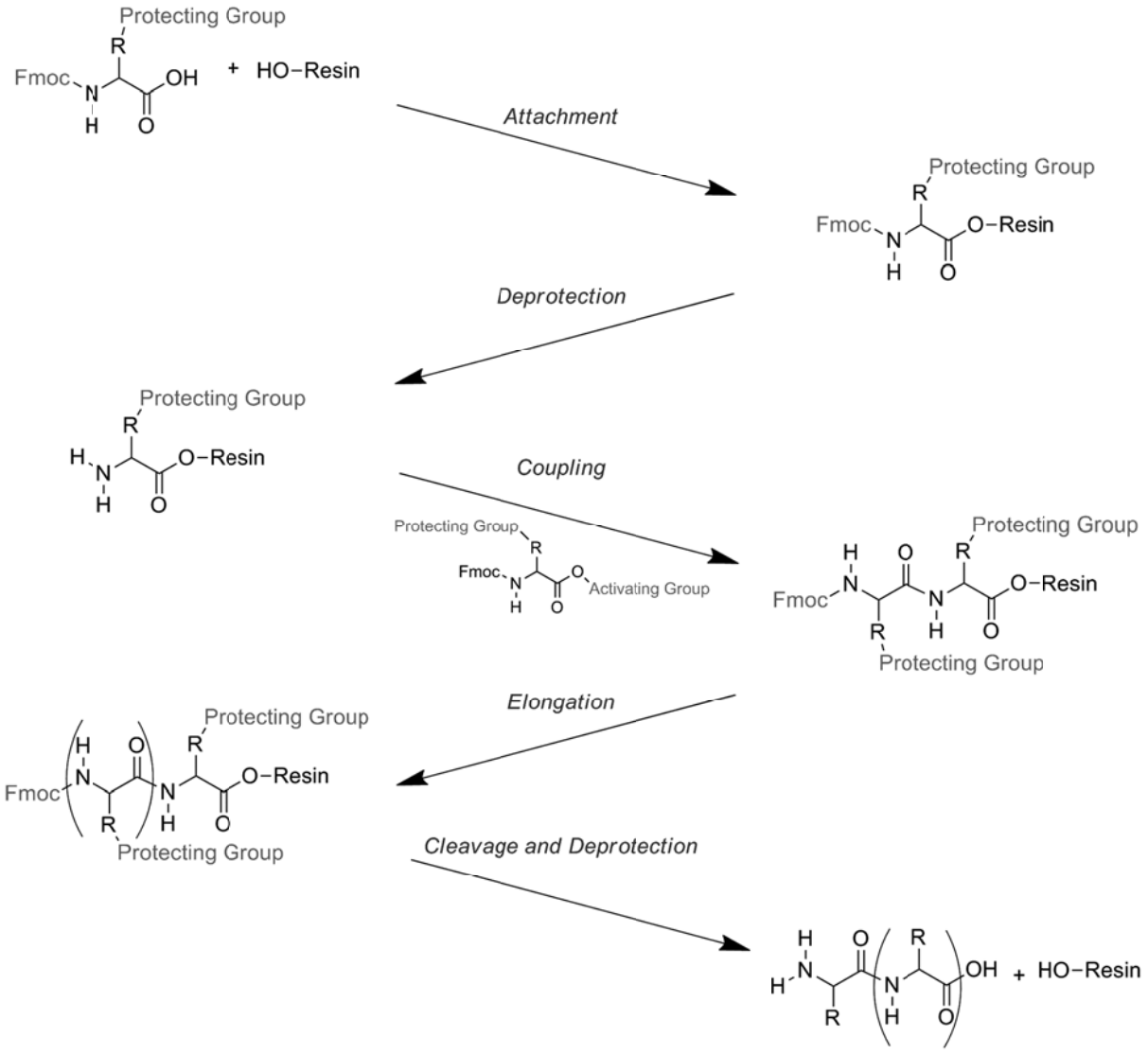

Fig. 1.3 Reaction scheme of solid-phase peptide synthesis using Fmoc strategy.[22]

Purification of the crude product can be performed with RP-HPLC providing good yield, purity, and little time spent to adjust purification protocols. Eluent systems are as varied as column materials. The latter can be end-capped C18 material, often used for peptide purification and a starting point for protocol development. Common eluent systems are:

- ACN/aq. 0.1% TFA
- ACN/aq. 2% HOAc
- ACN/aq. 1% TEAP, pH 2.3
- ACN/aq. 1% TEAP, pH 7-7.5
- ACN/aq. 0.4% NH_4OAc, pH 6.5
- ACN/aq. 0.3% H_3PO_4-$NaClO_4$, pH 2.8

Salt formation, especially with spatial counter-ions such as Tris or perchlorate, usually causes troublesome interactions and changes in peptide properties. Potassium and chloride are alternative counter-ions, providing compatibility in physiological conditions. Ion exchange is performed by removing excess salt by solid-phase extraction, followed by ion exchange chromatography towards the desired counter ion. The usage of acids and bases is necessary to ensure the recovery of uncharged peptides. Excess, unbounded salt can again be removed by solid-phase extraction. At most, ammonia or acetic acid can be used to create ammonium acetate which can be removed by repeated lyophilization.

1.5.3. Recombinant protein expression

Production of large peptides (>50 AAs) and proteins is dedicated to recombinant protein expression. Recombinant proteins are produced by genetically modified organisms after inserting the desired gene, *i.e.* recombinant DNA, into their genome or chromosome. Thereby the expression vector, which inserts the information into the host system, is one of the crucial elements. The recombinant proteins are expressed after the successful transformation of the host system. *Escherichia coli* cell lines are often used due to its safety, easy cloning, genetic manipulation, inexpensive cultivation, rapid growth and fast expression. However, secreted and oxidized proteins might be better expressed in other systems such as yeast (*Pichia pastoris*, *Saccharomyces cerevisiae*), insect cells (for secreted, membrane, and intracellular proteins) or mammalian cells. Therefore, this technique allows the production of collagen, elastin and *de novo* designed, self-assembling peptides or spider silk.[8, 23]

1.6. Approaches towards controlling and understanding self-assembly of peptide-based material

In the last decade self-assembly of peptide-based materials has been mostly studied on block copolypeptides using natural AAs as building units and polymers such as poly(ethylene oxide) (PEO), polystyrene (PS), poly(2-methyloxazoline) (PMOXA) or poly (acrylic acid) (PAA), poly(dimethylsiloxane) (PDMS) as hydrophilic or hydrophobic blocks.

Hybrids combine the known behavior of mainly hydrophobic entities such as polymers or alkyl chains with the beneficial properties of AAs. A recent review[24] summarized the latest achievements, referring to '*peptide amphiphiles*'. Cui *et al.*[25] presented the self-assembly of the so-called alkylated peptide amphiphiles into flat giant nanobelts. The hydrophilic part exhibits two sides due to the alternating valine and glutamic acid sequence, which then associate and form the hydrophilic layer. Polymers can also be used to form superstructures, as illustrated by Kukula *et al.*[26] They synthesized poly(butadiene)-*block*-poly(L-glutamic acid) (PB-PGA) copolymers, which formed vesicles or so-called polymersomes, or peptosomes due to their partial peptide sequence. Furthermore, the peptosomes showed no pH-dependence, *i.e.* no relevant morphological changes even though the PGA underwent a helix-coil transition.

Polypeptides result from hydrophobic AAs such as leucine, isoleucine, phenylalanine or tryptophan and hydrophilic AAs such as, at neutral pH, positively charged arginine and lysine, or negatively charged aspartic acid or glutamic acid. Deming *et al.* designed block copolypeptides that self-assembled into vesicular structures using poly(lysine)$_x$-block-poly(leucine)$_y$ (PLL_x-PL_y with $20<x<80$, $10<y<30$) and PGA_{60}-b-PL_{20}.[27] Rodriguez-Hernandez *et al.*[19a] managed reversible, inside-out PGA_{15}-b-PLL_{15} polypeptide vesicles. Upon a change in pH from < 4 to > 10 the core-forming PGA exchanges with the corona-forming PLL and vice versa. However, as the name 'block copolymer' implies, one block consists of only one kind of monomer. Therefore, it is not in the nature of polymerization to create a defined AA-sequence. Moreover, blocks created by polymerization inherently exhibit a size distribution.

Amphiphilic peptides, also termed *purely peptidic amphiphiles* in this text to clearly discriminate them from peptide-based materials obtained by polymerization and hybrid materials, are synthesized by SPPS or bioengineering techniques. Several systems have been invested. Wiradharma *et al.* investigated a series of six 32-mers in the context of a

medical application.[28] Thus, they designed these peptides with a constant hydrophilic part and a varying hydrophobic part on the basis of the phenylalanine/alanine ratio in order to fine-tune drug and gene co-delivery within the created nanoparticles. Micellization of the 28-mer Pep-L12 was shown by Hashimoto *et al.*[29] and the systems is regarded to be a potential, biodegradable gene carrier system. Amphiphilic peptide self-assembly based on ionic self-complementary peptides from solid-phase peptide synthesis was investigated by Zhang and co-workers.[30] They also used very short amphiphilic peptides *such as* V_6K_2 which assembled into net-like structures of tubes and vesicles.[31] This research was very inspiring for many scientists in this field, however these structures proved to be highly sensitive to the purity of the peptides.[32] Catanionic $A_6K^{\pm}$ was found by Qui *et al.* to successfully assemble into fibers.[33] However, the mentioned studies neglected investigations of the peptide secondary structure.

In contrast, secondary structure was examined on a 24-meric peptide, designed from a 20 kDa barnacle cement protein. [12b] It was found constant while self-assembling into its filamentous structure; however, the peptide did not exhibit an amphiphilic character and self-assembly was actually induced by salt addition. Shera *et al.*[34] compared a 15-mer-designed amphiphilic peptide to its alternating analogue with identical AAs, but a different sequence. The researchers linked the self-assembled morphologies to the observed primary β-sheet conformation, which was not present in the analogue. Further, Mastrobattista *et al.*[35] reported recombinantly produced amphiphilic peptides with a conical geometry of the hydrophobic part to direct self-assembly towards nano-sized vesicles. However, the polyproline II (PP II) secondary structure displayed the hydrophilic backbone and therefore lacked a completely hydrophobic part.

1.7. Scope of the thesis

Peptides represent a biologically, highly relevant material, fulfill crucial functions, and processes of life, with an alphabet consisting of only 20 AAs (with D- and L-configuration). Therefore, they are an excellent material to investigate self-assembly, often part of hierarchical organization, depend on intrinsic parameters such as the AA sequence and environmental conditions ranging from pH, T and salt concentrations to solvent mixtures.

The major topic of this thesis is the development of a better understanding of hierarchical self-organization of amphiphilic peptides. As a consequence, a higher degree of precision and a better adaptability towards the desired properties is one important aim. The focus is on the creation of nanometer-sized materials in the range of 100 to 400 nm which offer a high degree of chemical functionality and, at the same time, a defined response to environmental stimuli, so-called 'smart materials'. However, the response has to be directed in terms of the stimuli and the corresponding environment in which it should act.

Approaches to address these outlines are listed below.

- ✓ *Two hydrophobic parts*, derived from gramicidin A, have been used to determine their potential for amphiphilic design. Both, the 15-mer (gA) using the total alternating D, L AA-sequence of gramicidin A and the second, truncated, 7-mer (gT) consisting of just the repetitive [DL-LW] unit proved to be applicable as a hydrophobic contributor.
- ✓ For the *hydrophilic part* charged AAs, *i.e.* glutamic acid or lysine, have been used, which guarantees amphiphilic properties. Furthermore, acetylated oligolysine was used, which is water insoluble but relatively hydrophilic compared to gT, and was sufficient to induce self-assembly.
- ✓ *pH responsiveness* was linked to the acidic and basic properties of the AA incorporated in the hydrophilic part and a change in pH beyond the pK_a is commonly accompanied by changes in the secondary structure, and consequently affects the self-assembly itself.
- ✓ *Point mutation*, *i.e.* the replacement of lysine by acetylated lysine

represents a fine-tuning of lysine residue properties by acetylation and has linked the primary structure with self-organization.

- ✓ *Dimerization / oligomerization* of two or more amphiphilic peptides using hydrophobic interactions, H-bonds or charge compensation was used to initialize and stabilize membrane formation within vesicles or lamellar phases.
- ✓ *Complete acetylation* of the oligolysine part was used to remove all possible charges on the hydrophilic side and to change amphiphilic properties of the peptides.
- ✓ *Environmental conditions* such as temperature, salt conditions and solvent composition were used to accomplish general property and conformational changes with impact on self-assembled structures.
- ✓ *Interfacial techniques* have been applied to further investigate peptide properties, not only in solution but also at the interface.

Various techniques were combined to investigate amphiphilic peptide self-assemblies in solution, including light scattering, ζ-potential, electron paramagnetic resonance (EPR), transmission electron microscopy (TEM), cryogenic TEM, atomic force microscopy (AFM), scanning electron microscopy (SEM), tensiometry, and confocal laser scanning microscopy (CLSM). At the water-air interface and surfaces, film balance, Brewster angle microscopy (BAM), infrared spectroscopy and AFM have been used and are presented in this thesis.

The contribution to the field of colloids, soft matter and self-assembly lies in the achievement of using small peptides to study self-organization, and thus to better understand the formation process of hierarchical structures in living mater. The created structures and the applied approaches can be used as a basis for the development of advance functional smart materials with potential application in the medical sector as drug and gene delivery systems, vaccinations, interfaces between implants and living tissue or as sensor device, etc.

1.8. References

[1] D. F. Evans, *The Colloidal Domain: Where Physics, Chemistry, Biology, and Technology Meet, 2nd*, **1998**, p. 640 pp.

[2] L. Zhang and A. Eisenberg, *Science (Washington, D. C.)* **1995**, *268*, 1728-1731.

[3] a) J.-F. Gohy in *Block Copolymer Micelles*, *Vol. 190* (Ed. V. Abetz), Springer Berlin / Heidelberg, **2005**, pp. 65-136; b) C. Giacomelli and R. Borsali in *Disordered Phase and Self-Organization of Block Copolymer Systems*, *Vol.* Eds.: R. Borsali and R. Pecora), Springer Netherlands, **2008**, pp. 133-189.

[4] a) J. Sun, Q. Shi, X. Chen, J. Guo and X. Jing, *Macromol. Chem. Phys.* **2008**, *209*, 1129-1136; b) K. Yu and A. Eisenberg, *Macromolecules* **1996**, *29*, 6359-6361; c) H. Shen, L. Zhang and A. Eisenberg, *J. Am. Chem. Soc.* **1999**, *121*, 2728-2740; d) L. Liu, X. Gao, Y. Cong, B. Li and Y. Han, *Macromol. Rapid Commun.* **2006**, *27*, 260-265.

[5] a) S. Kubowicz, J.-F. Baussard, J.-F. Lutz, A. F. Thuenemann, H. von Berlepsch and A. Laschewsky, *Angew. Chem., Int. Ed.* **2005**, *44*, 5262-5265; b) J.-F. Lutz and A. Laschewsky, *Macromol. Chem. Phys.* **2005**, *206*, 813-817; c) H. von Berlepsch, C. Boettcher, K. Skrabania and A. Laschewsky, *Chem. Commun. (Cambridge, U. K.)* **2009**, 2290-2292; d) C. Zhong and D. Liu, *Macromol. Theory Simul.* **2007**, *16*, 141-157; e) K. Delak, S. Collino and J. S. Evans, *Langmuir* **2007**, *23*, 11951-11955.

[6] H. Ringsdorf, P. Lehmann and R. Weberskirch, **1999**, pp. BTEC-001.

[7] A. Laschewsky, *Curr. Opin. Colloid Interface Sci.* **2003**, *8*, 274-281.

[8] F. Hagn, L. Eisoldt, J. G. Hardy, C. Vendrely, M. Coles, T. Scheibel and H. Kessler, *Nature (London, U. K.)* **2010**, *465*, 239-242.

[9] a) E. Jahnke, J. Weiss, S. Neuhaus, T. N. Hoheisel and H. Frauenrath, *Chemistry--A European Journal* **2009**, *15*, 388-404; b) E. Jahnke, I. Lieberwirth, N. Severin, J. P. Rabe and H. Frauenrath, *Angew. Chem., Int. Ed.* **2006**, *45*, 5383-5386.

[10] N. Houbenov, A. Nykanen, H. Iatrou, N. Hadjichristidis, J. Ruokolainen, C. F. J. Faul and O. Ikkala, *Adv. Funct. Mater.* **2008**, *18*, 2041-2047.

[11] J. Rao, Z. Luo, Z. Ge, H. Liu and S. Liu, *Biomacromolecules* **2007**, *8*, 3871-3878.

[12] a) A. A. Ismail and H. H. Mantsch, *Biopolymers* **1992**, *32*, 1181-1186; b) M. Nakano, J.-R. Shen and K. Kamino, *Biomacromolecules* **2007**, *8*, 1830-1835; c) T. Makovec, *Biochem. Mol. Biol. Educ.* **2000**, *28*, 244-247; d) F. Checot, S. Lecommandoux, Y. Gnanou and H.-A. Klok, *Angew. Chem., Int. Ed.* **2002**, *41*, 1339-1343; e) E. Navarro, E. Fenude and B. Celda, *Biopolymers* **2004**, *73*, 229-241.

[13] Y. Zhang and P. S. Cremer, *Curr. Opin. Chem. Biol.* **2006**, *10*, 658-663.

[14] S. Durani, *Acc. Chem. Res.* **2008**, *41*, 1301-1308.

[15] a) C. Zhao and P. L. Polavarapu, *Biospectroscopy* **1999**, *5*, 276-283; b) L. E. Townsley, W. A. Tucker, S. Sham and J. F. Hinton, *Biochemistry* **2001**, *40*, 11676-11686; c) B. A. Wallace, *J. Struct. Biol.* **1998**, *121*, 123-141; d) B. A. Wallace, *Biophys. J* **1986**, *49*, 295-306.

[16] N. Bruns, K. Pustelny, L. M. Bergeron, T. A. Whitehead and D. S. Clark, *Angew. Chem., Int. Ed.* **2009**, *48*, 5666-5669, S5666/5661-S5666/5617.

[17] M. Heim, L. Roemer and T. Scheibel, *Chem. Soc. Rev.* **2010**, *39*, 156-164.

[18] D. G. Angelescu and P. Linse, *Soft Matter* **2008**, *4*, 1981-1990.

[19] a) J. Rodriguez-Hernandez and S. Lecommandoux, *J. Am. Chem. Soc.* **2005**, *127*, 2026-2027; b) J. Sun, X. Chen, C. Deng, H. Yu, Z. Xie and X. Jing, *Langmuir* **2007**, *23*, 8308-8315.

[20] T. J. Deming, *Nature* **1997**, *390*, 386-389.

[21] P. H. H. Hermkens, H. C. J. Ottenheijm and D. C. Rees, *Tetrahedron* **1997**, *53*, 5643-5678.
[22] R. S. Tu and M. Tirrell, *Adv. Drug Delivery Rev.* **2004**, *56*, 1537-1563.
[23] S. Kyle, A. Aggeli, E. Ingham and M. J. McPherson, *Trends Biotechnol.* **2009**, *27*, 423-433.
[24] H. Cui, J. Webber Matthew and I. Stupp Samuel, *Biopolymers* **2010**, *94*, 1-18.
[25] H. Cui, T. Muraoka, A. G. Cheetham and S. I. Stupp, *Nano Lett.* **2009**, *9*, 945-951.
[26] H. Kukula, H. Schlaad, M. Antonietti and S. Forster, *J. Am. Chem. Soc.* **2002**, *124*, 1658-1663.
[27] a) E. G. Bellomo, M. D. Wyrsta, L. Pakstis, D. J. Pochan and T. J. Deming, *Nat. Mater.* **2004**, *3*, 244-248; b) E. P. Holowka, D. J. Pochan and T. J. Deming, *Journal of the American Chemical Society* **2005**, *127*, 12423-12428; c) E. P. Holowka, V. Z. Sun, D. T. Kamei and T. J. Deming, *Nat. Mater.* **2007**, *6*, 52-57.
[28] N. Wiradharma, Y. W. Tong and Y.-Y. Yang, *Macromol. Rapid Commun.* **2010**, *31*, 1212-1217.
[29] T. Hashimoto, R. Iwase, A. Murakami and T. Yamaoka, *Polym. Degrad. Stab.* **2009**, *94*, 1349-1353.
[30] a) S. G. Zhang and X. J. Zhao, *J. Mater. Chem.* **2004**, *14*, 2082-2086; b) S. G. Zhang, *Nat. Biotechnol.* **2003**, *21*, 1171-1178.
[31] G. von Maltzahn, S. Vauthey, S. Santoso and S. Zhang, *Langmuir* **2003**, *19*, 4332-4337.
[32] D. J. Adams, K. Holtzmann, C. Schneider and M. F. Butler, *Langmuir* **2007**, *23*, 12729-12736.
[33] F. Qiu, Y. Chen and X. Zhao, *J. Colloid Interface Sci.* **2009**, *336*, 477-484.
[34] J. N. Shera and X. S. Sun, *Biomacromolecules* **2009**, *10*, 2446-2450.
[35] a) A. J. van Hell, A. Klymchenko, P. P. Burgers, E. E. Moret, W. Jiskoot, W. E. Hennink, D. J. A. Crommelin and E. Mastrobattista, *J. Phys. Chem. B* **2010**, *114*, 11046-11052; b) A. J. van Hell, C. I. C. A. Costa, F. M. Flesch, M. Sutter, W. Jiskoot, D. J. A. Crommelin, W. E. Hennink and E. Mastrobattista, *Biomacromolecules* **2007**, *8*, 2753-2761.

2. Reversible peptide particle formation using a mini amino acid sequence

Thomas B. Schuster[1], Dirk de Bruyn Ouboter[1], Enrica Bordignon[2], Gunnar Jeschke[2], Wolfgang Meier[1]

[1]Department of Chemistry, University of Basel, Klingelbergstrasse 80, CH- 4056 Basel, Switzerland

[2]Laboratory for Physical Chemistry, ETH Zürich, Wolfgang-Pauli-Str. 10, CH- 8093 Zürich, Switzerland

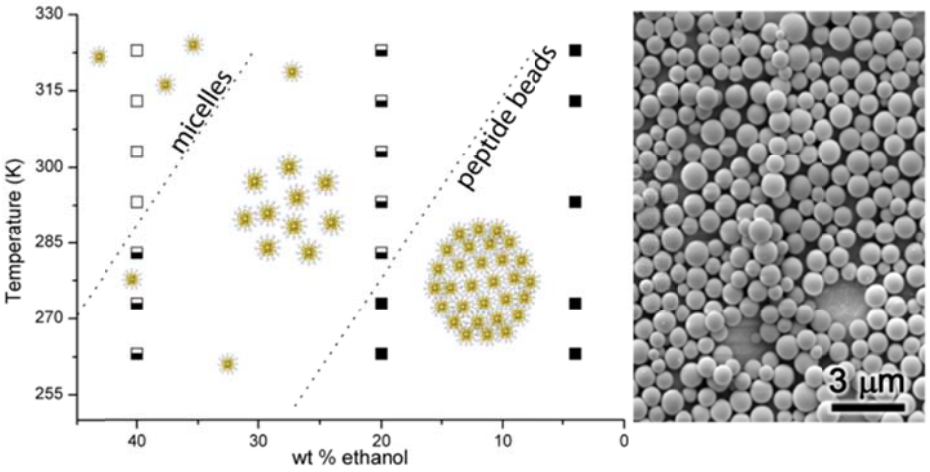

Phase diagram (left) of the self-assembly process of amphiphilic peptides from dissolved molecules to form self-assembled micelles and spherical peptide beads (right)

Parts published in: *Soft Matter* **2010,** *6* (21), 5596-5604

2.1. Introduction

The increased effort and interest in the self-assembly of nanostructures in recent decades, especially in aqueous solution, have led to manifold morphologies as exhibited by micelles, cylindrical micelles, and vesicles. Block copolymers have been explored to tailor-make micelles for the encapsulation of hydrophobic compounds.[1] Inspired by nature and imitating lipid membranes, block copolymer vesicles are now being used to create nanocompartments that encapsulate dyes[2] and active enzymes,[3] insert active proteins,[4] perform molecular recognition[5] and form stimuli-responsive nanoreactors and drug delivery systems (DDSs).[6] Vesicular structures are interesting candidates for DDSs because they permit the simultaneous encapsulation of hydrophobic and hydrophilic compounds in their membranes and aqueous cores.[7] Other self-assembled structures that could serve as DDSs are large compound micelles[8] (LCM) or multicompartment micelles[9] (MCM). These nanosized systems have a hydrosoluble shell and are characterized by segregated, incompatible subdomains that entrap drugs as a function of hydrophobicity, potentially followed by controlled release. MCM and LCM consist of micellar and inverse micellar-type subunits, respectively.

Hybrid materials composed of polypeptides and polymers combine the advantages of the two, *e.g.* solubility and processability.[10] Polypeptides contribute positive aspects in terms of chemical functionality due to a diversity of amino acid (AA) side chains, combined with specific AA sequences that act, *e.g.* as a specific recognition site[11] (RGD sequence for cell adhesion or arginine rich sequences for cell penetration[12]). Another characteristic feature of polypeptides is their secondary structure, which permits exploiting their geometry.[13] The primary sequence, along with environmental conditions (pH, ionic strength, temperature, solvent), *i.e.* intrinsic and external factors, determine the secondary structure and therefore also control the overall morphology of the assembly.

Peptide-based materials can respond to environmental triggers with sensitivity and specificity. In the biological context this smartness makes a multitude of applications possible, including triggered drug release, biosensors, tissue repair, and also patterning.[14] For example, applying changes in pH and temperature triggered the inversion of a micellar structure based on the properties of the two blocks used in a peptide-containing block copolymer.[15] In another system, the release of a drug was

controlled by the presence of poly(L-glutamic acid) within the block copolymer micelle's corona, leading to a pH-triggered increase in permeability.[16]

The importance of charges was also demonstrated by the charge-driven complexation of oppositely charged peptide-based blocks, yielding vesicles with a semipermeable membrane.[17]

Recently, amphiphilic biopolymers have also been reported that comprise only natural amino acids and hence are expected to display enhanced biocompatibility. For example, Deming *et al.*[12, 18] and Rodriguez-Hernandez *et al.*[19] designed block copolypeptides that self-assemble into vesicular structures. It should be noted that the systems described so far were generated by conventional polymerization techniques. Despite the fact that rather narrow molar mass distributions can be reached[12, 18] the resulting polymers are not monodisperse and polymerization allows only limited control of the sequence.

These problems are overcome by genetic engineering techniques that result in excellent control of sequence and length.[20] In this regard, Scheibel *et al.* reported the use of a natural 47.7 kDa spider silk protein to form microspheres.[21]

Solid-phase synthesis also offers optimal tuning of properties by point mutation, but is limited to oligo- and polypeptides (up to 50 AA).

Santoso *et al.* reported the self-assembly of small amphiphilic peptides having no defined secondary structure into well-defined superstructures[22] which, however, proved to be highly sensitive to the purity of the peptides.[23] The continued search for an essential amyloid-forming sequence led to still smaller molecules containing just two amino acids capable of forming superstructures, *i.e.* nanotubes.[24]

In summary, manifold architectures of self-assembled nanostructures exist. All are intrinsically very interesting and have potential application not only in medicine and nanobiotechnology but also in solar cells and optical and electronic devices. Naturally occurring amino acids, as hydrophobic or hydrophilic components, contribute to the self-assembly and can respond to external stimuli. After performing their mission they degrade to prevent accumulation in the body.

Here, we report the synthesis and characterization of amphiphilic oligopeptides while focusing on the self-assembly process. Inspired by gramicidin A (gA), the C-terminal sequence of the peptides consists of a truncated gA (gT) – a repetitive L-tryptophan – D-

leucine [LW-DL] motif. The motif results in distinct *phi* and *psi* angles of the peptide backbone, whereas similarities in the sequence between gramicidin and the amphiphilic peptides should also imply similarities in secondary structure.[25] Overall, the peptide is amphiphilic due to the N-terminus-attached lysines (K) or acetylated lysines (X).

An overview of the synthesized peptides is given in Table 2.1 (for details, see Table 2.3). We investigated the amphiphilic mini (11 AA) peptides using electron paramagnetic resonance (EPR), dynamic (DLS) and static light scattering (SLS) as well as transmission (TEM) and scanning electron microscopy (SEM). The focus was centered on the process that forms the superstructures as a function of temperature and solvent composition.

To investigate the effect of electrostatic interactions on self-assembly, charges on the molecule were removed by acetylation, while shielding accomplished by the addition of counter ions also proved effective.

2.2. Results and discussion

2.2.1. Peptides and their potential to dimerize

Similar to other amphiphiles, amphiphilic peptides are also expected to self-assemble into well-defined superstructures in aqueous solution. Here, we focused on peptides with a given hydrophobic [LW-DL]$_3$-LW-*NH$_2$* sequence that was coupled to a hydrophilic tripeptide either based on a positively charged [LK]$_3$ sequence or the corresponding, electrically neutral [LK*(Ac)*]$_3$.

The repetitive [LW-DL] sequence of our model peptides derives from gA, which is known to form dimers in an apolar environment.[24b] Hence, we expected that the C-

Table 2.1 Code and sequence of charged (K) and uncharged (X = LK(*Ac*)) amphiphilic peptides.

Code	Sequence
K$_3$-gT	*H*-LK$_3$-[LW-DL]$_3$-LW-*NH$_2$*
C-K$_3$-gT	*H*-LC-LK$_3$-[LW-DL]$_3$-LW-*NH$_2$*
Ac-X$_3$-gT	*Ac*-[LK*(Ac)*]$_3$-[LW-DL]$_3$-LW-*NH$_2$*
AcC-X$_3$-gT	*Ac*-LC-[LK*(Ac)*]$_3$-[LW-DL]$_3$-LW-*NH$_2$*
(AcC-X$_3$-gT)$_2$	*(Ac*-LC-[LK*(Ac)*]$_3$-[LW-DL]$_3$-LW-*NH$_2$)$_2$*
AcC(sl)-X$_3$-gT	*Ac*-LC*(acetamidoproxyl)*-[LK*(Ac)*]$_3$-[LW-DL]$_3$-LW-*NH$_2$*

terminus of our peptides would also be accessible for such intermolecular organization. The nature of the building blocks (monomeric *vs.* dimeric peptides) is expected to directly influence the structure of the resulting self-assemblies in aqueous media. Therefore, we performed model experiments in organic solvents to probe the dimerization capacity of the peptides by gel permeation chromatography (GPC) and EPR. The GPC elution profile for gramicidin shows separation into mono- and dimers in different solvents[26] (THF, ethanol, Fig. 2.12). The elution profile of the amphiphilic peptide was characterized by a slightly broader peak with no indication of distinct dimerization.

EPR was used to further verify possible dimerization in solution. The spin-labeled amphiphilic peptide AcC(sl)-X_3-gT was dissolved in ethanol, in which gA is known to lead to dimerization.[26] Dimerization of the molecule can occur by association of the hydrophobic component in a head-to-head or in an intertwining configuration, both well-established forms for gA.[27] Either means of dimerization is expected to bring the two spin labels at the hydrophilic ends of the peptide into close proximity (2 − 3 nm range). Dzikovski[28] *et al.* found direct evidence of a head-to-head gA dimer in the dimyristoylphosphatidylcholine (DMPC) membrane with an interspin distance of 3.1 nm by double-quantum coherence (DQC) EPR.

Here, double electron-electron resonance (DEER), which is sensitive in the 1.7 − 8 nm range,[29] was performed on AcC(sl)-X_3-gT in double-distilled water (dd H_2O). No DEER signal modulation from dipole-dipole interaction between electron spins was detected. Therefore, the trace clearly confirmed that no dimerization occurred (Fig. 2.1A). To verify the possible presence of short interspin distances (< 2 nm), the spin labeled AcC(sl)-X_3-gT was spin-diluted with unlabeled AcC-X_3-gT. The continuous wave (cw) EPR spectra of AcC(sl)-X_3-gT at 100 wt % and 8.7 wt % (2:23 dilution with unlabeled AcC-X_3-gT) in ethanol are superimposed in Fig. 2.1B. The identical spectral shapes at room temperature ruled-out the presence of short interspin distances.

In conclusion, both GPC and EPR showed that the amphiphilic peptides are monomeric in ethanol.

2.2.2. Charged amphiphilic peptides – C-K_3-gT

The hydrophilic building block C-K_3-gT possesses free amine functionalities on the

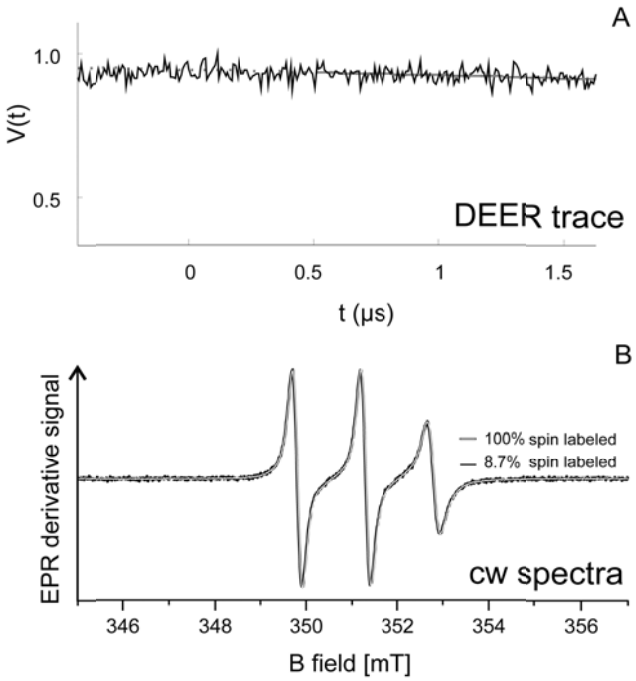

Fig. 2.1 (A) Pulse double electron-electron resonance on 150 µM AcC(sl)-X_3-gT in ethanol in the presence of 50 v % deuterated glycerol and (B) cw EPR spectra of an AcC(sl)-X_3-gT/AcC-X_3-gT mixture (100 µM, black line) as well as AcC(sl)-X_3-gT (300 µM, white line (superimposed on the black line)) in ethanol.

lysine residues as well as a free N-terminus. Therefore, at neutral pH (pK_a of 10.2) the peptide is charged and self-assembly is constrained by electrostatic repulsion.

The peptide C-K_3-gT can be directly dissolved in an aqueous environment. In such, it exhibits a confined critical micelle concentration (cmc) of 0.23 mmol L^{-1} (*cf.* Fig. 2.15), thus suggesting assembly into micelles and conventional surfactant behavior.

This is confirmed by DLS, indicating spherical micelles with a hydrodynamic radius of $R_h \approx 10$ nm. In addition – particularly at higher peptide concentrations – DLS indicates the presence of a minor fraction of larger aggregates with a hydrodynamic radius of approximately 160 nm. Indeed, TEM micrographs also show that, besides the dominant micelle fraction, spherical objects of the mentioned dimension were occasionally found (Fig. 2.16). We hypothesize that these structures are formed by the aggregation of individual micelles into 'multicompartment micelles', herein termed 'peptide beads'. Since the assembly of C-K_3-gT is strongly influenced by electrostatic interactions of the positively charged oligolysine groups, we expected that an equilibrium between micelles and peptide beads would be directly influenced by shielding the charges with appropriate counter ions. The Hofmeister series orders such ions according to their

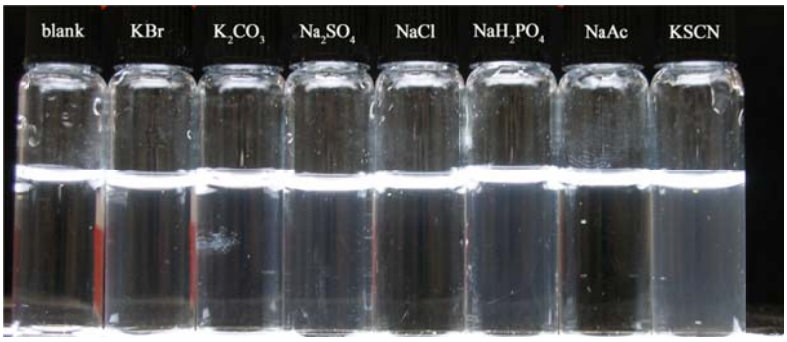

Fig. 2.2 Effect of cosmotrop, neutral and chaotropic anions on the self-assembly.

properties at interfaces.[21b, 30] Chaotropic ions, *e.g.* decrease surface tension and protein stability, in contrast to cosmotropic ions having the opposite effects.

Indeed, stepwise addition of small aliquots of concentrated salt solution to C-K_3-gT increased the fraction and size of the beads as monitored by DLS, and can even be suggested by the turbidity (Fig. 2.2). The growth in size was similar for the different ions. The size of the peptide beads increased up to a salt concentration of 0.3 mol L^{-1}. Beyond that value only minor size changes were observed, indicating saturation and maximum shielding.

The final radii of the formed particles at salt concentrations of 0.6 mol L^{-1} essentially followed the Hofmeister series (Fig. 2.3). Cosmotropic and chaotropic ions influenced the size and the relative fraction of the corresponding aggregates while 'neutral' ions led to a minor response in the peptide assemblies. For cosmotropic ions, we monitored salting out due to a decrease in solubility of the peptide, and therefore the

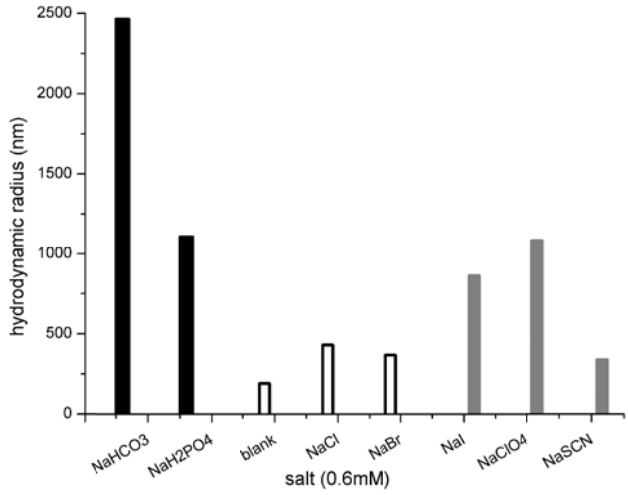

Fig. 2.3 Effect of cosmotropic (black) neutral (white) and chaotropic anions (gray) on self-assembly (radius).

amplification of the tendency to agglomerate.

Chaotropic ions lowered the interfacial tension and therefore affected the curvatures and dimensions of the peptide beads. Exemplary SEM of peptide particles in the presence of PO_4^{3-} and SCN^- are given in Fig. 2.17.

We found only one exception to the Hofmeister series. Despite their chaotropic nature, SCN^- ions (Fig. 2.3) still led to particles with relatively small radii. This is possibly due to a specific interaction that stabilizes the structure.[31]

2.2.3. Uncharged amphiphilic peptides – acetylated AcC-X_3-gT

It is obviously possible to manipulate self-assembly of the charged amphiphiles by external factors (*e.g.* correct choice of counter ions). Therefore, we expected that a similar or even stronger effect could be induced by acetylation of the lysine residues, thus eliminating the electrostatic interactions. Consequently, the only difference between C-K_3-gT and AcC-X_3-gT is a lack of charges due to the acetylation of the primary amine function. It should be noted, however, that acetylation to AcC-X_3-gT reduces hydrophilicity to the extent that the entire amphiphilic molecule does not dissolve directly in dd H_2O. Therefore, self-assembly process is induced by dissolving the peptide in ethanol and changing the surrounding polarity by exchanging the ethanol with dd H_2O.

The self-assemblies formed by AcC-X_3-gT were characterized by SEM and TEM (Fig. 2.4A and B). Indeed, this peptide also assembled into micelles and larger peptide beads.

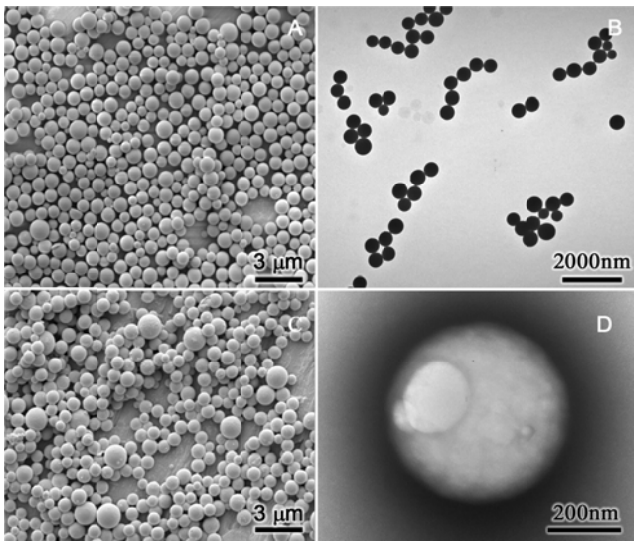

Fig. 2.4 Representative SEM of (A) AcC-X_3-gT and (C) Ac-X_3-gT and TEM of (B) AcC-X_3-gT (D) AcC(sl)-X_3-gT after solvent exchange to dd H_2O.

Interestingly, in TEM the spherical particles display an indentation as shown in Fig. 2.4D for AcC(sl)-X_3-gT. This phenomenon might be caused by solvent evaporating from the assembly during the sample preparation (drying). The self-assembly behavior proved to be insensitive to minor structural changes in the peptides. For example, for Ac-X_3-gT, AcC-X_3-gT (with an additional acetylated cysteine) or AcC(sl)-X_3-gT (carrying a spin label at the hydrophilic end), no difference was observed with any of the methods used (Fig. 2.4 and Fig. 2.18). Thus, the labeled AcC(sl)-X_3-gT can be used as a valid 'tool' to probe its self-assembly and that of its analogues. Furthermore, no significant difference was observed between C-K_3-gT and K_3-gT. Therefore, a transfer of the information concerning the self-assembly process of the AcC-X_3-gT/C-K_3-gT system to the Ac-X_3-gT/K_3-gT system appears justified.

To obtain further insight into the self-assembly process upon solvent displacement, samples at different final ethanol concentrations (40 wt % – 0 wt % EtOH) were prepared and analyzed by EPR, DLS, and SLS.

The self-assembly process for AcC-X_3-gT (with 8.7% of AcC(sl)-X_3-gT and total initial peptide concentration of 1 mg mL^{-1} to ensure sufficient signal/noise ratio) was followed using EPR. The cw EPR spectra performed at different final ethanol concentrations showed two distinct species (Fig. 2.19), one characterized by narrow lines (so-called 'mobile species', with fast rotational correlation times) and one characterized by broad lines, large pseudo hyperfine splitting, which is typical of powder-like spectra (so-called 'immobile species', with slow rotational correlation times). The ratio of the two species varied with temperature and final ethanol concentration (Fig. 2.5): increasing the temperature together with the ethanol concentration led to an increase in the mobile species population. The mobile species was predominant at 40 wt % ethanol, with 65% of the total spectral area at 273 K. The immobile species, on the other hand, was the prevalent species at 4 wt % ethanol, with 100 to 98% of the spectral area in the 263 to 335 K range (Fig. 2.5). The rotational correlation time (τ = 0.530 ns at 293 K and 40 wt %) calculated for the micelle fraction at a size of 5.65 nm matched the rotational correlation time (τ = 0.531 ns) obtained by simulating the spectrum with the fast motion regime EasySpin[32] 'garlic' function using an isotropic model of motion. Thus, the mobile EPR species correlates with the micellar fraction. Similarly, the high correlation times of the immobile species (> 20 ns) correlate to the large dimensions observed for the peptide

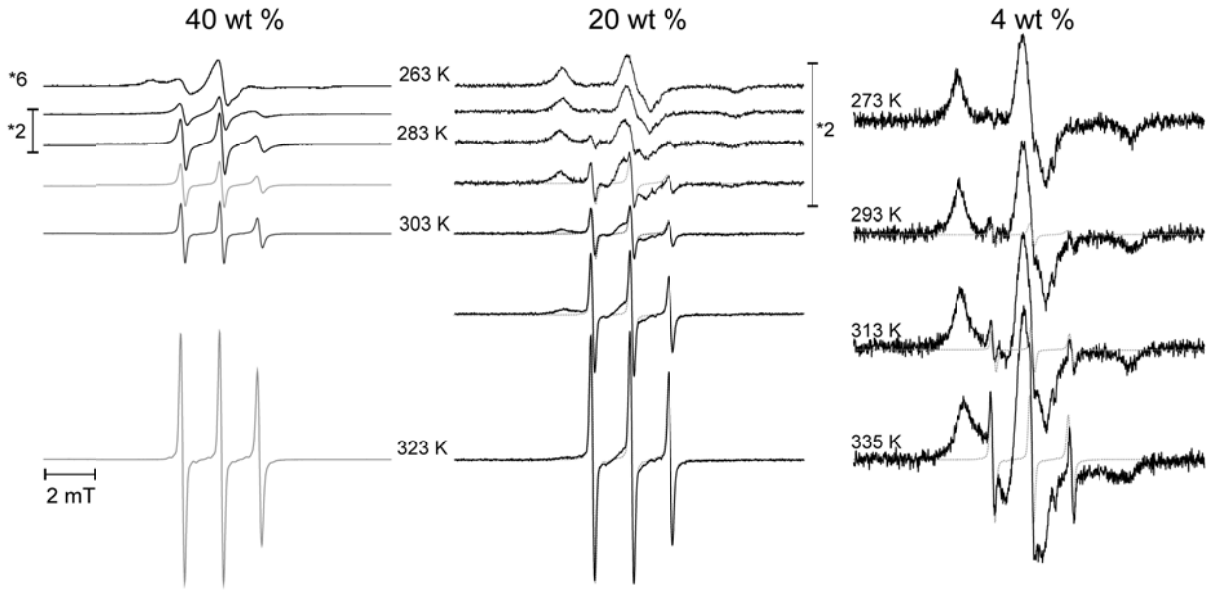

Fig. 2.5 EPR spectra of AcC(sl)-X_3-gT / AcC-X_3-gT mixture as a function of final ethanol concentration and temperature. The spectra at 40 wt % EtOH were scaled and superimposed to the spectra obtained at the same temperature with different EtOH concentrations.

beads. The temperature and ethanol dependence of the EPR spectral fractions confirmed that both external factors can shift the equilibrium between the micelle and the peptide bead population.

The self-assembly process for the same AcC-X_3-gT/ AcC(sl)-X_3-gT mixture (8.7%, c_{tot} = 1 mg mL^{-1}) and final ethanol concentrations was monitored by DLS, which confirmed the observations from EPR. In the dissolved state in pure ethanol, no significantly higher scattering intensity was observed than for that of pure ethanol, indicating molecularly dissolved peptides. For water/ethanol mixtures, data were analyzed by the CONTIN algorithm and this revealed up to three different species (correlation functions are given in in Fig. 2.20). One species was found with a hydrodynamic radius in the range of 5 – 10 nm, which corresponds well with the size of micelles. With decreasing ethanol concentration an increasing fraction of larger particles at 100 – 150 nm was also present. At less than 20 wt % ethanol a third species with a greater radius (*e.g.* $R_h \approx 350$ nm at 4 wt %) appeared and became the dominant species. It apparently emerged from the second species, since we found no structurally different morphologies in the final stage of the self-assembly. Nevertheless, these particles have an increased radius and thus are considered a 'matured' second species. It should be emphasized that the formation of the final particles was fully reversible; upon addition of ethanol the fraction of the

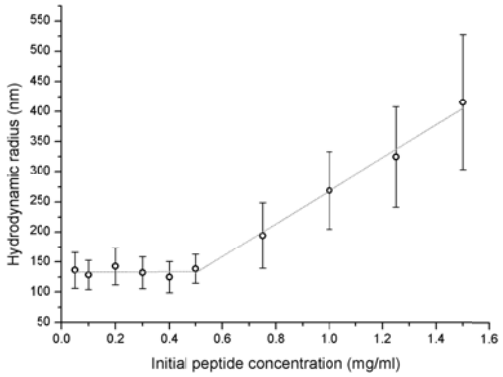

Fig. 2.6 Size-dependence of final peptide beads in dd H_2O on the initial peptide concentration. Error bars reflect the relative peak width from DLS (2nd cumulant analysis).

second species increased at the expense of the third. Also, the self-assembly of the synthesized peptides into micelles and peptide beads was found to be a reversible process and the equilibrium between the different species was independent of the sample preparation (for example, see Fig. 2.21). The transition was also able to be induced by temperature variation: absorbance measurements allowed us to directly track the reversible formation of the final 'matured' peptide particles (see Fig. 2.22 for temperature dependent absorbance measured at 20 wt % ethanol). Interestingly, the formation of the final 'matured' peptide particles in dd H_2O also depends on the initial concentration of the peptide in ethanol. The hydrodynamic radius remained constant at $R_h \approx 130$ nm up to an initial peptide concentration of approx. 0.5 mg mL^{-1}. For concentrations higher than 0.5 mg mL^{-1} the size of the peptide beads increased linearly with the initial peptide concentration (Fig. 2.6 and SEM micrographs Fig. 2.23). Obviously, the onset of the second growth process requires a certain 'critical peptide concentration' similar to the critical micelle concentration of detergents. However, further experiments are needed to understand this process.

To derive further information on the structure and composition of the different peptide particles we performed static light scattering for dispersions at different final ethanol concentrations. For all samples the initial peptide concentration in pure ethanol was 1 mg mL^{-1}. The desired solvent composition was adjusted by solvent exchange and kept constant during the subsequent dilution steps. Fig. 2.7A shows a representative Guinier-Plot for a peptide dispersion in a solvent mixture at 4 wt % ethanol. Under these conditions the radius of gyration of the particles was only minimally dependent on the

Table 2.2 SLS summary for peptide beads in different ethanol concentrations.

EtOH wt %	R_g nm	M_w g mol^{-1}	A_2 mol dm^{3}g^{-2}	N_{AG}
40	179	3.76E+07	8.342E-10	2.14E+04
30	189	1.61E+08	-2.43E-08	9.16E+04
20	201	2.44E+09	-4.231E-11	1.39E+06
12	210	1.01E+10	2.857E-10	5.77E+06
4	218	1.73E+10	2.895E-10	9.87E+06

final solvent composition. At the same time, the molar mass (Mw) of the particles drastically increased (*i.e.* by a factor of 500) as the fraction of ethanol decreased in the final dispersion. At the lowest final ethanol concentration of 4 wt % the particles had a Mw of $1.73 \cdot 10^{10}$ g mol^{-1}, corresponding to a particle composed of approximately 10^7 peptide molecules (Table 2.2). Assuming the particles behave like homogenous hard spheres, an apparent density δ of the particles can be calculated accordingly.[33] Interestingly, the apparent density of the particles increased from 0.006 g cm^{-3} at 40 wt % ethanol to 1.44 g cm^{-3} at 4 wt % ethanol. Molar masses and apparent densities at higher final ethanol concentrations (> 20%) can only be used as a rough estimate, since here a considerable fraction of small micelles, coexisting with the peptide beads, contributed negligibly to the scattering intensity. Nevertheless, our data clearly indicate a transition from a loosely packed, highly solvent-swollen aggregate to more homogenous particles mainly consisting of densely packed peptides. Indeed, the observed value is in agreement with typical data for peptides[34] and consistent with the observed sedimentation of the particles.

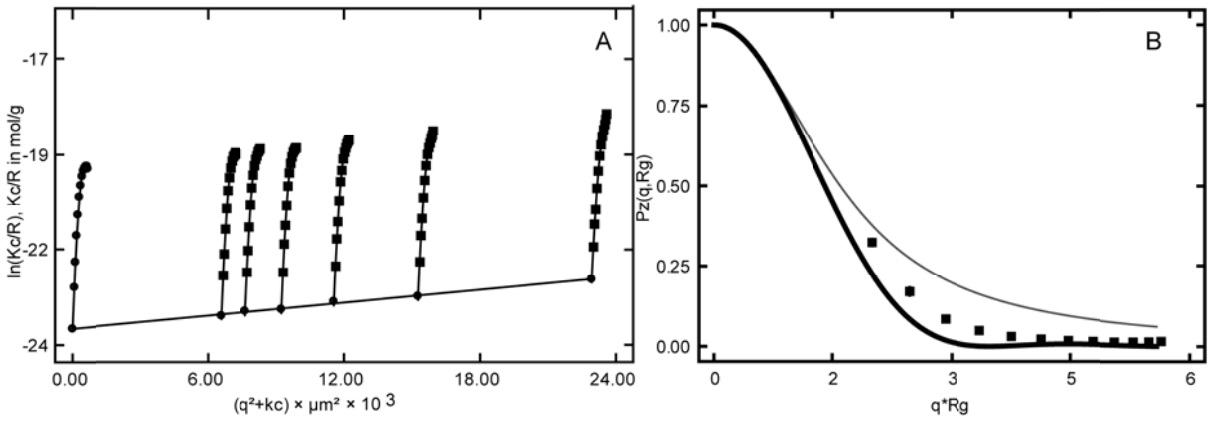

Fig. 2.7(A) Guinier plot of 4 wt % ethanol extrapolated to zero angle and concentration (B) Dependence of the particle scattering factor Pz on q for hard sphere (black line) and coil (gray line) compared with representative experimental data for 4 wt % Guinier plot(■).

Fig. 2.7B shows the angular dependence of the particle scattering factor of the peptide beads. For comparison, the well-established theoretical functions for homogenous hard spheres (Fig. 6B, black line, eq. 3) and monodispersed polymer coils (Fig. 2.7B, gray line, eq. 4) have been included in the plot. Indeed, our data resemble the function for hard spheres, thus supporting the assumption of particles with a rather homogenous density distribution. It should be noted that the data for different final ethanol concentrations hardly differed, indicating that, during the 'condensation' to more densely packed particles, their basic structure did not change significantly.

Thus, we hypothesize that the particles are formed by a hierarchical assembly process, starting with the formation of micelles that further aggregate into 'multicompartment micelles' or peptide beads that increase their packing density and aggregation number with decreasing ethanol concentration.

In complementary experiments we used fluorescence quenching to analyze the accessibility of tryptophan within the aggregates. Here, the tryptophan fluorescence of the peptide AcC-X_3-gT in 40 wt % ethanol was quenched with acrylamide. The comparison to lower ethanol concentrations was not possible due to scattering; therefore a pure tryptophan solution was used. The Stern-Volmer plots (Fig. 2.8) deviate from a straight line, exhibiting a distinct upward curvature. Therefore, the data were fitted taking the contributions from static quenching and transient effects into account.[35] The Stern-Volmer constant K_{SV} for AcC-K_3-gT (4.8 ± 0.3 M^{-1}) is in good agreement with literature values for gA in its molecularly dissolved state, indicating that

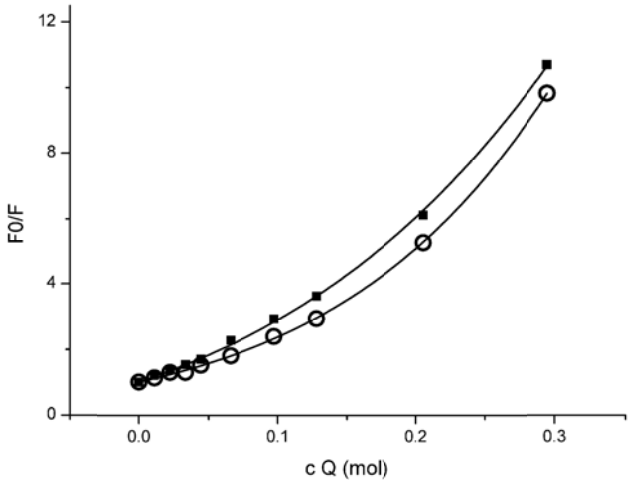

Fig. 2.8 Stern-Volmer-Plot of AcC-X_3-gT in 40 wt % ethanol (○) and tryptophan (■) with increasing quencher concentration.

the tryptophans are freely accessible for the quencher.[34b] Obviously, there is no significant difference in accessibility between molecularly dissolved Trp-OH and the peptide self-assembly at 40 wt % ethanol (Fig. 2.8). Hence, our results show that the micelles and peptide beads at 40 wt % ethanol do not possess barriers to penetration by acrylamide. This is in good agreement with the data from SLS, indicating a low packing density of the peptides inside the particles at rather high ethanol concentrations.

2.2.4. Dipeptide - $(AcC\text{-}X_3\text{-}gT)_2$

Depending on environmental conditions the thiol of the cysteine forms a disulfide-bridge and thus can be used to form dipeptides. The disulfide bond is established via the hydrophilic end, forming $(AcC\text{-}X_3\text{-}gT)_2$. The self-assembly into peptide beads is very similar, however the sizes are bigger as can be deduced from Fig. 2.9. The identical superstructures suggest that the interactions and orientations on a molecular level are not significantly altered by the disulfide bridge. Also the formation of micelles as a first step in the peptide bead formation therefore would still be in agreement for a dipeptide. The orientation of the hydrophilic ends towards the solvent brings the peptides thiol-functionality already in close approximation. However, the covalent bond decreases the degree of freedom and likely makes the dipeptide more rigid, and therefore increases the size of the micelles and consequently increases the size of the peptide beads.

2.2.5. Multicompartment micelle hypothesis

In order to further evaluate the MCM hypothesis we intended to remove single micelles from the aggregate by means of freeze-thaw cycles and ultra-sonication. Indeed, as illustrated in Fig. 2.10 it was possible to remove material mostly from the particle

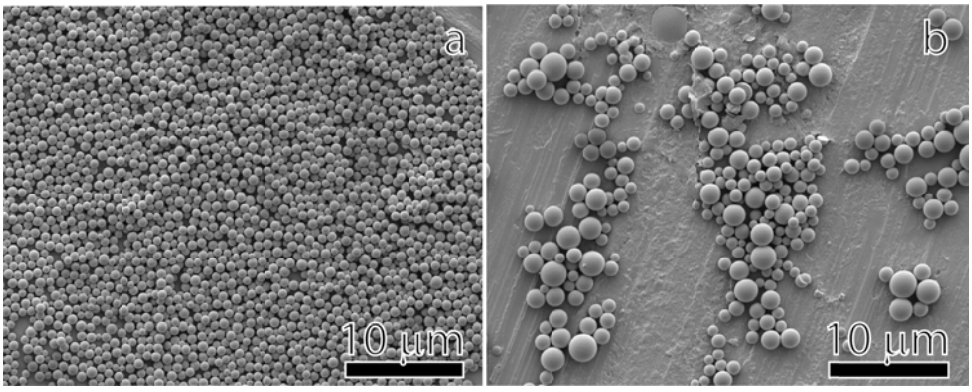

Fig. 2.9 SEM image of $(AcC\text{-}X_3\text{-}gT)_2$ peptide beads at a) 0.5 mg mL^{-1} b) 1.0 mg mL^{-1}.

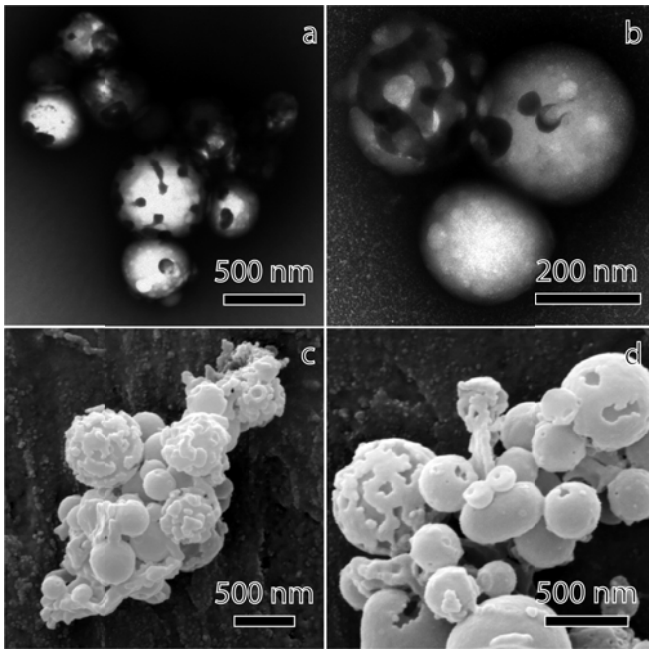

Fig. 2.10 AcC-X_3 gT peptide beads in 10 mM Ac-buffer after freeze-thaw cycles and ultra-sonication treatment imaged in a) and b) TEM and c) and d) SEM.

surface of AcC-X_3-gT peptide beads. However, the dimensions of the created holes and channels are too big to be assigned to single micelles but suggested that groups of micelles were released.

2.3. Conclusion

In this chapter we described an amphiphilic undecapeptide capable of forming micelles and peptide particles in aqueous-ethanol mixtures as a function of ethanol concentration and temperature. We introduced a repetitive [LW-DL] motif, which is the essential part of the peptide and which can be used as a general hydrophobic contributor in an amphiphilic molecule. The sequence was extended with a positively charged, hydrophilic lysine, or an uncharged, acetylated lysine group. The peptide with a charged oligolysine showed a well-defined cmc in aqueous solution and initially formed spherical micelles. An increasing fraction of larger aggregates, presumably multicompartment micelles, is formed as a result of increasing charge screening with appropriate counter ions. The acetylated lysine of the hydrophilic component of AcC-K_3-gT is less water soluble than the amphiphilic peptide, based on the non-acetylated lysine. Generally, for the acetylated peptide, decreased solubility obviously favors a secondary aggregation of the individual micelles. The self-assembly process was initiated by solvent exchange. Our experiments suggest that the hierarchical self-assembly of spherical aggregates from the

investigated mini amphiphilic peptides starts in a dissolved monomeric state in pure ethanol. With increasing water concentration a micellar solution evolves. Once a threshold of solvent polarity is exceeded (*i.e.* decreasing ethanol concentration) the micelles themselves start aggregating into highly solvent-swollen particles or multicompartment micelles. The 'open' and liquid structure of these primary multicompartment micelles is also reflected by fluorescence quenching experiments with acrylamide, indicating free access of the quencher to the tryptophan residues within the aggregates. The peptide beads further condense and presumably fuse with residual small micelles below 20 wt % ethanol. This is reflected by a drastically increasing aggregation number and a considerably higher apparent density. It should be emphasized that a decreasing ethanol concentration ultimately led to rather rigid peptide particles that preserved their shape and dimensions even after isolation from the aqueous dispersion, as by lyophilization.

Macroscopically, the system can be described as an emulsion or suspension, depending on the concentration of ethanol. The organic solvent acts as the softener that keeps the separated peptide phase in a liquid state. As it is removed, the droplets harden and form a suspension. Additional experiments are necessary, however, to fully clarify

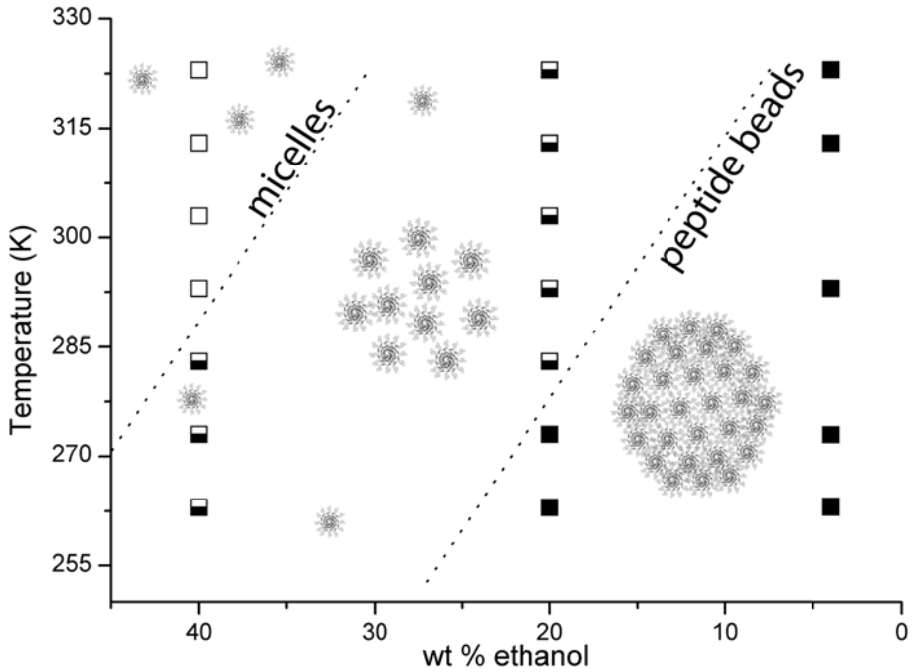

Fig. 2.11 Phase diagram of the self-assembly of amphiphilic peptides in the multicompartment micelle model deduced from EPR measurement (■) >95% peptide beads, (◘) > 95% micelles, half-full squares refer to coexistence of micelles and peptide beads.

the 'inner' structure of the peptide beads and the parameters that determine their final size. Fig. 2.11 shows a phase diagram summarizing our findings. It should be emphasized that the transitions between the different species and/or their fractions in the mixtures were fully reversible. For the construction of the phase diagram we used data points from EPR measurements that allowed a convenient quantification of the respective species in the dispersions. Data from light scattering are in good agreement with these results. Furthermore, the structure of these multicompartment micelles or peptide beads at the same time offers hydrophilic and hydrophobic compartments that could potentially be used to embed, for example, drugs. Indeed, the system presented here was shown to encapsulate water soluble and –insoluble model drugs in high concentrations[25] and is promising as a novel and bio-compatible drug delivery tool, as it is exclusively composed of amino acids.

2.4. Supporting information

2.4.1. Results

2.4.1.1. Dimerization probed by GPC

Fig. 2.12 illustrates GPC elution profiles of Ac-X_3-gT and gramicidin in THF and EtOH, whereby a clear separation of monomer and dimer was visible as two peaks for gramicidin only. The amphiphilic peptide elution profile was characterized by a slightly broader peak and no indication of distinct dimerization.

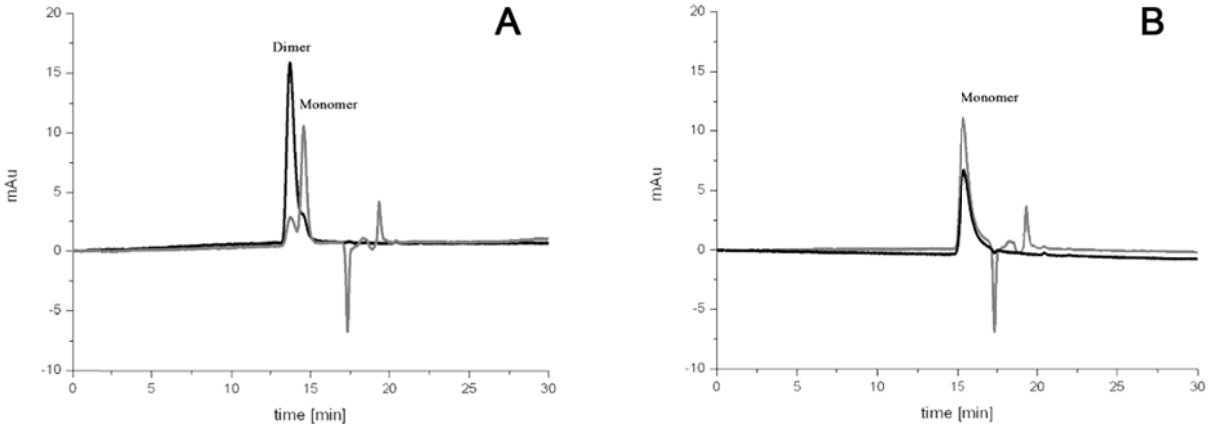

Fig. 2.12 A) GPC elution profiles of gramicidin mono and dimer, and B) Ac-X_3-gT monomers in different solvents (THF black line, EtOH gray line).

2.4.1.2. Peptide purification and characterization

Preparative HPLC profiles with the collected fractions for K_3-gT are presented in Fig. 2.13.

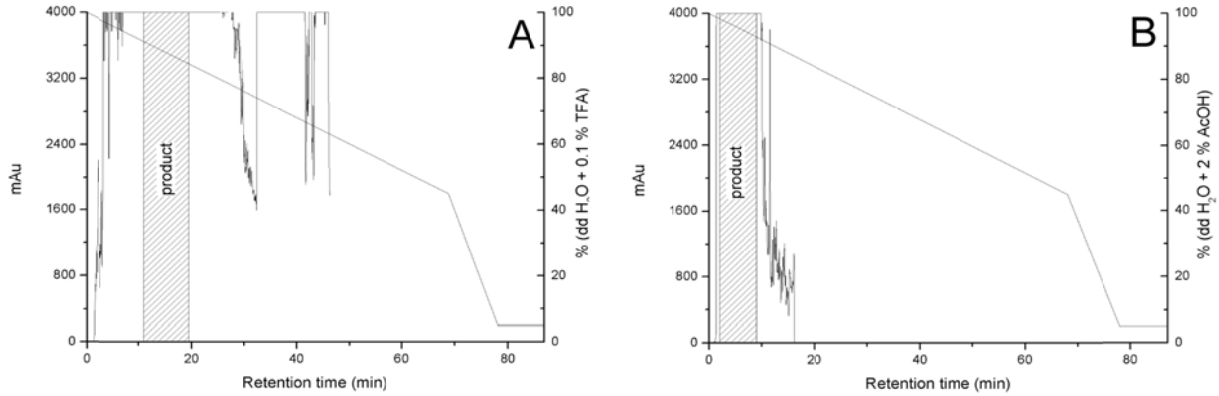

Fig. 2.13 Preparative HPLC elution profile of K_3-gT A) first run with ACN/dd H_2O 0.1 % TFA B) second run using ACN/dd H_2O 2 % AcOH.

Verification of mass and purity of the collected fractions was analysed by MALDI-TOF-MS and HPLC. Examples are illustrated in Fig. 2.14.

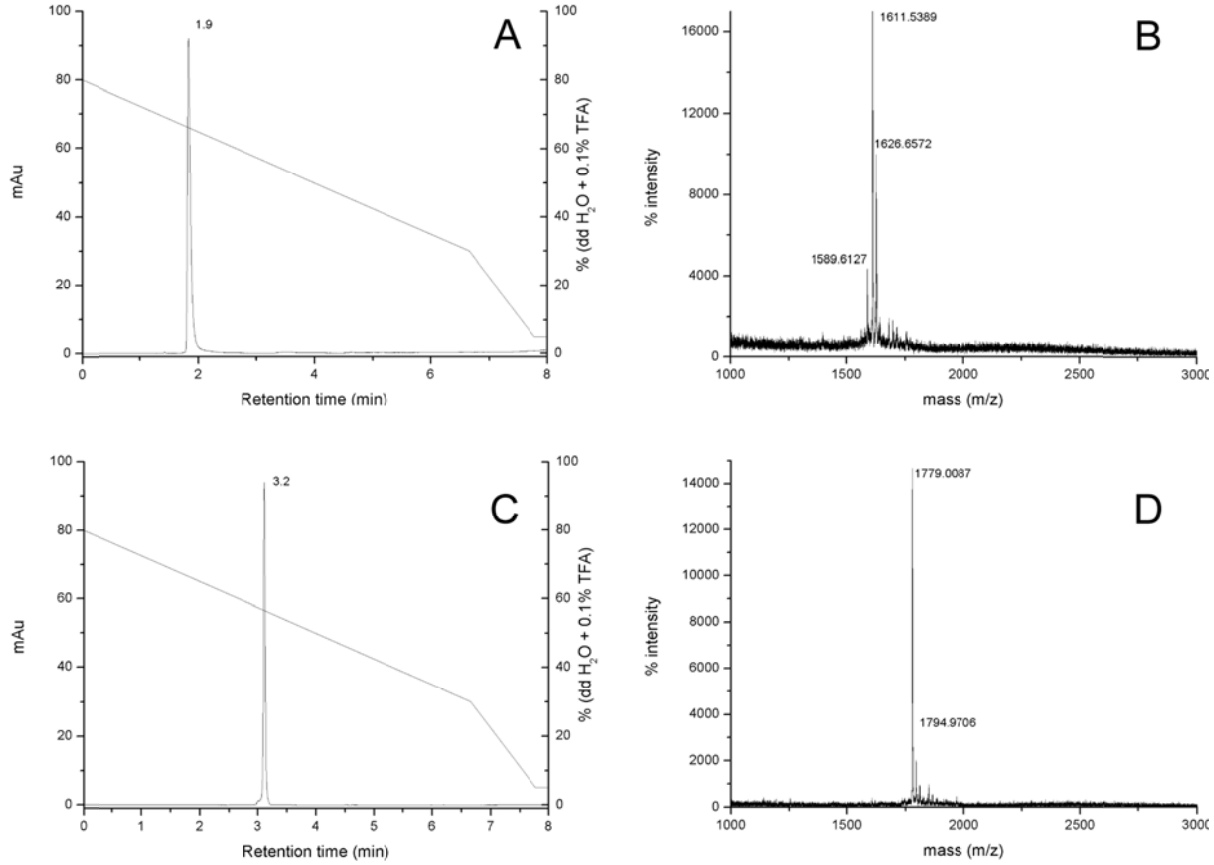

Fig. 2.14 Analysis of C-K_3-gT A) HPLC profile B) MALDI-TOF-MS and AcC-X_3-gT C) HPLC profile D) MALDI-TOF-MS.

Table 2.3 presents a summary of the measured mass and purity of the purified compounds.

Table 2.3 Verification of mass and purity of the amphiphilic peptides used.

code	mass g mol^{-1}	mass m z^{-1}	purity
K_3-gT	1485,9	1486.7	> 99 %
C-K_3-gT	1589,9	1588.6	97 %
Ac-X_3-gT	1653,9	1677.3 ($M+Na^+$)	98 %
AcC-X_3-gT	1757,9	1779.0 ($M+Na^+$)	96 %
AcC(sl)-X_3-gT	1947,0	1948.5	97 %

2.4.1.3. Behavior of C-K_3-gT

Amphiphilic peptides behave like surfactants. It was therefore possible to determine a critical micelle concentration (cmc), as illustrated in Fig. 2.15).

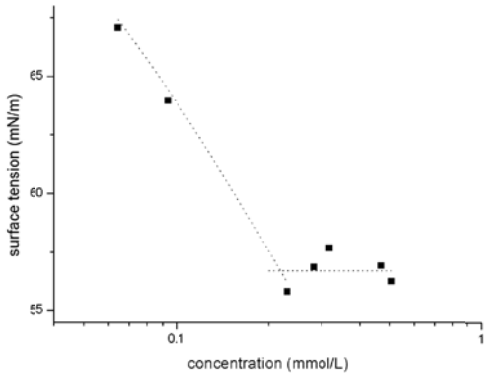

Fig. 2.15 Cmc of C-K_3-gT.

Self-assembly of C-K_3-gT into micelles is suggested by Fig. 2.16.

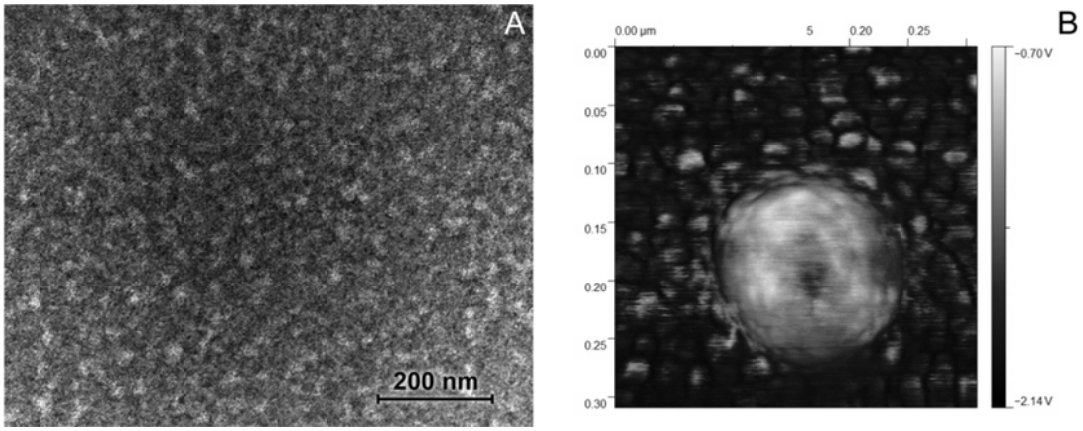

Fig. 2.16 Representative TEM image of C-K_3-gT micelles and AFM phase image of micelles, together with one peptide bead.

Peptide bead formation due to charge shielding is illustrated in Fig. 2.17.

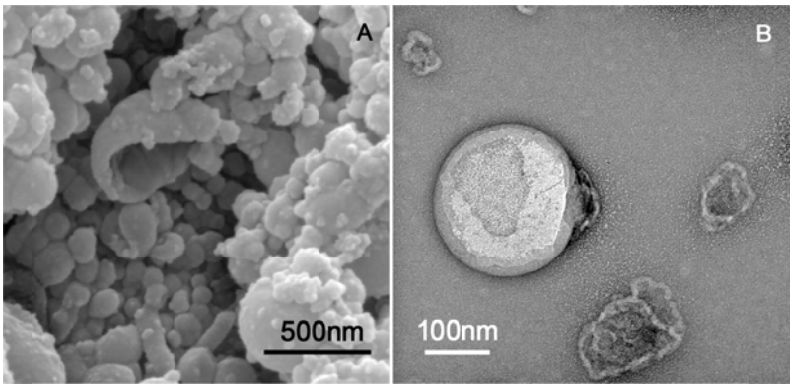

Fig. 2.17 A) SEM of C-K_3-gT with NaH_2PO_4 (0.025 mol L^{-1}) B) TEM of AcC-K_3-gT with NaSCN (0.1 mol L^{-1}L).

2.4.1.4. Self-assembly of Ac-X_3-gT

Self-assembled spherical structures - so-called 'peptide beads' - from Ac-X_3-gT were imaged using SEM, TEM, and AFM (Fig. 2.18).

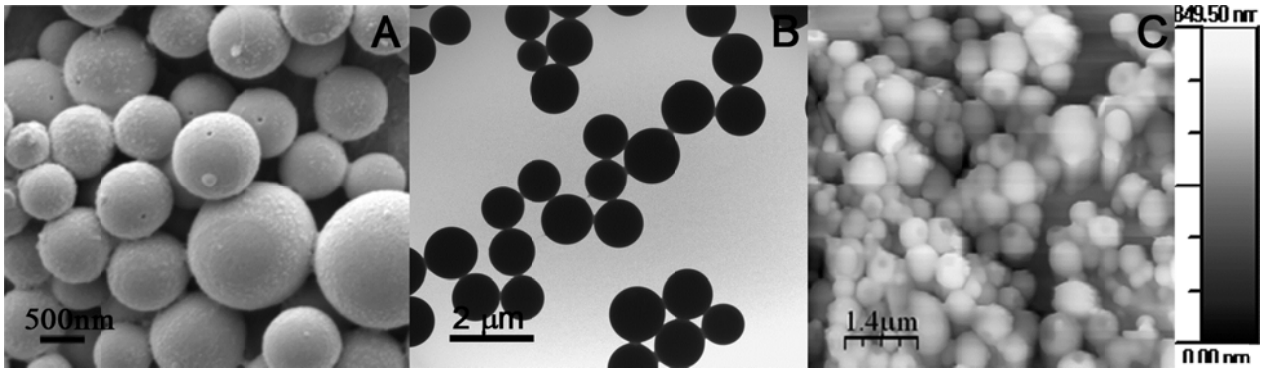

Fig. 2.18 A) SEM of Ac-X_3-gT peptide beads, B) TEM and C) AFM.

Cw EPR measurements in different ethanol/water mixtures

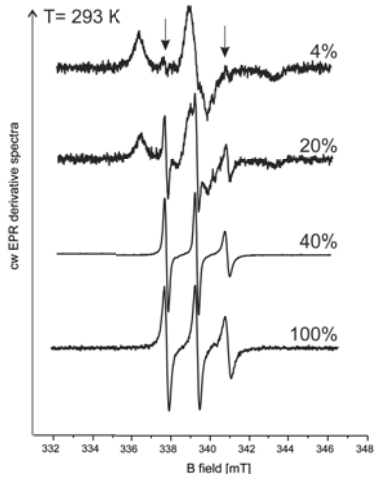

Fig. 2.19 cw EPR spectra of AcC-X_3-gT / AcC(sl)-X_3-gT mixtures depending on ethanol concentration. Arrows mark the characteristic features of the mobile species, which become dominant with increasing ethanol concentration.

Correlation functions

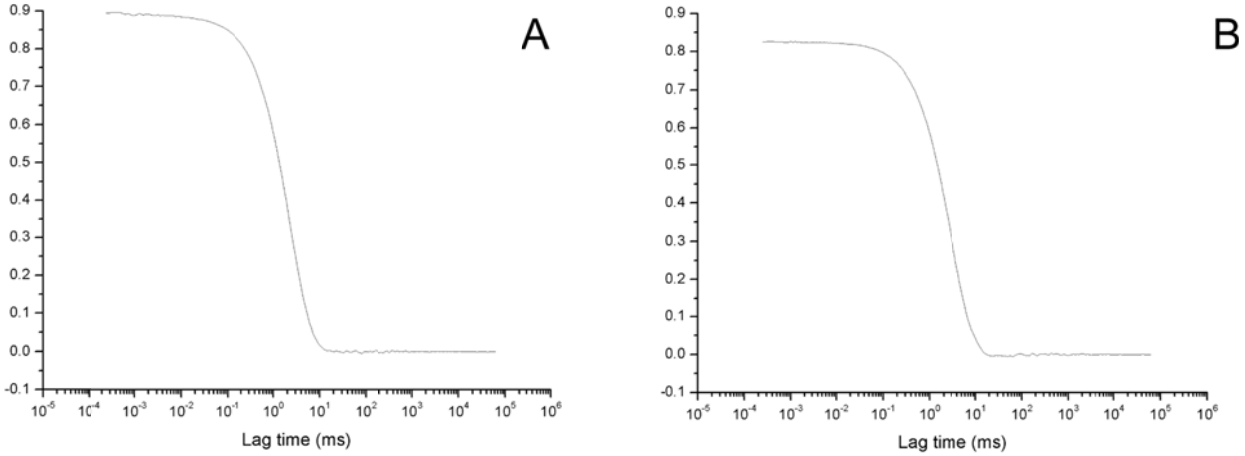

Fig. 2.20 Correlation functions of AcC-X_3-gT/AcC(sl)-X_3-gT mixture in A) 40 wt % ethanol and B) 4 wt % ethanol.

Equilibrium between Ac-X_3-gT micelles and peptide beads arises in ethanol/water mixtures. Converting peptide solutions at 4 wt % ethanol to 40 wt % ethanol and vice versa (using dialysis) always produces the same characteristic DLS signals, proving the reversibility of the system. A diagram of the experiment and the corresponding results are presented in Fig. 2.21.

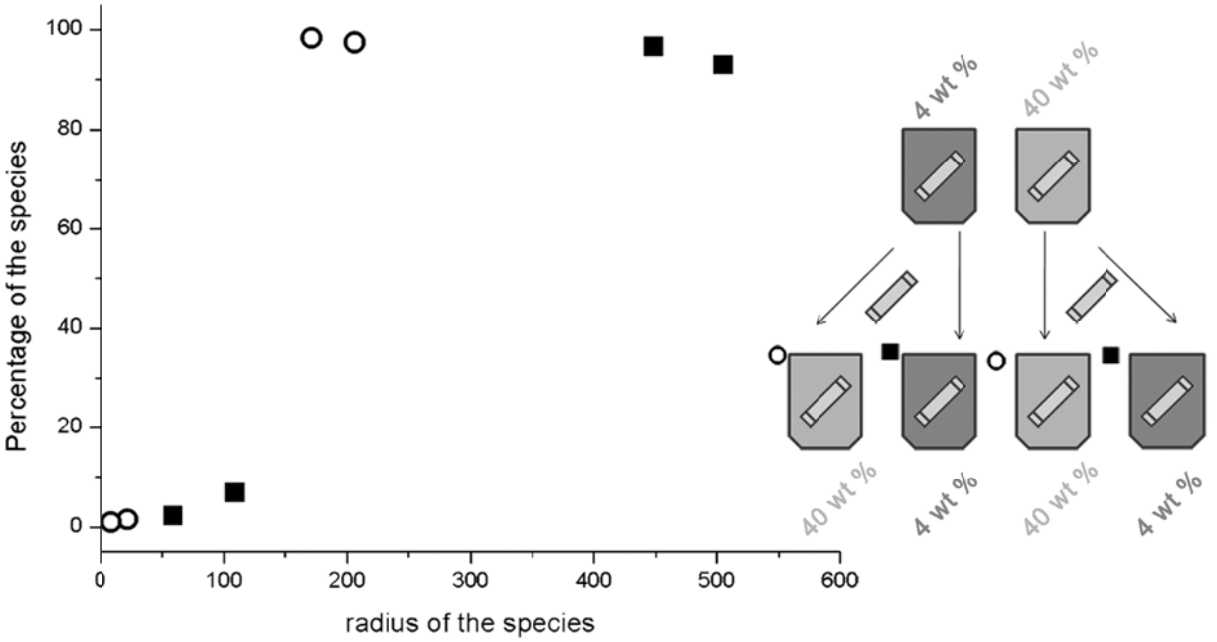

Fig. 2.21 Reversibility of the system: Two different starting points (4 wt % and 40 wt %) yield the same DLS features at 4 wt % (■) and at 40 wt % (○) final ethanol content.

The self-assembly of Ac-X_3-gT is strongly temperature-dependent. The self-assembly process was initiated by solvent displacement from 100 wt % to 20 wt % ethanol. Reversible, temperature-dependent peptide bead formation was monitored at that ethanol concentration. Temperature-dependent UV absorption measurements tracked bead formation as absorption increased due to scattering. As Fig. 2.22 shows, peptide beads begin to assemble below 25 °C at 20 wt % ethanol. This process was reversible. The cooling (black line) - heating (gray line) cycle exhibits a slight hysteresis due to the experimental setup.

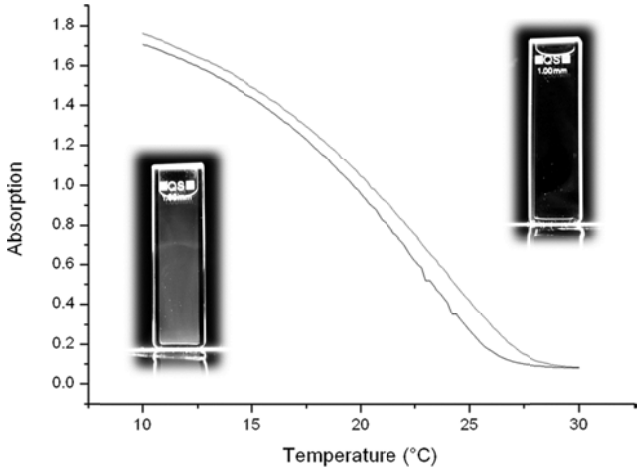

Fig. 2.22 UV measurement of temperature-dependent bead formation (heating (gray line), cooling (black line)) using Ac-X_3-gT at 20 wt % EtOH. Photographs were taken at 4 °C (left) and RT (22 °C, right).

Size-dependence of peptide beads in dd H_2O upon initial peptide concentration is shown in Fig. 2.23.

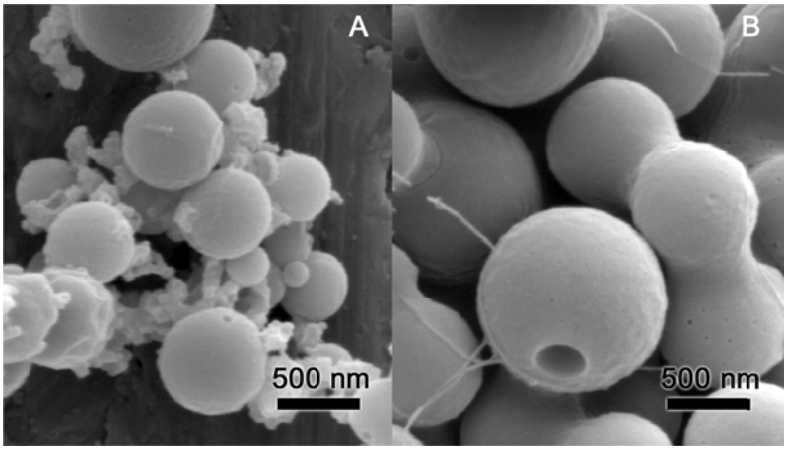

Fig. 2.23 SEM micrographs of Ac-X_3-gT at A) 1.0 mol L^{-1} B) 1.5 mol L^{-1}.

2.5. References

[1] C. Allen, D. Maysinger and A. Eisenberg, *Colloid Surface B* **1999**, *16*, 3-27.

[2] G. Pace, M. Venanzi, P. Castrucci, M. Scarselli, M. De Crescenzi, A. Palleschi, L. Stella, F. Formaggio, C. Toniolo and G. Marletta, *Mater. Sci. Eng., C* **2006**, *26*, 918-923.

[3] a) F. Axthelm, O. Casse, W. H. Koppenol, T. Nauser, W. Meier and C. G. Palivan, *J. Phys. Chem. B* **2008**, *112*, 8211-8217; b) N. M. D. Brown and H. X. You, *J. Struct. Biol.* **1991**, *107*, 250-258.

[4] Y. H. George Barany, Balazs Hargitta, Rong-Qiang Liu, Jaya T. Varkey, *Biopolymers* **2003**.

[5] R. Nehring, C. G. Palivan, O. Casse, P. Tanner, J. Tuxen and W. Meier, *Langmuir* **2009**, *25*, 1122-1130.

[6] a) C. E. Dempsey and P. E. Mason, *J. Am. Chem. Soc.* **2006**, *128*, 2762-2763; b) L. Braco, M. C. Bano and C. Abad, *J. Chem. Educ.* **1992**, *69*, A113-A116.

[7] F. Ahmed, R. I. Pakunlu, A. Brannan, F. Bates, T. Minko and D. E. Discher, *J. Controlled Release* **2006**, *116*, 150-158.

[8] a) J. Sun, Q. Shi, X. Chen, J. Guo and X. Jing, *Macromol. Chem. Phys.* **2008**, *209*, 1129-1136; b) S. B. Lei, R. Tero, N. Misawa, S. Yamamura, L. J. Wan and T. Urisu, *Chem. Phys. Lett.* **2006**, *429*, 244-249; c) V. P. Ivanova, I. M. Makarov, T. E. Schaffer and T. Heimburg, *Biophys. J.* **2003**, *84*, 2427-2439.

[9] J.-F. Lutz and A. Laschewsky, *Macromol. Chem. Phys.* **2005**, *206*, 813-817.

[10] A. Carlsen and S. Lecommandoux, *Curr. Opin. Colloid Interface Sci.* **2009**, *14*, 329-339.

[11] W. R. Veatch and E. R. Blout, *Biochemistry* **1974**, *13*, 5257-5264.

[12] E. P. Holowka, V. Z. Sun, D. T. Kamei and T. J. Deming, *Nat. Mater.* **2007**, *6*, 52-57.

[13] V. Malinova, S. Belegrinou, D. de Bruyn Ouboter and W. P. Meier, *Adv. Polym. Sci.* **2010**, *224*, 113-165.

[14] R. Fairman and K. S. Akerfeldt, *Curr. Opin. Struct. Biol.* **2005**, *15*, 453-463.

[15] J. Rao, Z. Luo, Z. Ge, H. Liu and S. Liu, *Biomacromolecules* **2007**, *8*, 3871-3878.

[16] J. Lin, J. Zhu, T. Chen, S. Lin, C. Cai, L. Zhang, Y. Zhuang and X.-S. Wang, *Biomaterials* **2009**, *30*, 108-117.

[17] a) M. Balakirev, G. Schoehn and J. Chroboczek, *Chem. Biol.* **2000**, *7*, 813-819; b) A. Koide, A. Kishimura, K. Osada, W.-D. Jang, Y. Yamasaki and K. Kataoka, *J. Am. Chem. Soc.* **2006**, *128*, 5988-5989.

[18] a) E. G. Bellomo, M. D. Wyrsta, L. Pakstis, D. J. Pochan and T. J. Deming, *Nat. Mater.* **2004**, *3*, 244-248; b) E. P. Holowka, D. J. Pochan and T. J. Deming, *Journal of the American Chemical Society* **2005**, *127*, 12423-12428.

[19] J. Rodriguez-Hernandez and S. Lecommandoux, *J. Am. Chem. Soc.* **2005**, *127*, 2026-2027.

[20] a) M. R. Dreher, A. J. Simnick, K. Fischer, R. J. Smith, A. Patel, M. Schmidt and A. Chilkoti, *J. Am. Chem. Soc.* **2008**, *130*, 687-694; b) A. J. van Hell, C. I. C. A. Costa, F. M. Flesch, M. Sutter, W. Jiskoot, D. J. A. Crommelin, W. E. Hennink and E. Mastrobattista, *Biomacromolecules* **2007**, *8*, 2753-2761.

[21] a) M. Heim, L. Roemer and T. Scheibel, *Chem. Soc. Rev.* **2010**, *39*, 156-164; b) U. K. Slotta, S. Rammensee, S. Gorb and T. Scheibel, *Angew. Chem., Int. Ed.* **2008**, *47*, 4592-4594.

[22] S. Santoso, W. Hwang, H. Hartman and S. G. Zhang, *Nano Lett.* **2002**, *2*, 687-691.

[23] C. Masens, J. Schulte, M. Phillips and S. Dligatch, *Microsc. Microanal.* **2000**, *6*, 113-120.

[24] a) M. Reches and E. Gazit, *Science (Washington, DC, U. S.)* **2003**, *300*, 625-627; b) W. R. Veatch, E. T. Fossel and E. R. Blout, *Biochemistry* **1974**, *13*, 5249-5256.

[25] C. Dittrich and W. Meier, *Macromol. Biosci.* **2010**, *10*, 1406-1415.

[26] L. Braco, M. C. Bano and C. Abad, *Journal of Chemical Education* **1992**, *69*, A113-A116.
[27] B. A. Wallace, *J. Struct. Biol.* **1998**, *121*, 123-141.
[28] B. G. Dzikovski, P. P. Borbat and J. H. Freed, *Biophys. J.* **2004**, *87*, 3504-3517.
[29] S. M. Schiller, R. Naumann, K. Lovejoy, H. Kunz and W. Knoll, *Angew. Chem., Int. Ed.* **2003**, *42*, 208-211.
[30] W. Kunz, P. Lo Nostro and B. W. Ninham, *Curr. Opin. Colloid Interface Sci.* **2004**, *9*, 1-18.
[31] A. Aroti, E. Leontidis, M. Dubois, T. Zemb and G. Brezesinski, *Colloids Surf., A* **2007**, *303*, 144-158.
[32] K. Kitagawa, T. Morita and S. Kimura, *Kyoto Daigaku Nippon Kagaku Sen'i Kenkyusho Koenshu* **2006**, *63*, 29-34.
[33] O. Stauch, R. Schubert, G. Savin and W. Burchard, *Biomacromolecules* **2002**, *3*, 565-578.
[34] a) W. S. Davidson and G. M. Hilliard, *J. Biol. Chem.* **2003**, *278*, 27199-27207; b) S. S. Rawat, D. A. Kelkar and A. Chattopadhyay, *Biophys. J.* **2004**, *87*, 831-843.
[35] M. Hegner, P. Wagner and G. Semenza, *Surf. Sci.* **1993**, *291*, 39-46.

3. Highly ordered gold nanoparticles - peptide composites

Dirk de Bruyn Ouboter, Thomas B. Schuster, Wolfgang Meier

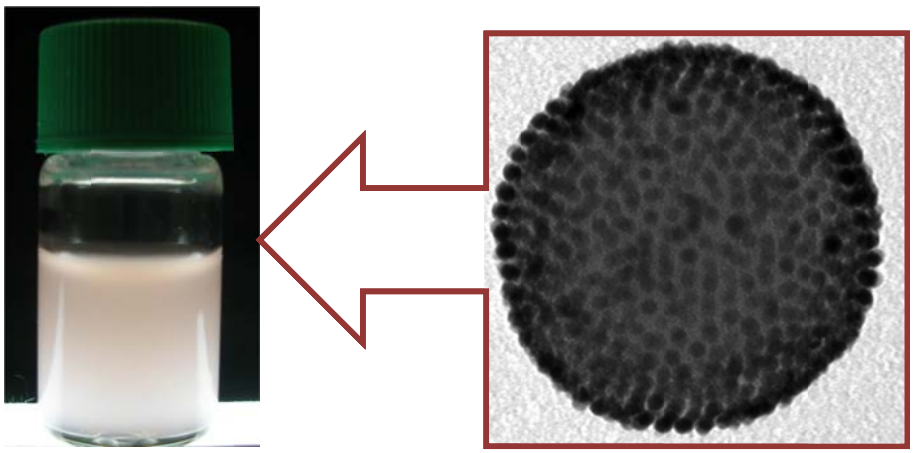

Suspension of self-assembled peptide gold nanoparticle (Au-NP) composites exhibiting a highly order within the peptide nanoparticles.

Parts are considered for publication: *manuscript in preparation, 2011*

3.1. Introduction

Composite materials are of great academic and industrial interest because they usually combine the advantages of different materials and try to reduce their drawbacks. In particular, increasing attention is being drawn to the development of polymersomes loaded with magnetic nanoparticles, MRI contrast agents, gold nanoparticles, and quantum dots that may provide noninvasive images of organs and living tissues.[1] Gold nanoparticles, as a polymer composite material, are further intended to find use as drug delivery systems such as the development of poly(ethylene oxide) -*b*- poly(ε-caprolactone) coated gold nanoparticle.[2] In order to release the co-localized content, near-infrared light absorbing gold nanoparticles were incorporated into a capsule in which they caused heating and degradation of the inner shell of the capsule, as a result of irradiation using near-infrared laser light.[3] Therefore, combining biocompatible materials such as peptides, which consist of natural amino acids and thus display a favorable material, with gold nanoparticles, may lead to advanced materials as mentioned above, yielding even better performance.

The self-assembly process using amphiphilic peptides AcC-X_3-gT was investigated in the previous chapter. The resulting structures are hypothesized to be either multicompartment micelles (MCM) or large compound micelles (LCM). The latter imply the formation of peptide beads by aggregation of inverted peptide micelles, enclosed in an outer shell of amphiphile. Multicompartment micelles, on the other hand, refer to a supramolecular aggregate with a hydrophilic shell and segregated hydrophobic regions within. In order to gain additional information on the hierarchical self-assembly, we designed an analogue to AcC-X_3-gT – namely Ac-X_3-gT-C – which exhibits the thiol-functionality on the hydrophobic side and permits the attachment of labels. The first objective was to evaluate the impact of the C-terminal cysteine on the peptide's properties and the self-assembled structures. Furthermore, with the label - a covalently attaching gold nanoparticle (Au-NP) - we intended to visualize and follow the events within the micelles and the formation of hierarchical self-assembly of micelles into peptide beads.

3.2. Results and discussion

Self-assembly of charged K_3-gT-C

Table 3.1 presents the synthesized amphiphilic peptide sequence. TEM and SEM images (Fig. 3.1) of K_3-gT-C self-assembled structures demonstrated that the peptide's properties were affected by placing the terminal cysteine not on the hydrophilic but on the hydrophobic end. As demonstrated in the previous chapter, C-K_3-gT forms micelles while the structures of K_3-gT-C that were able to be imaged appeared net-like. However, due to the meta-stability of the self-assembled structure, preparation artifacts cannot be excluded. Therefore it is also possible that micelles were present in solution, and these then fused into elongated micelles and finally net-like structures within the preparation step of TEM samples. In Fig. 3.1b two spherical structures, *i.e.* species with a radius of ~ 300 nm and a smaller one at ~ 20 nm, can be seen and might be assigned to peptide beads and micelles, respectively. Also DLS confirmed the existence of a second species in the large nm range; its detected R_h was ~ 190 nm.

Self-assembly of uncharged Ac-X_3-gT-C

Ac-X_3-gT-C similarly self-assembled into peptide beads as AcC-X_3-gT (Fig. 3.2a). The surface did not appear perfectly smooth but instead showed substructural features. The latter originated from aggregated Ac-X_3-gT-C micelles that self-assembled into peptide beads, as revealed by SEM images (Fig. 3.2b). The C-terminal cysteine slightly disturbed the perfect packing of the micelles into peptide beads, which allowed us to visualize the inner structure, *i.e.* aggregated micelles, which were already postulated by the results from EPR and DLS in chapter 2. However, size distribution is relatively large for Ac-X_3-gT-C peptide beads (*cf.* Fig. 3.2a), the hydrodynamic radius was determined to be 256 nm by DLS and is consistent with SEM.

Table 3.1 Code and sequence of charged (K) and uncharged (X = LK(*Ac*)) amphiphilic peptides.

Code	Sequence
K_3-gT-C	[LK]$_3$-[LW-DL]$_3$-LW-LC-NH_2
Ac-X_3-gT-C	*Ac*-[LK*(Ac)*]$_3$-[LW-DL]$_3$-LW-LC-NH_2

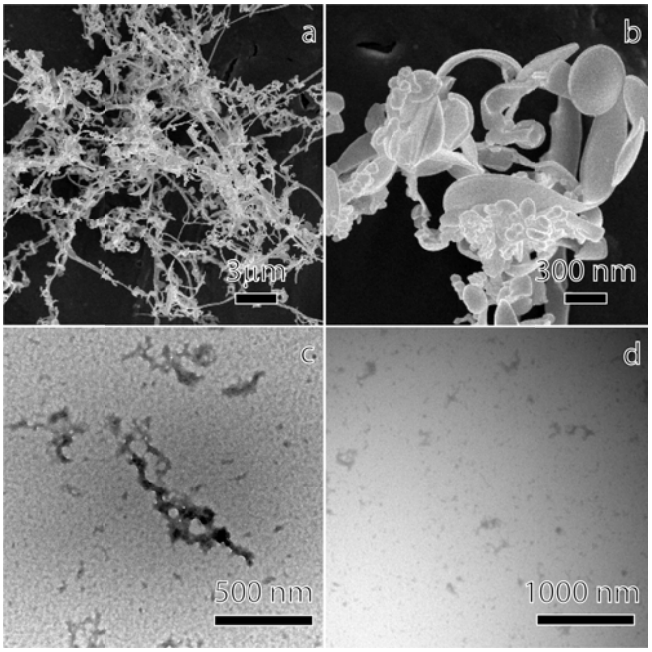

Fig. 3.1 Self-assembled net-like structures of K_3-gT-C a) and b) in SEM and c) and d) TEM.

Gold nanoparticle (Au-NP) Ac-X_3-gT-C composites

To provide further evidence on the hypothesized aggregated micelles, *i.e.* MCM structure and equally to investigate composite formation, Au-NP were intended to be embedded within the micellar cores via the thiol-functionality of Ac-X_3-gT-C on the hydrophobic end. As seen in Fig. 3.3, the solution obeys a typical reddish color due to the Au-NP, but only simultaneous sedimentation indicates successful bonding and self-assembly. The TEM images show that the gold nanoparticles peptide composites possess

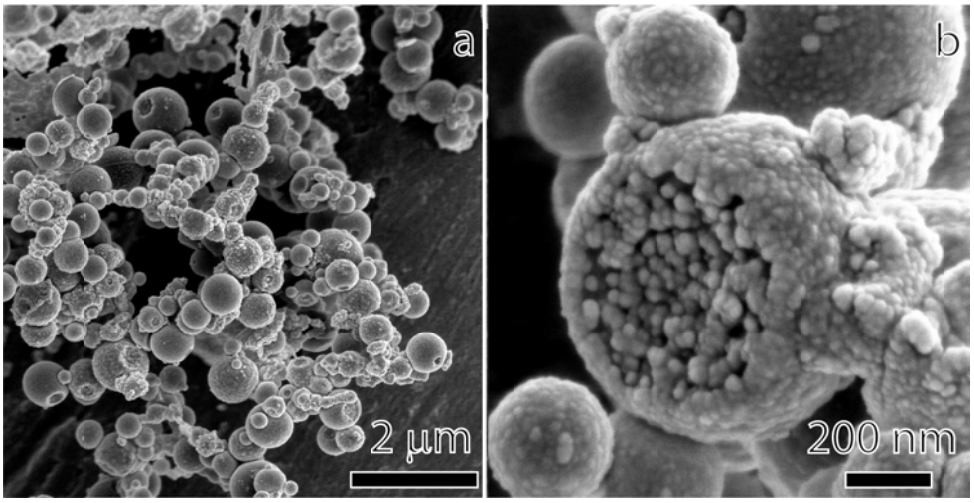

Fig. 3.2 a) Self-assembled peptide beads of Ac-X_3-gT-C, b) view of the inside of one peptide bead, built-up of smaller spherical subunits.

Fig. 3.3 Gold nanoparticle (Au-NP) Ac-X_3-gT-C composites.

homogenously distributed gold nanoparticles in very close arrangement. However, different radii were present within the sample and their analysis suggest that particle growth may occur by fusion of smaller aggregates, as shown in Fig. 3.4. DLS detects two different species, one with an R_h of 50 nm of small micelle aggregates and a second one with an R_h of 350 nm assigned to peptide beads.

SEM confirmed the hydrodynamic radius for the second species and further provided insight into the process of building the peptide beads (Fig. 3.5). It seems that

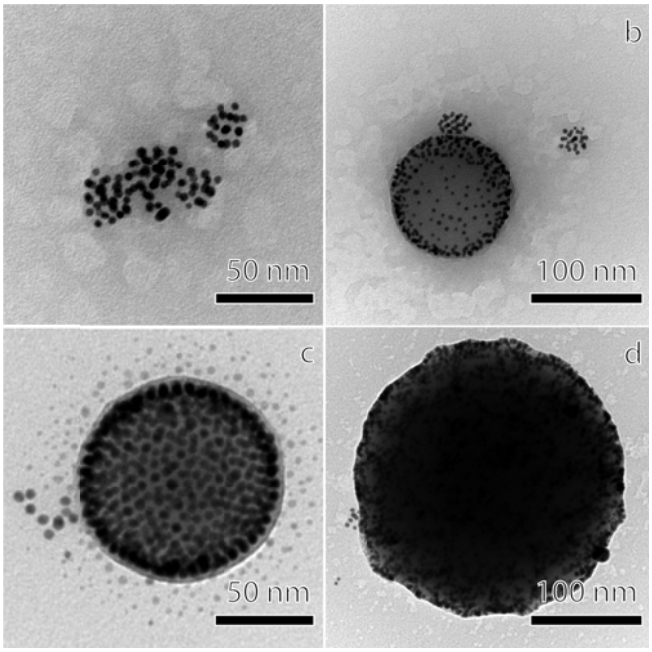

Fig. 3.4 TEM micrographs of self-assembled peptide beads of Au-NP Ac-X_3-gT-C. Within one sample several objects were observed, as from a) a few aggregated micelles to, b) bigger aggregates, c) ordered distribution of Au-NP within the beads, and d) bigger composite bead.

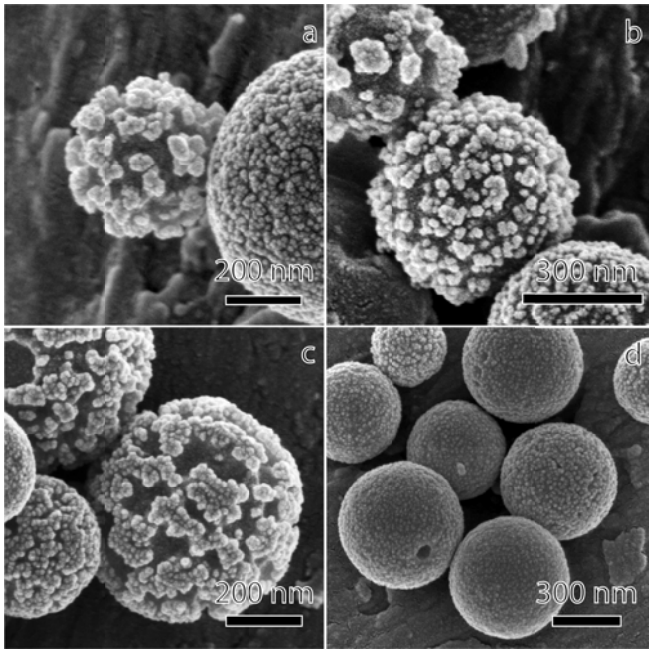

Fig. 3.5 Different surfaces of Au-NP peptide composites were observed, from a) small beads with islands, to b) larger islands and small gaps c) almost complete outer shell, and d) a homogeneous and smooth surface.

the formation starts at small micellar aggregates, while new, small aggregates dock onto the existing particle, and thus form little islands. These islands grow further while increasing the overall radius and decreasing the gaps between them by finally closely packing and presenting a smooth and closed surface.

3.3. Conclusion

C-terminal introduction of a cysteine within the amphiphilic peptide 'Ac-X_3-gT' did not disturb the self-assembly in general, but rather led to non-homogeneous peptide bead surfaces. On the other hand, the modification allowed us to gain insights into the peptide beads and to validate the multicompartment micelle hypothesis, and into their formation process, *i.e.* growing islands and filling gaps until all material was consumed.

We furthermore succeeded in creating gold nanoparticle Ac-X_3-gT-C composites by covalently linking Au-NP to the C-terminal thiol functionality of the peptide in the micellar core. This method allowed us to visualize the peptide bead inner structure and suggests that the driving force for the assembly from micelle to peptide beads is the solubility of the acetylated lysine residues.

Gold nanoparticles have garnered more and more interest in recent years due to their exceptional electronic and optical properties.[4] Various concepts for applications

have been developed.[5] The distance of only a few nanometers between the individual gold nanoparticles lets us assume that these effects are also present in our system.

3.4. References

[1] F. Meng, Z. Zhong and J. Feijen, *Biomacromolecules* **2009**, *10*, 197-209.
[2] T. Azzam and A. Eisenberg, *Langmuir* **2007**, *23*, 2126-2132.
[3] O. Kreft, A. G. Skirtach, G. B. Sukhorukov and H. Moehwald, *Adv. Mater. (Weinheim, Ger.)* **2007**, *19*, 3142-3145.
[4] M.-C. Daniel and D. Astruc, *Chem. Rev. (Washington, DC, U. S.)* **2004**, *104*, 293-346.
[5] D. A. Giljohann, D. S. Seferos, W. L. Daniel, M. D. Massich, P. C. Patel and C. A. Mirkin, *Angew. Chem., Int. Ed.* **2010**, *49*, 3280-3294.

4. Molecular thin films produced by short amphiphilic peptides

Thomas B. Schuster, Dirk de Bruyn Ouboter, Wolfgang Meier

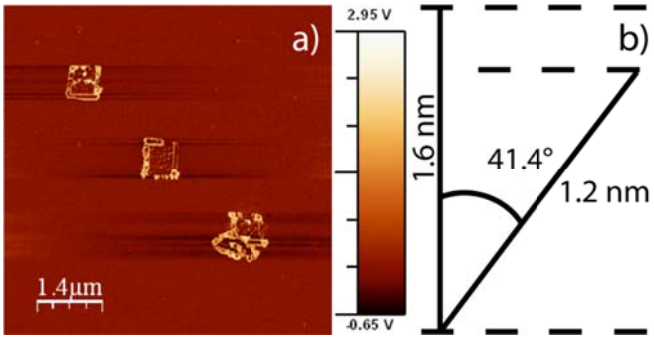

AFM images of molecular thin peptide film on an Si-wafer scratched with the tip revealed a film thickness of 1.2 nm.

Parts are considered for publication: *manuscript in preparation, 2011*

4.1. Introduction

Interface regions, for example molecular thin films, are of special interest to the design of novel functional materials including nature-made, highly elaborated structures that range from magnetite in chiton teeth, to calcite in sea urchin spicules to skeletons of corals and crustaceans.[1] Such structures, which are produced by the process of mineralization, comprise primarily calcium carbonate[2] or phosphate.[3] An understanding of the underlying process will facilitate recreating these structures in the laboratory and is of great relevance to medical applications, for example in the design and creation of interfaces in human-implants.[4] The mineralization process in living organisms produces minerals to harden or stiffen existing tissues and typically develops at an interface region on a template, which itself is usually of a peptidic or proteinaceous nature. To create and mimic nature-made structures, a suitable template must first emerge at an interface in order to foster correct mineralization. The mineralization itself is then regulated at the initiating template by various chemical parameters that include, among others, ionic strength and pH of the subphase.

New templates and interfaces that exhibit different surface dynamics and properties compared to conventional lipid and polymer membranes, such as diffusion and flexibility, are necessary in order to develop new biomaterials. Such new structures can be derived by forming stable interfacial peptides structures,[5] an as yet rare source of potential templates for mineralization in the literature.[6] In this regard, it is interesting to note that such templates are commonly used by nature to guide the growth of structures such as teeth and bones.

As mentioned, interfaces offer areas of control of the crystallization of minerals[7] but equally define protein crystallization. Protein crystals are required to determine the molecular structure for any given protein by means of crystallography. The first step in protein crystallization that occurs at an interface is nucleation, or seeding, which is difficult to control in practice.[8] Therefore, the strategy to create 2D crystals at an interface uses templates, for example block copolymers, which offer specific chemical interaction sites for the protein such as Ni^{2+}/NTA,[9] or carboxy-terminated SAMs,[10] to allow their adsorption onto the surface and higher local concentrations in order to facilitate the nucleation step on a template. This template, as mentioned, is usually made of acidic and basic block copolymers[3] but can alternately also be produced by other

amphiphiles.

In chapter two the self-assembly of thiolated short amphiphilic peptides in solution was investigated, while this chapter focuses on the creation of stable peptide layers at the water-air interface and on a solid support. The amphiphilic peptide combines a truncated hydrophobic part (gT) – adapted from the gramicidin family[11] and a hydrophilic basic tri-lysine (K_3) or acetylated tri-lysine (X_3) and self-assembled into micelles and solid peptide nanoparticles in aqueous solution.[12]

In the present study we investigate the behavior at the air-water interface of our amphiphilic peptides, their film forming properties under different conditions (pH, buffer, etc.) as well as the influence of an N-terminal cysteine and the effect of acetylated amine functionalities on film stability. Interfacial studies including peptides have usually been focused on their interaction within either lipids or polymer monolayers but far less peptides have been investigated on their potential to form a stable thin molecular layer on their own. We are interested in such films but, since gramicidin – a major component in our amphiphilic peptides - is known to form aggregates[13] and interacts with lipids[14] it is necessary to first investigate lipid, *i.e.* dipalmitoylphosphatidylcholine (dppc) - peptide mixtures before characterizing pure peptide films. Furthermore we were interested in a facile method to produce pure peptide films directly on solid substrate. Therefore, we used a Langmuir trough and a Brewster angle microscope (BAM) setup to measure and image the surface pressure – area (π-A) isotherms and followed the formation of thin films. The latter could then be transferred via the Langmuir-Blodgett (LB) technique onto solid support to be analyzed by atomic force microscopy (AFM).

4.2. Results and discussion

4.2.1. Dppc peptide mixtures and pure peptide films at the air-water interface

Three different amphiphilic peptides had been synthesized (Table 2.1). Fig. 4.1a illustrates π-A isotherms of C-K_3-gT and dppc mixtures on the Langmuir trough with increasing peptide content. The characteristic transition of dppc from the liquid-extended (LE) phase to the liquid-condensed (LC) phase at 7 mN m^{-1} quickly disappeared

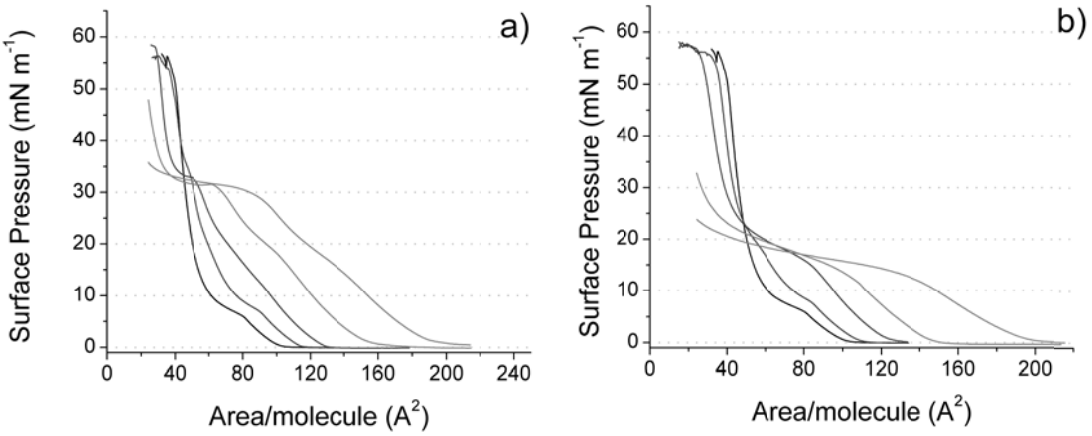

Fig. 4.1 π-A isotherms of a) C-K_3-gT/dppc mixtures and of b) K_3-gT/dppc mixtures on carbonate buffer, pH 10 with increasing peptide contents of 0, 10, 25, 50 and 95% peptide with increasing - from left to right - area/molecule values, respectively.

with increasing peptide content while the peptide π-A isotherm features appeared. For example, a transition within the LC phase is visible in the isotherms around 30 mN m^{-1} (60-100 $Å^2$ $molecule^{-1}$).

The subphase, the aqueous phase underlying the film is an important factor, in addition to others, for film stability; therefore several subphases have been tested. Carbonate buffer as a modest basic buffer subphase (pH 10) performed best and produced the most stable films with a decrease to 80% of the initial π-value within 1.5 h (*cf.* Fig. 4.2a) compared to neutral (dd H_2O or HEPES/KCl) or even high basic conditions (phosphate buffer, pH 12). Protonation of the amine group of the tri-lysine and thus the removal of charges caused a reduced hydrophilicity, which causes the increased film stability.

Noteworthy is the positive free energy of mixing values (ΔG) over the whole range of the measured molar fraction x (Fig. 4.2b), which suggests phase separation *i.e.* peptide raft formation. Actually, it is known that wild-type gA forms rafts in lipid bilayers[13a, 15] and also C-K_3-gT exhibits lateral interaction leading to formation of micelles.[12] Further evidence of phase separation and of the formation of highly irreversible 2D peptide aggregates was given by hysteresis for the first and second compression curves of C-K_3-gT films at the air-water interface (*cf.* Fig. 4.2c). These aggregates, which are likely stabilized by tryptophan-tryptophan (π–π stacking) interactions[15] have been induced as a result of film compression while differences in compression speed also led to different hysteresis profiles.

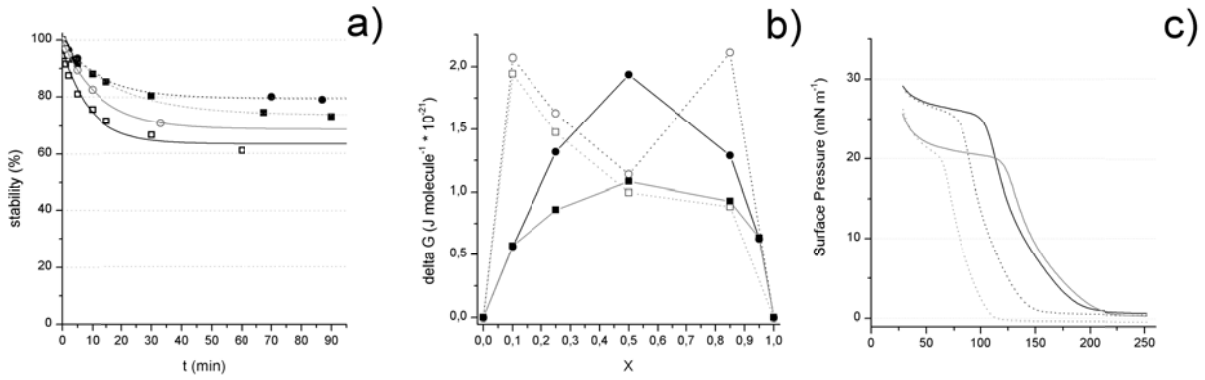

Fig. 4.2 a) film stability monitored by the decrease in the initial π-value of C-K_3-gT on different subphases (●) carbonate buffer (pH 10),(■) phosphate buffer (pH 12), (❍) dd H_2O (pH 7) and (□) HEPES buffer (pH 7); b) free energy of mixing values (ΔG) for C-K_3-gT in dppc mole fractions for dif. subphase pHs and π-values: (black solid line) pH 10 at π = 15 mN m^{-1}, (gray solid line) pH 10 at π = 8 mN m^{-1}, (dashed black line) pH 7 at π = 15 mN m^{-1} and (dashed gray line) pH 7 at π = 8 mN m^{-1}; c) π-A isotherms of 100% C-K_3-gT, comparison of a (black line) fast and (gray line) slow speed (dashed lines represent the second compression cycle).

Self-assembled structures and properties of C-K_3-gT and K_3-gT are similar in solution.[12] However, using a Langmuir trough, the presence of the peptide's N-terminal cysteine at the interface between the peptide layer and the subphase becomes much more important. Consequently K_3-gT exhibited decreased film stability compared to C-K_3-gT, as illustrated in Fig. 4.1b, caused by the missing hydrophobic AA. Furthermore, in K_3-gT/dppc mixtures the transition from LE to LC occurred at much lower π, between 12 and 20 mN m^{-1} (120 - 80 Å^2 molecule^{-1}). This transition occurred in a fashion similar to *cyclo*-[(LW-DL)$_4$],[16] which exhibits the same alternating LW-DL sequence as gT, the truncated gramicidin sequence. Actually, at a high area per molecule the curves are almost identical; this implies that the dimensions should be identical as well. Therefore, we estimated a single helical turn – different helical configurations are known for gramicidin A (gA) – to be preserved.[11] This was not previously evident, since the original sequence had been considerably condensed from 15 AA to only 7 AA and transferred into an amphiphilic peptide by N-terminal attachment of tri-lysine. Moreover, we calculated the minimal area required for a K_3-gT molecule in the dppc monolayer (extrapolation related to the 10% sample in the dppc matrix) to 223 ± 25 Å^2 molecule^{-1}, which reflects a helix radius (r) of 8 Å (area= (2r) 2sin60°) and is consistent with literature values for the gA helices.[11c, 17] With further compression, areas per molecules exceeded the values for

dppc, which is ruled-out by molecular dimensions and thus can be an artifact only, likely due to K_3-gT molecules forced into the subphase. This might be due either to the character of the K_3-gT being too hydrophilic or to its denaturation caused by the compression force.

ΔG values and compression hysteresis already indicated raft formation for these peptides. However, BAM showed homogenous film formation but could not resolve corresponding features for K_3-gT/dppc films. Thus, we transferred peptide Langmuir films to freshly cleaved mica substrates for AFM analysis, which indeed showed raft formation (d = 10 - 80 nm) within the dppc matrix for low peptide content, as expected.[13a] Examples are provided in Fig. 4.3 and Fig. 4.4 for different K_3-gT contents in dppc (0.08% and 4.4%). However, raft formation turned out to be strongly affected by environmental conditions. Further, the transfer from the air-water interface onto the solid support may result in artifacts and thus displays a critical point.

The third peptide under investigation, AcC-X_3-gT, did not exhibit any chargeable group due to the acetylated amine groups, and thus should only be slightly interdependent with pH of the subphase. However AcC-X_3-gT films were sensitive to the buffer used and, similar to the other peptides, showed the highest stability on carbonate buffer with loss of only 5% of the initial π-value (Fig. 4.2a). Comparing the π-A isotherm of AcC-X_3-gT and C-K_3-gT revealed overlapping regions at high surface areas, whereas the transition from the LE to the LC phase occurred more pronouncedly (Fig. 4.5b). The similar offsets for all three peptides also indicate a preserved gT helix as the most space demanding group, at least at high surface areas.

A reflectivity curve was recorded during compression of AcC-K_3-gT in order to follow the development of film thickness. The signal consistently increased until the liquid-extended to liquid-condensed (LE-LC) phase transition took place, which confirmed the formation of a peptide film (Fig. 4.6 und Fig. 4.7). Afterwards the intensity increased further, which is not in agreement with material loss to the subphase, but could indicate a forced formation of dimers at corresponding π as shown for wild-type gA.[18] An alternative explanation is an elongation and denaturation of the molecule, due to the applied forces.

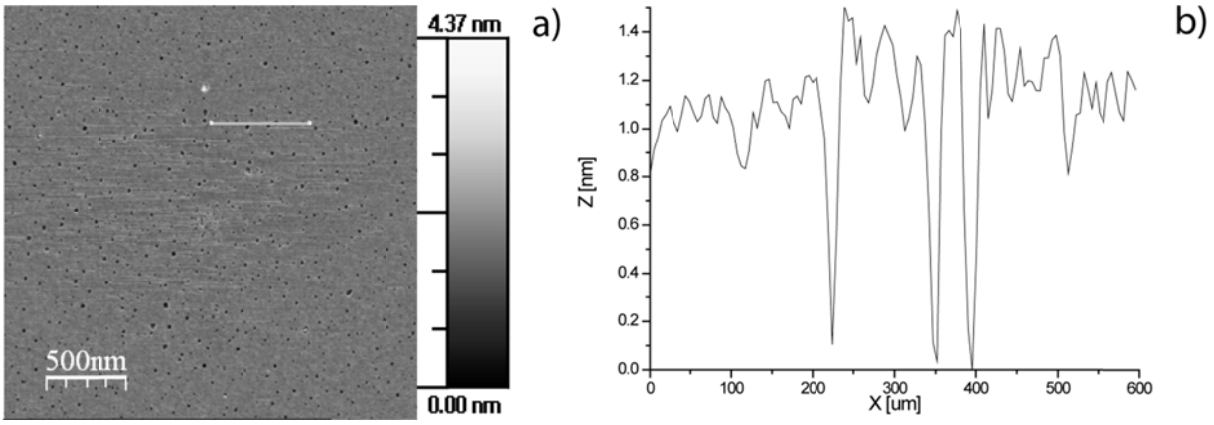

Fig. 4.3 a) AFM image of 0.08% K_3-gT in dppc compressed on HEPES buffer subphase (pH 7) and transferred to mica at a surface pressure of 25 mN m^{-1} and b) height profile as indicated in a).

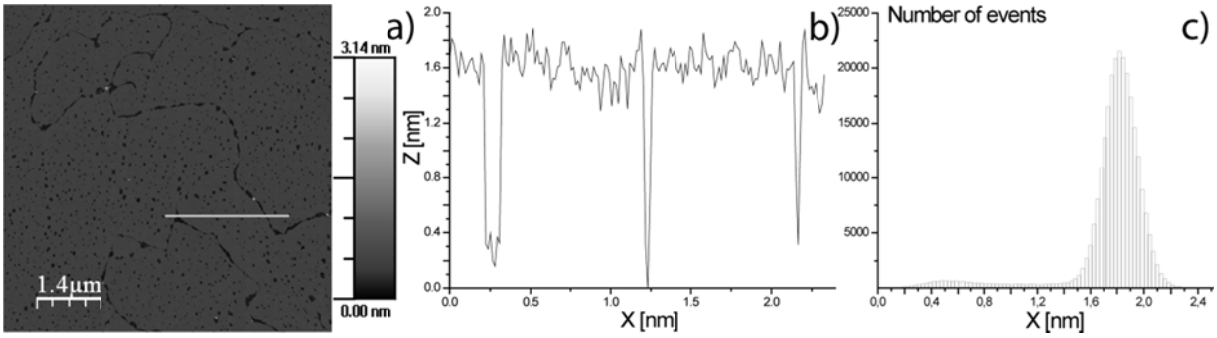

Fig. 4.4 a) AFM image of 4.4% K_3-gT in dppc compressed on HEPES buffer subphase (pH 7) and transferred to mica at a surface pressure of 25 mN m^{-1}; b) height profile as indicated in a); and c) height histogram illustrating two different population, dppc phase and peptides.

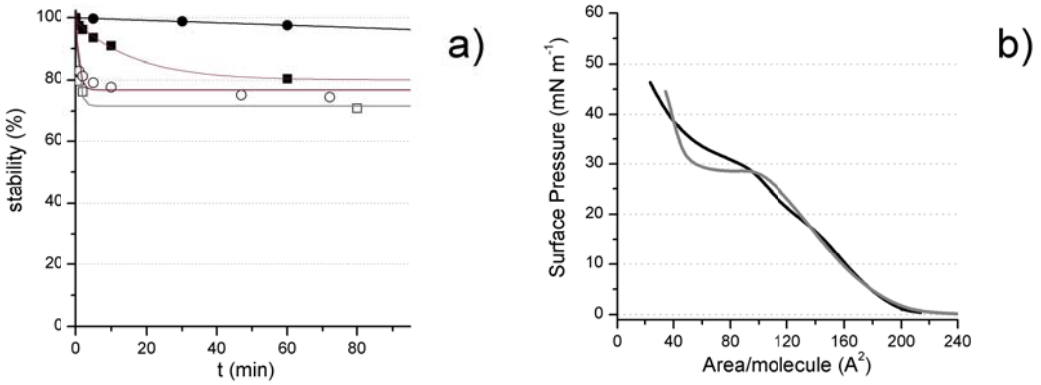

Fig. 4.5 a) film stability monitored by the decrease in the initial π-value of AcC-X_3-gT for dif. subphases and initial -values (●) carbonate buffer (pH 10), π = 25 mN m^{-1} (■) AcC-X_3-gT pH 10, carbonate buffer, π = 35 mN m^{-1} (○) AcC-X_3-gT pH 7, dd H_2O, π = 25 mN m^{-1} (□)AcC-X_3-gT pH 7, dd H_2O, π = 35 mN m^{-1} and b) π-A isotherms of (black line) C-K_3-gT and (gray line) AcC-X_3-gT on a carbonate buffer subphase (pH 10).

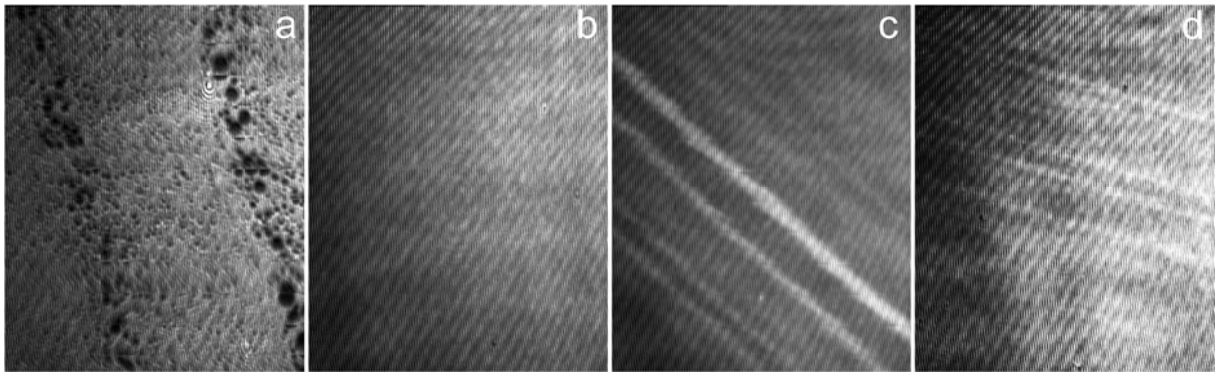

Fig. 4.6 BAM images for a) 7.2 min b) 23.3 min c) 33.3 min d) 36.7 min as indicated in Fig. 4.

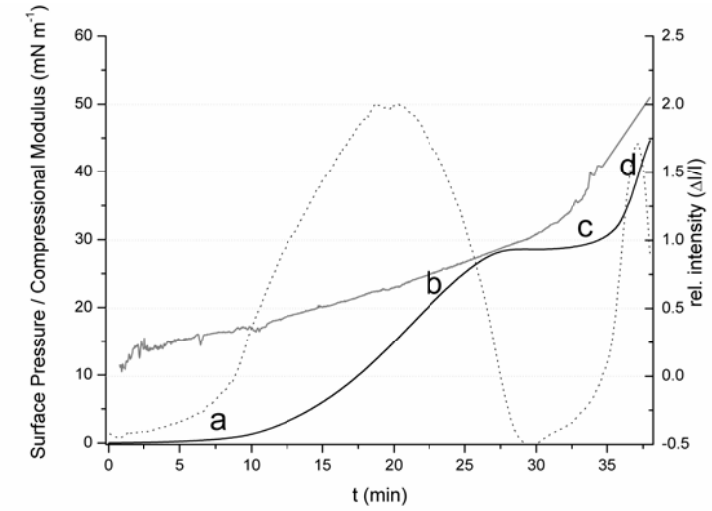

Fig. 4.7 Compressional modulus and relative intensity of π-A isotherm of AcC-X_3-gT on carbonate buffer (pH 10).

4.2.2. AcC-X_3-gT films on template-stripped gold (TSG)

In general, transferring the peptide film from the air-water interface to a substrate is performed using the Langmuir-Blodgett technique, by slowly pulling out the substrate from the subphase through the interface at constant surface pressure. Fig.4.10b presents an AFM image of the transferred AcC-X_3-gT film on freshly cleaved template stripped gold (TSG). Films showed a very homogenous, featureless and smooth surface. A comparison of the blank TSG surface and the AcC-X_3-gT LB monolayer shows that the roughness increased only slightly, which indicates the deposition but also illustrates the quality of the peptide films (Fig.4.8).

AcC-X_3-gT was also deposited on a Si-wafer. The partial removal of the peptide film upon scratching with the AFM tip and subsequent scanning further indicated the successful transfer of the LB film onto the solid substrate. Furthermore, it revealed a

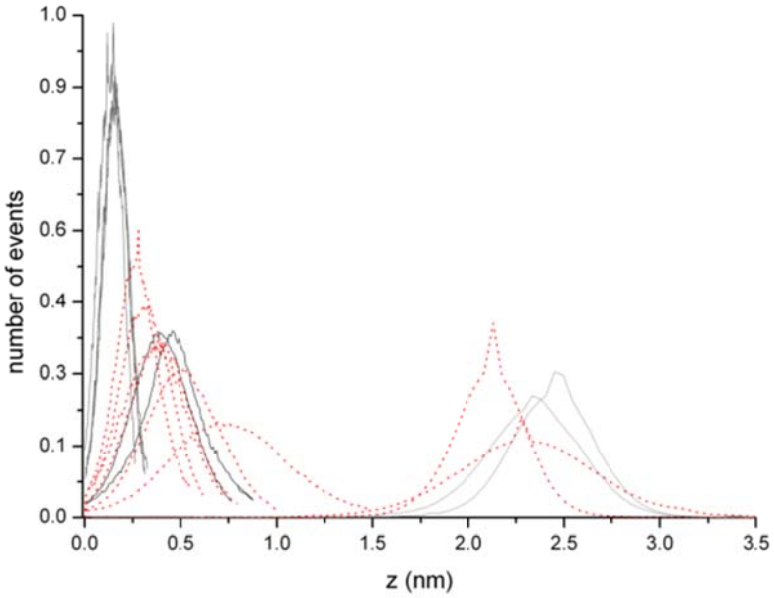

Fig. 4.8 AFM roughness analysis (height distribution) derived from transferred AcC-X_3-gT films on TSG (red, dashed in the same scan size) and the TSG control (scan sizes: black 0.25 nm x 0.25 nm, gray 1 μm x 1 μm, light gray 7 μm x 7 μm).

thickness of the peptide film of about 1.2 nm. Considering a molecule length of 1.6 nm this value might arise from either a low surface coverage or a tilt angle of approximately 41° (Fig. 4.). A tilt angle of 30° was found for wild-type gA monolayers at the air-water interface.[17] Both cases are in agreement with the transfer of a unimolecular peptide layer.

LB films represent a convincing method to produce homogenous monolayers on solid supports. Nevertheless it is rather time- and labor-consuming. Therefore, the question arises as to whether a homogenous peptide monolayer can be produced by faster and easier methods such as spin-coating or direct immersion of a substrate into a

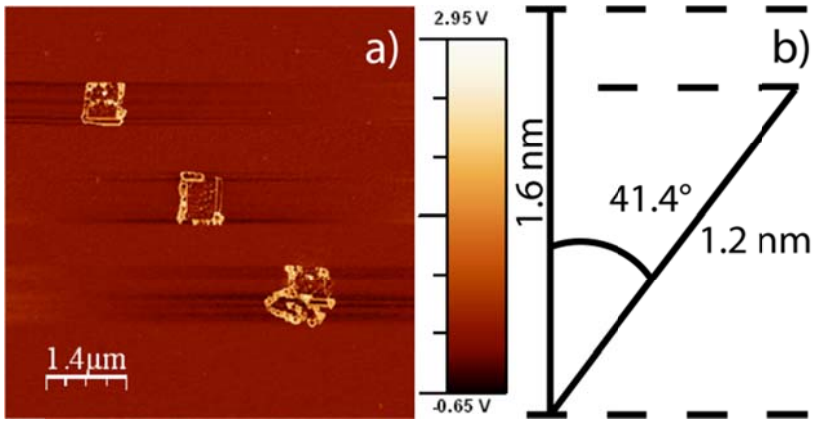

Fig. 4.9 a) AFM image of a partly removed AcC-X_3-gT film on an Si-wafer via scratching shows a thickness of 1.2 nm, b) geometrical considerations based on a peptide length of 1.6 nm.

thiolpeptide solution leading to a self-assembled monolayer (SAM). The original design of C-K_3-gT and AcC-X_3-gT includes the thiol functionality of the cysteine for covalent sulfur-gold linkage, which would then be used to create a stable SAM on TSG. SAMs are usually formed by alkyl chains but the rod-like structure of the hydrophobic gT-trunk should induce an ordered alignment of the peptide as well.[19]

Both methods, spin coating and immersion, were applied to form AcC-X_3-gT thin films. Since, in aqueous solution, AcC-X_3-gT forms spherical peptide particles in the nanometer size range,[12] different methods have been compared with the TSG blank (a) and the LB film (b): spin coating and immersion of an aqueous peptide bead solution (c and d) and an ethanol peptide solution (e and f), followed by a cleaning protocol to remove excess peptide from the surface. TSG exhibit a very flat surface with a molecular plane gold patterns over 100 nm in length, which is necessary to form SAMs (Fig.4.10a). The thin films produced by immersion in AcC-X_3-gT ethanol solution or spin coating showed, similarly to the LB-films, very smooth surfaces, as is illustrated in the profiles in Fig.4.10c and Fig.4.10d. Using an aqueous peptide particle solution led to an increased surface roughness and spin coated samples showed circular structures (r ~ 6 nm, 20 - 25 nm and 50 - 90 nm). Similar structures were found by Diociaiuti *et al.* in phospholipid (dppc) LB monolayers which they described as 2D gA-assemblies.[13a] In the present study, due to the preparation method, they might also originated from covalently bound peptide beads while the washing procedure caused the removal of all non-bonded material and the peptide beads' outer layers thereby remained. To confirm this theory the adsorption of intact peptide bead on a gold surface had to be analyzed. Indeed, the absorption in the form of complete peptide beads, in contrast to the mechanism for vesicle spreading as known,[20] was confirmed by QCM (Fig.4.11). In comparison to the thiolpeptide solution in ethanol, the peptide bead in aqueous solution exhibited a different adsorption profile. The continuous increase in mass and the constant dissipation indicated the adsorption of dissolved peptide molecules or peptide beads - without any morphological change.

Mean molecular areas, derived for Ac-X_3-gT from the π-A isotherms suggested an intact single helical turn; however, it is difficult for small molecules to fold back and form a stable secondary structure. In order to determine discrepancies from the gA structure we performed IR, *i.e.* polarization modulation infrared reflection absorption spectroscopy (PM-IRRAS) measurements on the presented AFM samples. First, the

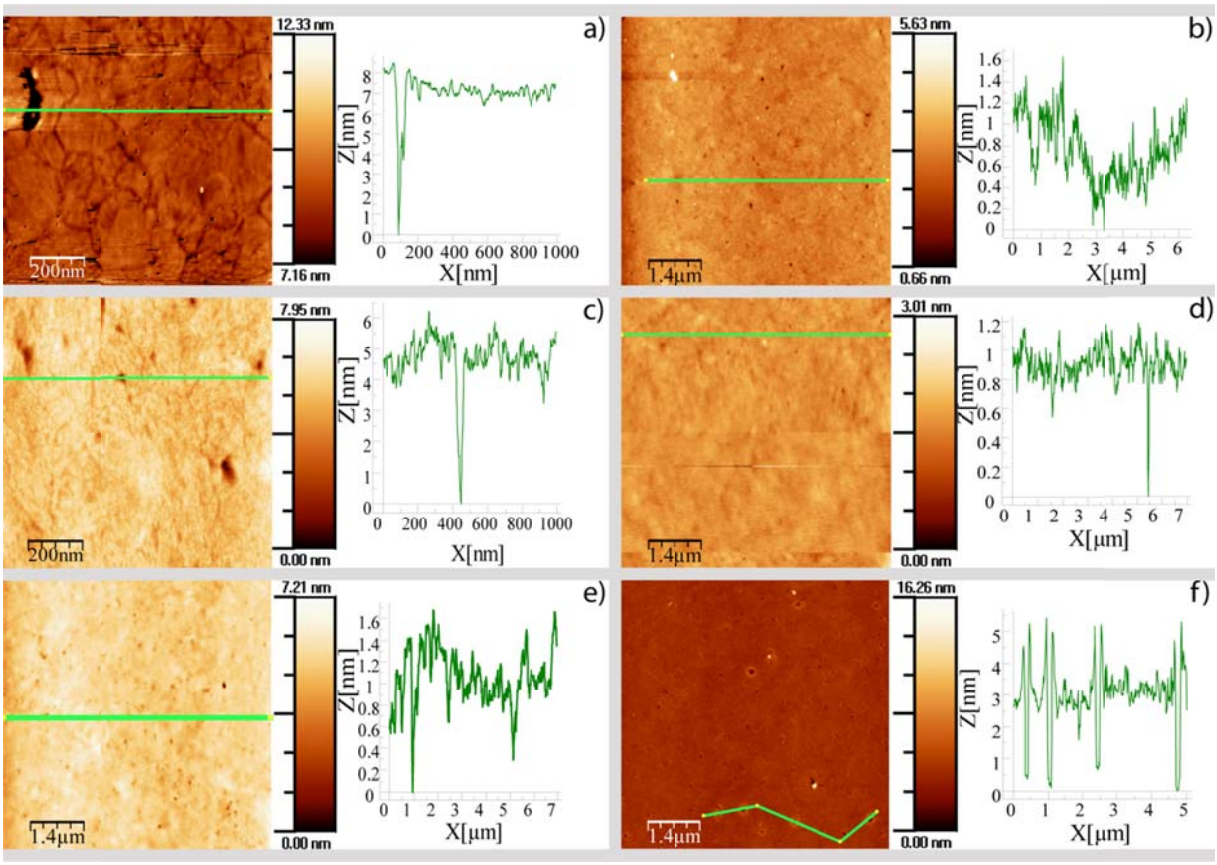

Fig. 4.10 AFM images of a) TSG blank b) LB-film (π_{TR} = 25 mN m^{-1}) c) immersion in ethanol solution d) immersion in peptide bead solution e) spin coating with ethanol solution f) spin coating with peptide bead solution with their height profiles as indicated in the respective scans.

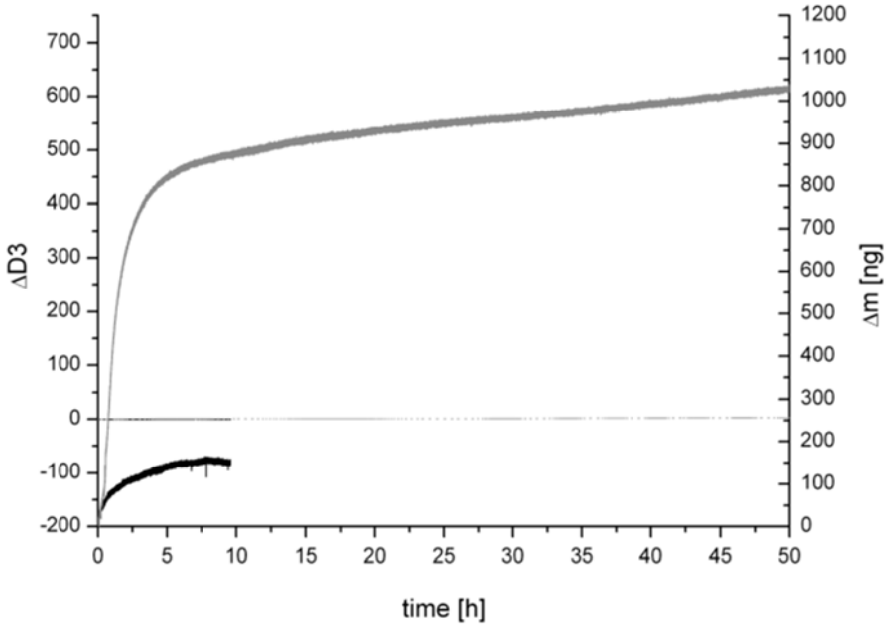

Fig. 4.11 QCM mass adsorption of a peptide bead in aqueous solution (gray) and an ethanol solution (black) and their dissipation (dashed lines).

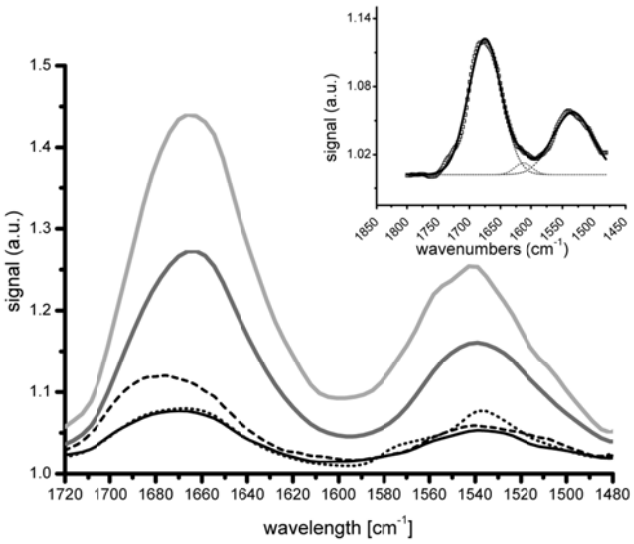

Fig. 4.12 Polarization modulation infrared reflection absorption spectroscopy (PM IRRAS) of peptide layer formed by: light gray: spin coating of AcC-X_3-gT ethanol solution; gray: spin coating of AcC-X_3-gT peptide bead solution; black: immersion in AcC-X_3-gT ethanol solution; dashed: AcC-X_3-gT LB-film; dotted: immersion in AcC-X_3-gT peptide bead solution, Inset: AcC-X_3-gT LB-film, deconvolution shows peak at 1612 cm^{-1}.

results proved the presence of a peptide film on the TSG (Fig.4.12, Table 4.1). Second, the amide I adsorptions at 1662 - 75 cm^{-1} (weak signal at ~ 1612 cm^{-1}) differ significantly from the known spectra for gA conformations, namely β-helical structures (1675 - 95 cm^{-1} and ~ 1625 - 40 cm^{-1}), and as well as from the random coil spectra (~ 1630 - 40 cm^{-1}).[21] In principle, parallel aligned hydrophobic parts of the peptides create a hydrophobic environment such as in inner-membrane regions, leading to corresponding shifts in the spectra. However, this effect of the peptides on each other can be neglected, since pure gA monolayers on the air-water interface did not show such influences.[22] The Amide I adsorption at ~ 1670 cm^{-1} was assigned to a β-turn and weak hydrogen-bonding. It is known for gramicidin S – a cyclic decapeptide analogue – to have a II' β-turn/ antiparallel

Table 4.1 Summary of amide I and II bands for LB film, Immersions in peptidic ethanol solution and aqueous peptide bead solution, spin coated ethanol solution and peptide bead solution.

Sample	Amide I [cm^{-1}]	Intensity	Amide II [cm^{-1}]	Intensity	Ratio I/II
Langmuir-Blodgett technique	1675.88	1.12	1538.95	1.06	1.06
Immersion in ethanol solution	1670.09	1.08	1538.95	1.05	1.02
Immersion in peptide bead solution	1666.23	1.08	1538.95	1.08	1.00
Spin coating of ethanol solution	1666.23	1.44	1542.81	1.25	1.15
Spin coating of peptide bead solution	1662.38	1.27	1538.95	1.16	1.10

β-sheet conformation.[23] Similarly, we propose the secondary structure of gT to contain a β-turn and weak hydrogen bonding.

Considering the similar IR results for all the preparation methods and AFM analysis, the most convincing method is immersion of the solid support into an AcC-X_3-gT ethanol solution, which is an easy method and led to similar smooth monomolecular films as the LB-transfer.

4.2.3. First steps towards a sensor platform using short amphiphilic peptides

The streptavidin-biotin interaction has a binding affinity K_a of 10^{14}-10^{15} M^{-1}, which is one of the strongest biological non-covalent binding events known. It is the basic platform for many sensing applications and preparation of functional surfaces. However, a lower receptor – ligand binding affinity, *i.e.* a reversible controllable binding event, depending on ionic strength, temperature and pH may find application as a reusable sensor platform. Thereby, the reloading of the next receptor layer is performed by desorption adsorption cycles. Our amphiphilic peptides might be able to be applied in such a sensor platform if they were to exhibit reversible, controllable gA intrinsic dimerization. By covalently linking a first peptide layer onto a solid support and controlling the dimerization state of a second, detecting layer, *i.e.* labeled with a binding site etc., the reusable sensor can be created. It was found that dimerization of gT amphiphiles did not take place in solution.[12] Therefore, we synthesized an amphiphilic peptide with a similar hydrophilic to hydrophobic ratio but with the complete gA-sequence (Table 4.2).

Table 4.2 Code and sequence of the amphiphilic peptides containing gA as hydrophobic contributor.

Code[a)]	Sequence
wild-type gA	*CHO*-LV-G-LA-DL-LA-DV-LV-DV-[LW-DL]$_3$-LW-*NHCH$_2$CH$_2$OH*
K_4-gA	*H*-LK-G-LK$_3$-LV-G-LA-DL-LA-DV-LV-DV-[LW-DL]$_3$-LW-*NH$_2$*
Biotin-K_6-gA	*Biotin*-LK$_3$-G-LK$_3$-LV-G-LA-DL-LA-DV-LV-DV-[LW-DL]$_3$-LW-*NH$_2$*
K_8-gA	*H*-LK$_2$-G-LK$_3$-G-LK$_3$-LV-G-LA-DL-LA-DV-LV-DV-[LW-DL]$_3$-LW-*NH$_2$*
OG488-K_8-gA	*OregonGreen488*-LK$_2$-G-LK$_3$-G-LK$_3$-LV-G-LA-DL-LA-DV-LV-DV-[LW-DL]$_3$-LW-*NH$_2$*

[a)] formerly named CD3[7], changed for a consistent nomenclature; [b)]X=K(Ac);

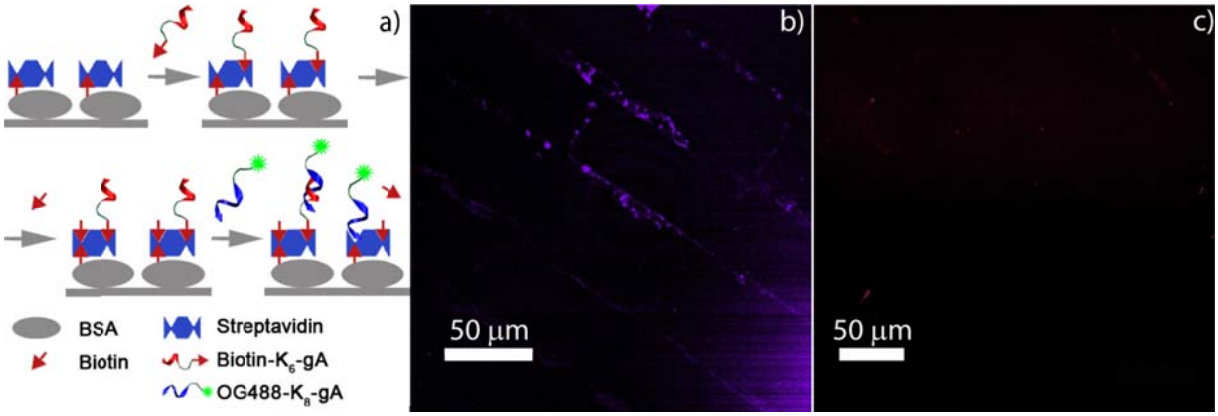

Fig. 4.13 a) schematic representation of the sensor setup b) with the addition of OG488-K_6-gA c) saturation with biotin.

The setup used was based on micro-contact printing to create a streptavidin pattern on the glass surface while the biotinylated peptide was used to create the peptide layer, presenting the gA part for gA dimerization. To detect the dimerization event we synthesized a fluorescent Oregon Green 488 modified peptide labeled OG488-K_8-gA. A monolayer as presented with covalently linked peptides via a thiol group on TSG would quench the fluorescent signal due to the gold adsorption. Therefore, biotinylated amphiphilic peptides biotin-K_6-gA were linked to a streptavidin stamped glass surface to reveal hydrophobic tails as illustrated in Fig. 4.13. However, dimerization was not detected. Instead, unspecific binding of the hydrophobic tryptophan rich part of the amphiphile with the hydrophobic tryptophan rich binding pocket of the streptavidin gave rise to a fluorescent signal. If the binding pockets of streptavidin were *a priori* saturated with biotin, then no fluorescence signal would be detected, meaning that dimerization of the presented peptide and the fluorescent-labeled amphiphilic peptide did not occur (Fig.4.13). Therefore, sensor application in this setup was not successful and further experimental efforts and even synthetic approaches had to be considered to guarantee a high degree of dimerization and thus a successful creation of a sensor platform.

4.2.4. Mineralization at the air-water interface

The usability of C-K_3-gT films for mineralization of calcium phosphate at the air-water interface was evaluated. Therefore a peptide monolayer was compressed on a Langmuir trough and mineralization was initiated by the injection of $CaCl_2$ into the subphase of phosphate buffer. After two hours sampling of the resulting mineralization products was performed. As shown in the TEM image in Fig.4.14a, samples typically

consist of three layers: a first, presumably the peptide layer, a second more dense layer which might contain calcium phosphate and peptide, and a third 'layer' which contains crystals. The size of the crystals ranges from below 100 nm to over 1 μm (Fig.4.14a to c). Noteworthy is the net-like structure of the first layer as seen in Fig.4.14c. Also SEM (Fig.4.15) confirms the formation of crystals but only from energy dispersive X-ray spectroscopy crystal composition can be deduced. Indeed, calcium phosphate is commonly one signature in the EDXS spectra such as in Fig.4.15c representing the bright crystal in Fig.4.15b. EDXS spectra also includes the thiol-group of the amphiphilic peptide. However, the formation of NaCl crystals cannot be ruled out since it appeared in the EDXS spectra and also some of the crystals found in TEM appear cubic. The presented mineralized structures are not completely homogenous over the whole sample which might be due to artifacts of the sampling. TEM as well as SEM confirmed the formation of bigger aggregates or crystal in the micrometer range (Fig.4.15c), which do contain calcium phosphate. The presented experiments represent a proof-of-principle and simultaneous the potential to use purely amphiphilic peptides in order to induce mineralization. Optimization of the purely peptidic system depends on parameters such as subphase, ionic strength, pH, temperature, and agitation but further may be achieved by mixing uncharged AcC-X_3-gT with charged C-K_3-gT and with it a more controlled mineralization.

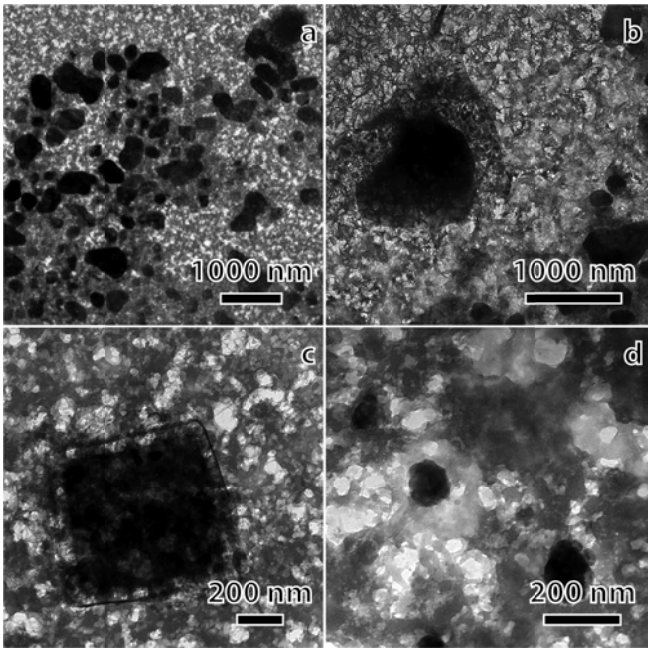

Fig. 4.14 TEM of crystals transferred from air-water interface onto a TEM grid.

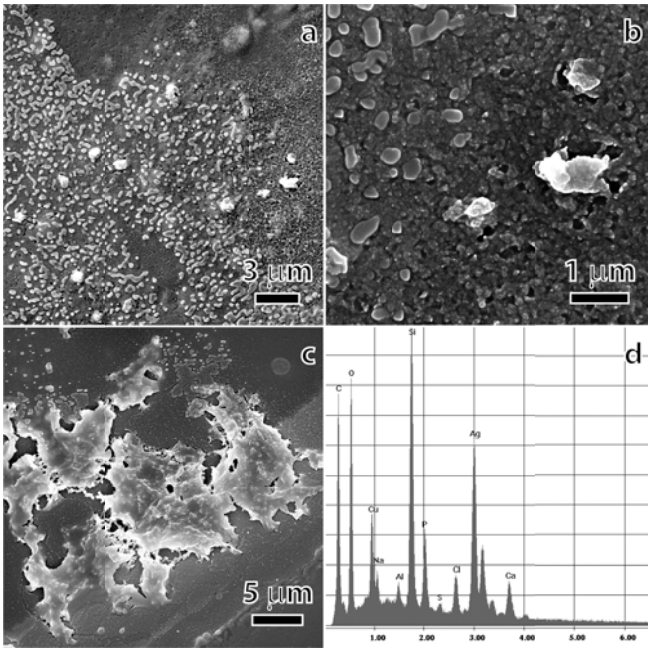

Fig. 4.15 (a-c) SEM images of mineralized crystals (d) example EDXS spectra of the bright crystal in (b).

4.3. Conclusion

LB films were affected by the subphase, its pH, and its ion composition as well as by the peptide's end-group at the interface, and whether the hydrophilic heads were acetylated or not. At the interface, we found the amphiphilic peptide AcC-X_3-gT with reduced hydrophilicity due to acetylation of the tri-lysine head group to be the most stable layer if a carbonate buffer was used as subphase. Introduction of an N-terminal cysteine or acetylation of the tri-lysine does not have an influence on the offset area per monomer. Those homogenous layers have already been successfully transferred onto a solid support, but similar results have been created more readily by means of immersion and spin-coating of an ethanol or aqueous solution. Therefore, fast and facile surface modification was also performed via direct surface coverage of the substrate. Surface modifications with purely peptidic films have been confirmed by AFM and IR measurements and enabled us to propose components of the peptide's secondary structure. The latter includes a defined and reproducible pattern, contains β-turn and weak hydrogen bonding, and the gT likely exhibits a single distorted turn with an average radius of approx. 8 Å.

We presented purely peptidic cationic amphiphiles, which formed stable monolayers at the air-water interface, using carbonate and phosphate buffer as a

subphase. Preliminary experiments showed the successful creation of calcium phosphate containing minerals. Therefore these monolayers can be used as a platform for mineralization. The presented peptidic system is of general importance for the future development of supramolecular structures and for the creation of new functionalities at interfaces. The thiol-functionality could thereby play an important role as an anchoring group.

4.4. References

[1] F. C. Meldrum and H. Colfen, *Chem. Rev. (Washington, DC, U. S.)* **2008**, *108*, 4332-4432.

[2] K. Gorna, R. Munoz-Espi, F. Groehn and G. Wegner, *Macromol. Biosci.* **2007**, *7*, 163-173.

[3] M. Junginger, K. Kita-Tokarczyk, T. Schuster, J. Reiche, F. Schacher, A. H. E. Mueller, H. Coelfen and A. Taubert, *Macromol. Biosci.* **2010**, *10*, 1084-1092.

[4] S. Schweizer, T. Schuster, M. Junginger, G. Siekmeyer and A. Taubert, *Macromol. Mater. Eng.* **2010**, *295*, 535-543.

[5] T. Nonoyama, M. Tanaka, T. Kinoshita, F. Nagata, K. Sato and K. Kato, *Chem. Commun. (Cambridge, U. K.)* **2010**, *46*, 6983-6985.

[6] a) S. Hayashi, K. Ohkawa and H. Yamamoto, *Macromol. Biosci.* **2006**, *6*, 228-240; b) V. Ball, M. Michel, F. Boulmedais, J. Hemmerle, Y. Haikel, P. Schaaf and J. C. Voegel, *Cryst. Growth Des.* **2006**, *6*, 327-334.

[7] a) M. Boncheva and H. Vogel, *Biophys. J.* **1997**, *73*, 1056-1072; b) S. Belegrinou, J. Dorn, M. Kreiter, K. Kita-Tokarczyk, E.-K. Sinner and W. Meier, *Soft Matter* **2009**, *6*, 179-186.

[8] J. L. Grey and D. H. Thompson, *Expert Opinion on Drug Discovery* **2010**, *5*, 1039-1045.

[9] E. Kang, J.-W. Park, S. J. McClellan, J.-M. Kim, D. P. Holland, G. U. Lee, E. I. Franses, K. Park and D. H. Thompson, *Langmuir* **2007**, *23*, 6281-6288.

[10] J. R. Cox, M. Dabros, J. A. Shaffer and V. R. Thalladi, *Angew. Chem., Int. Ed.* **2007**, *46*, 1988-1991.

[11] a) R. Sarges and B. Witkop, *J. Am. Chem. Soc.* **1965**, 2027-2030; b) D. W. Urry, *Proc. Natl. Acad. Sci. U. S. A.* **1971**, *68*, 672-676; c) B. A. Wallace, *J. Struct. Biol.* **1998**, *121*, 123-141; d) H. Rapaport, H. S. Kim, K. Kjaer, P. B. Howes, S. Cohen, J. Als-Nielsen, M. R. Ghadiri, L. Leiserowitz and M. Lahav, *J. Am. Chem. Soc.* **1999**, *121*, 1186-1191.

[12] T. B. Schuster, D. de Bruyn Ouboter, E. Bordignon, G. Jeschke and W. Meier, *Soft Matter* **2010**, *6*, 5596-5604.

[13] a) M. Diociaiuti, F. Bordi, A. Motta, A. Carosi, A. Molinari, G. Arancia and C. Coluzza, *Biophys. J.* **2002**, *82*, 3198-3206; b) J. Mou, D. M. Czajkowsky and Z. Shao, *Biochemistry* **1996**, *35*, 3222-3226.

[14] a) J. A. Killian and B. de Kruijff, *Biochemistry* **1985**, *24*, 7890-7898; b) H. Tournois, C. H. J. P. Fabrie, K. N. J. Burger, J. Mandersloot, P. Hilgers, H. Van Dalen, J. De Gier and B. De Kruijff, *Biochemistry* **1990**, *29*, 8297-8307.

[15] R. Brasseur, J. A. Killian, B. De Kruijff and J. M. Ruysschaert, *Biochim. Biophys. Acta, Biomembr.* **1987**, *903*, 11-17.

[16] H. Rapaport, *Peptide Science* **2005**, *41st*, 79-82.
[17] H. Lavoie, D. Blaudez, D. Vaknin, B. Desbat, B. M. Ocko and C. Salesse, *Biophys. J.* **2002**, *83*, 3558-3569.
[18] D. Ducharme, D. Vaknin, M. Paudler, C. Salesse, H. Riegler and H. Moehwald, *Thin Solid Films* **1996**, *284-285*, 90-93.
[19] Y. Miura, S. Kimura, Y. Imanishi and J. Umemura, *Langmuir* **1998**, *14*, 6935-6940.
[20] C. A. Keller and B. Kasemo, *Biophys. J.* **1998**, *75*, 1397-1402.
[21] a) M. Jackson and H. H. Mantsch, *Crit. Rev. Biochem. Mol. Biol.* **1995**, *30*, 95-120; b) B. A. Wallace, *Biophys. J* **1986**, *49*, 295-306.
[22] W. P. Ulrich and H. Vogel, *Biophys J* **1999**, *76*, 1639-1647.
[23] a) D. Mihailescu and J. C. Smith, *J. Phys. Chem. B* **1999**, *103*, 1586-1594; b) C. R. Jones, C. T. Sikakana, S. Hehir, M.-C. Kuo and W. A. Gibbons, *Biophys. J.* **1978**, *24*, 815-832.

5. From fibers to micelles using point mutated amphiphilic peptides

Thomas B. Schuster, Dirk de Bruyn Ouboter, Cornelia G. Palivan, Wolfgang Meier

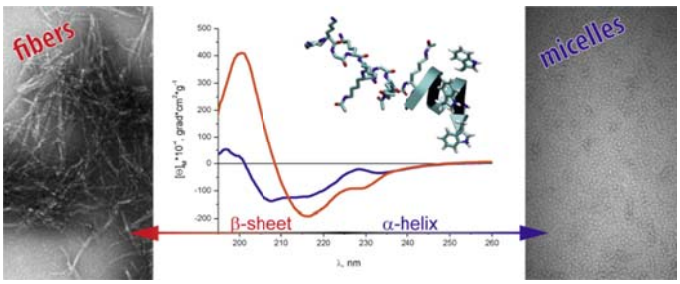

The secondary structure of the amphiphilic peptides defines their self-assembled morphology.

Reprinted in parts with permission from: *Langmuir* **2011**, *27*, 4578-4584.

http://pubs.acs.org/doi/abs/10.1021/la200443

5.1. Introduction

Self-assembled nanostructures are attracting ever more attention, in particular in aqueous solution, due to fundamental aspects that concern the nature of the folding processes as well as the wide range of applications as carriers in drug delivery, templates for surface oriented applications, or nanodevices in combination with active molecules.[1] At the focus of this interest is the fabrication of nanostructures such as micelles, nanotubes or vesicles that can be combined with active molecules, such as biological entities, to generate complex hybrid systems.[2] Ranging from systems that are completely synthetic (polymers, inorganic compounds) to biological (phospholipids, polypeptides), interest in medically-oriented applications stems from the possibility of producing suprastructures that are able to both accommodate the active entity and preserve its structure/function in biological conditions. Even if the diversity of the polymeric systems that are able to generate supramolecular structures is very extensive, biocompatibility plays a crucial role for any biomedical application.[1-3] This requirement limits significantly the types of polymers or copolymers to only those that are biocompatible, such as, for example, poly(ethylene oxide), poly(dimethylsiloxane) or poly(glutamic acid).[4] But this limitation does not apply to poly(amino acids) *i.e.* polypeptides, which appear ideal for the development of supramolecular structures, since it is anticipated that they will be both biocompatible and biodegradable. Furthermore, they offer broad chemical functionality due to the diversity of AA side chains combined with specific AA sequences that define specific recognition sites[5] (*e.g.* RGD sequence for cell adhesion) or act similar to cell penetrating peptides (arginine rich sequences).[6] Another important feature of peptides is their secondary structure, *e.g.* β-sheet or α-helix, reflecting a three dimensional conformation that supports specific interactions and properties. The complete folding and assembly of a protein into its quaternary structure is an outcome that depends on the interaction between the solvent and the protein structure, leading to often advantageous electrostatic interactions and hydrogen-bonding combined with the hydrophobic effect. Thus, in the self-assembly of natural systems the secondary, the tertiary, and the quaternary structures are interconnected and serve to create the final supramolecular conformation that favors a specific functionality. The secondary structure and the overall 3D conformation are encoded in the primary sequence, and these structures are then modulated via effects

on the secondary structure arising from environmental conditions such as pH, ionic strength, temperature, and type of solvent. A pH-induced, so-called helix – coil transition of poly(L-lysine) and poly(L-glutamic acid) was used to create micelles that are able to invert their corona and core regions in so-called 'schizophrenic' behavior.[7] The same approach was used when polypeptides were combined with biocompatible polymers, in a co-micellated system of poly(glutamic acid) -*b*- poly(propylene oxide) -*b*- poly(glutamic acid)/ poly(ethylene oxide) -*b*- poly(propylene oxide) for controlled drug release.[7-8] These examples illustrate in an excellent fashion how the self-assembly of polypeptides derived from polymerization techniques can be controlled by changes in a molecule's secondary structure. However, polypeptides obtained by polymerization techniques bear the inherent drawbacks of polymerization that produce a molecular weight distribution that can differ slightly from batch to batch, and that fails to provide a controlled, defined sequence of differing amino acids.

It is possible to overcome these limitations by using solid-phase peptide synthesis (SPPS), which is limited to peptides up to 50 AAs.[9] Zhang and co-workers produced ionic, self-complementary peptides by solid-phase peptide synthesis, and investigated their supramolecular architectures upon self-assembly.[10] When very short amphiphilic peptides, *e.g.* V6K2 self-assembled into net-like structures of tubes and vesicles,[11] the 3D structures have been found to be highly sensitive to the purity of the peptides.[12] Qui *et al.* showed the successful assembly of catanionic A6K$^{\pm}$ into fibers.[13] A series of six 32-mers with a constant hydrophilic part and a variable hydrophobic part based on a phenylalanine/alanine ratio was used to fine-tune drug and gene co-delivery.[14] Hashimoto *et al.*[15] showed that micelles using the 28-mer Pep-L12 are biodegradable and are a potential gene carrier system.[15] However, the mentioned studies do not include investigations on secondary structure. This was examined on a 24-meric peptide, designed from a 20 kDa barnacle cement protein, and was found to be constant while self-assembling into a filament structure. This peptide, however, does not exhibit an amphiphilic character and self-assembly was induced by salt addition.[16] Shera *et al.* compared a designed, amphiphilic 15-meric peptide to an alternating analogue, *i.e.* an analogue with identical AAs but differing in its sequence and related the self-assembled morphologies to the observed primary β-sheet conformation, not present in the alternating analogue.[17] General studies in solution that include the influence of the

secondary structure do exist – especially for polypeptides – but, to the best of our knowledge, a systematic study using a series of amphiphilic small (≤ 25 AAs) defined and controlled sequences – *i.e.* not synthesized by polymerization – for the purpose of undestanding superstructures that are generated by self-assembly, have not been reported yet.

As a key to understanding protein/polypeptide folding and self-assembly of the primary sequence, point mutation represents the best choice to induce, in a controlled way, a precise change of one specific AA in the primary sequence. In the present study we investigate the impact of point mutations on a short peptide series, on the control of amphiphilicity, on secondary structure and on the self-assembled morphologies. The amphiphilic peptides successfully synthesized by SPPS via Fmoc strategy[18] allowed us to create a library of ten peptides with progressively changing properties. Their constant hydrophobic part was inspired by the pentadecamer gramicidin A (gA), consisting of only hydrophobic AAs in an alternating D, L configuration, which generates β-helical membrane channels.[19] The C-terminal ethanolamine group of gA was replaced by an amide group and its N-terminus was used to start a hydrophilic sequence of lysine (K, pKa of 10.2) and acetylated lysine (X). Acetylated lysine results in the removal of a charge and thus elimination of electrostatic repulsion, with expected impact on the secondary structure and morphology of the resulting assemblies. Glycine was introduced after every third lysine or acetylated lysine to prevent a decrease in yield by creation of a homooligomer.

The degree of acetylation (DA) directly affects the number of charges and the corresponding hydrophilicity. The peptides of our library can be divided into three parts in terms of increasing hydrophilicity: (a) a highly hydrophilic-, charged lysine part with a space-demanding hydration shell, (b) a moderate hydrophilic, acetylated lysine part without electrostatic repulsion of the amine groups, and (c) a hydrophobic rod-like helix based on gA. Depending on the hydrophilic character of the peptides, the self-assembly process leads to different supramolecular structures that have been analyzed in relation to the primary structure.

5.2. Results and discussion

5.2.1. Design of amphiphilic peptides

We synthesized a peptide library based on SPPS via the Fmoc strategy, with the schematic structure K_mX_{8-m}-gA with: K_m (K - lysine, m – no of lysines), X_{8-m} (X - acetylated lysine), and a gA sequence of 14 highly hydrophobic amino acids, which remains constant and represents 56% of the total sequence (Table 5.1). Only one peptide, Ac-X_8-gA has an acetylated N-terminus, so that the peptide is completely neutral, while only one peptide, K_8-gA has no acetylated group. As an example, the peptide K_4X_4-gA has the following sequence: *H*-LLys$_2$-Gly-LLys$_2$-(LLys-Ac)-Gly-(LLys-Ac)$_3$-LVal-Gly-LAla-DLeu-LAla-DVal-LVal-DVal-LTry-DLeu-LTry-DLeu-LTry-DLeu-LTrp-*NH2* (Fig. 5.1).

The design of the peptide library provides a linear increase in charge starting at neutral (Ac-X_8-gA), until reaching a total number of nine charges/molecule, for K_8-gA. This is associated with the changes in the degree of acetylation (DA), which thus gradually tunes the hydrophobicity. The library of short peptides – each consisting of only 25 AAs with a precise primary sequence – was used to detect morphological transformations upon self-assembly in solution, based on the slightest changes in the amphiphilic design. Our interest concerned the study of whether and in what respect a very fine change to only one residue in the primary structure would affect the 3D conformation of the peptides.

5.2.2. Amphiphilic character of the peptide library

As expected from the design of the molecules, the properties of the peptides changed

Table 5.1 Properties of the peptide K_mX_{8-m}-gA library, together with its schematic representation (DA - degree of acetylation).

Label	Hydrophobicity	DA	No. of charges	Scheme
Ac-X_8-gA	0.62	9/9	0	
X_8-gA	0.57	8/9	1	
K_1X_7-gA	0.55	7/9	2	
K_2X_6-gA	0.53	6/9	3	
K_3X_5-gA	0.52	5/9	4	
K_4X_4-gA	0.50	4/9	5	
K_5X_3-gA	0.49	3/9	6	
K_6X_2-gA	0.47	2/9	7	
K_7X_1-gA	0.45	1/9	8	
K_8-gA	0.44	0/9	9	

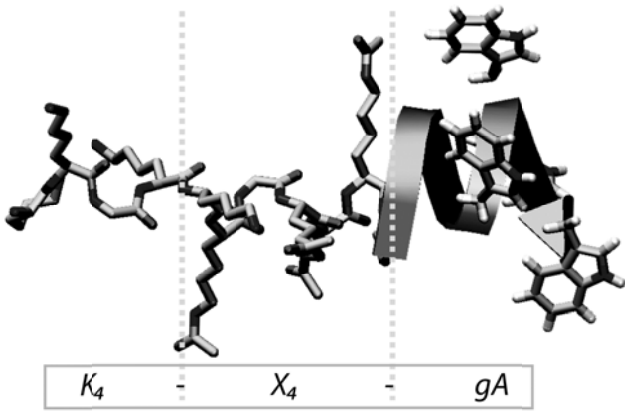

Fig. 5.1 Schematic representation of K_4X_4-gA including oligolysine (K_4), acetylated oligolysine (X_4), and β-helical gA.[20]

continuously within the library. For example, stepwise acetylation leads to a progressively increasing mass, and corresponds to a progressive increase in hydrophilicity of the peptide series. The variation in hydrophobicity was evidenced by the increased retention time on a RP-HPLC column (Fig. 5.2). While hydrophobic sequences such as gA are usually very difficult to produce,[21] our synthesis and purification provides peptides with very high purity.

As the self-assembly process takes place by solvent exchange from molecularly dissolved amphiphiles in solution, the solubility of the peptide library was analyzed in different solvents at concentration of 1 mg mL^{-1}. In DMF all of the peptides were soluble (Fig. 5.3a). We observed two types of behaviors with respect to solubility, in both ACN/water mixture and in ethanol: peptides partially soluble (Ac-X_8-gA to K_2X_6-gA) and

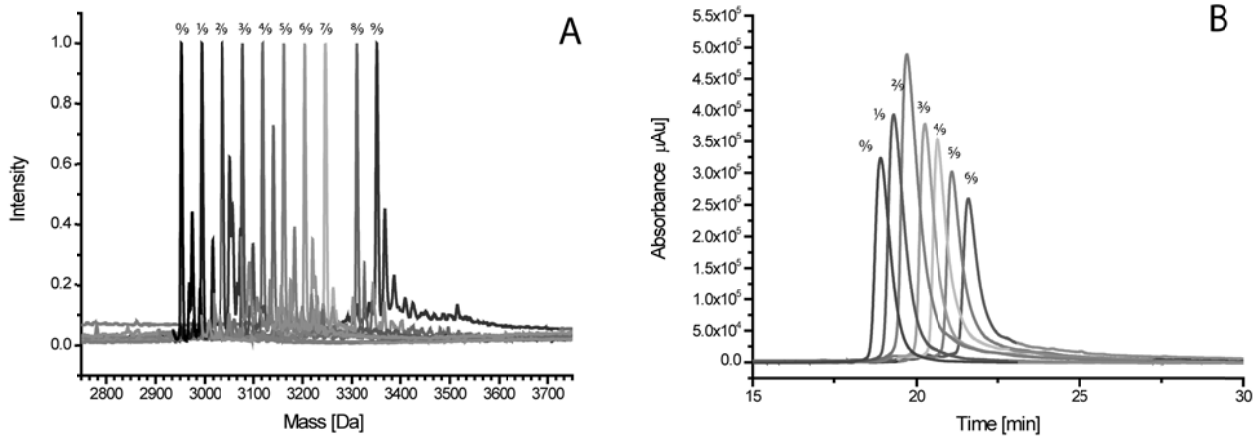

Fig. 5.2 A) MALDI-TOF-MS and B) HPLC overlay of the peptide library. The curves are assigned with the degree of acetylation (*cf.* Table 5.1).

peptides completely soluble for smaller DA (K_3X_5-gA to K_8-gA). Thus, we observed a breakpoint in solubility between K_2X_6-gA and K_3X_5-gA (DA 6/9 and 5/9), which was not expected due to the continuously increasing hydrophilicity of the amphiphiles and continuous increase in retention time. Consequently, we assume that conformational changes along the peptide backbone are responsible for inducing intermolecular interactions, thereby explaining the observed solubility behavior. Therefore, we analyzed the secondary structure and evaluated the folding themes in ethanol by circular dichroism (CD). Even though Ac-X_8-gA to K_3X_5-gA showed low solubility in ethanol, CD spectra were measured for diluted solutions. All CD spectra (Fig. 5.4A) corresponding to peptides ranging from Ac-X_8-gA (DA 8/9) to K_2X_6-gA (DA 6/9) exhibited a negative cotton effect around 218 nm and a positive cotton effect at around 200 nm (Fig. 5.4b, dotted line) and were assigned to a β-sheet configuration (217 nm and 198 nm).[22] Starting from K_3X_5-gA, different CD spectra were observed with a negative cotton effect around 208 nm and 219 nm, as well as a positive cotton effect at around 197 nm (Fig. 5.4b, solid line). These values correspond to an α-helical character (208 nm, 222 nm and 192 nm).[22] K_3X_5-gA contains only one acetylated lysine less as compared to K_2X_6-gA, but exhibits a completely different CD-spectrum and therefore marks the breakpoint in the behavior of the peptide series (Fig. 5.4b). Thus, the abrupt change in solubility behavior of peptides corresponds to a different secondary structure of the peptides, namely a β-sheet for K_2X_6-gA as compared to an α-helix for K_3X_5-gA. The low solubility found in different solvents for peptides Ac-X_8-gA to K_2X_6-gA can be explained by intermolecular

Fig. 5.3 Solubility of the amphiphiles in A) DMF B) ACN/water (1:1) C) ethanol.

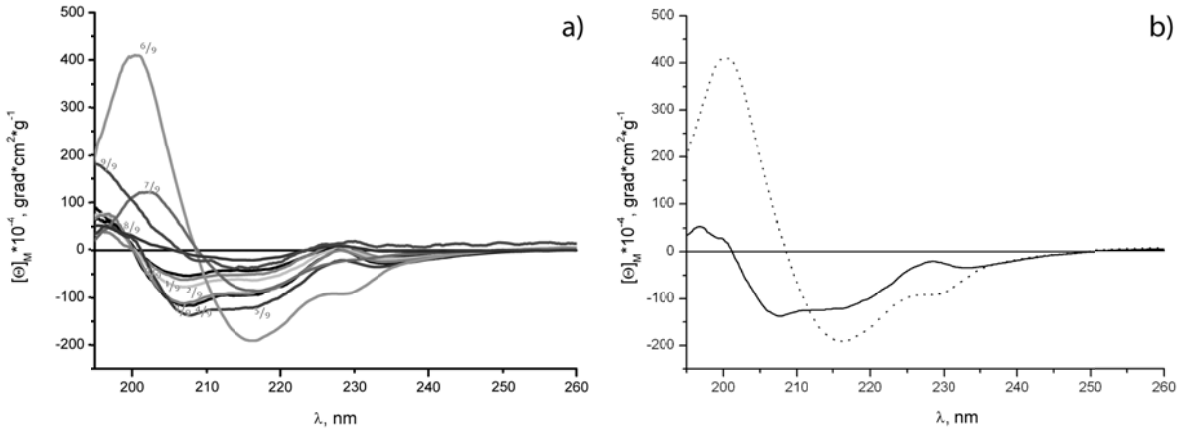

Fig. 5.4 CD spectra of a) the peptide library labeled with the degree of acetylation b) only K_2X_6-gA (dotted line, β-sheet) and K_3X_5-gA (solid line, α-helix) in ethanol.

interactions that are known for β-sheet-like structures that form higher-order assemblies of ribbons, fibers, and amyloids.[23] It is interesting to note that the α-helical and β-sheet-like secondary structures of the charged and uncharged peptides differ from that usually assigned to lysine homopolymer 2.5_1-helical and α-helical conformations, respectively.[24] However, this difference is not surprising and is caused by the introduction of a residue other than lysine (glycine) after each third AA. The deviation from a homooligomeric hydrophilic part is actually 20% and thus contributes significantly to the secondary structure.

The area in CD spectra between 210 and 260 nm is strongly affected by the structure adopted by the gA-sequence of peptide amphiphiles, and includes a characteristic maximum at 223 nm.[25] This is preserved throughout the whole library, even if the signal intensity is decreased by the superimposed spectra of the hydrophilic part. Therefore, we found the structure of the hydrophobic sequence little affected by the presence of the hydrophilic part of peptides and equally so by the variation of their DA character. This agrees with the stable structures known for gA and gA-analogues found in different conditions of solvents or matrices.[26] Analysis of overall shape of CD spectra therefore indicated that the variation in the primary sequence caused a transition in the secondary structure of the hydrophilic part from a β-sheet to an α-helix.

The hydrophobic contributor gA is based on the alternating D, L configuration and its secondary structure and self-assembly changes completely if only L-configured amino

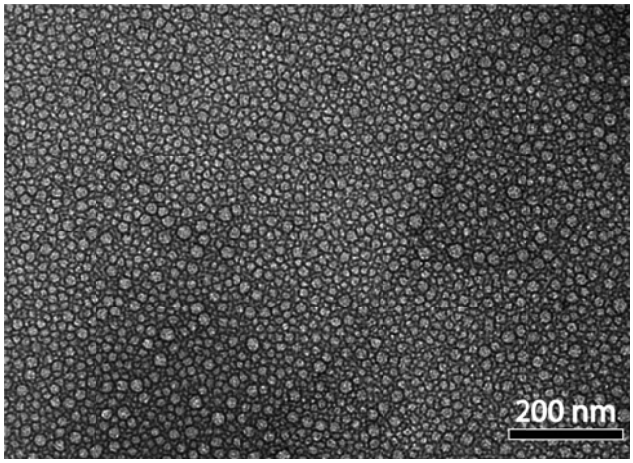

Fig. 5.5 TEM of K_6-gA micelles.

acids are used for its synthesis (LgA). This became evident by comparing the water soluble amphiphile K_6-gA with its analogue, the all L-configured K_6-LgA. While K_6-gA forms mainly micelles such as K_3X_6-gA to K_8-gA (Fig. 5.5), K_6-LgA exhibits a great tendency to form gels in ethanol and water, and was only soluble in trifluoroethanol (TFE). The CD spectra no longer exhibit the maximum at 223 nm, as observed for K_6-gA, and the secondary structure, as derived from CD in TFE (Fig. 5.6), was assigned to a β-sheet structure. Thus, the intramolecular hydrogen-bonds that stabilize the D, L configured gA helix are most likely intermolecular hydrogen-bonds between the β-sheet structures of the gA entirely L-configured. Therefore, the folding of the hydrophobic gA- helix is crucial to the amphiphilicity of the entire peptide and only occurs in the case of the D, L – alternating configuration.

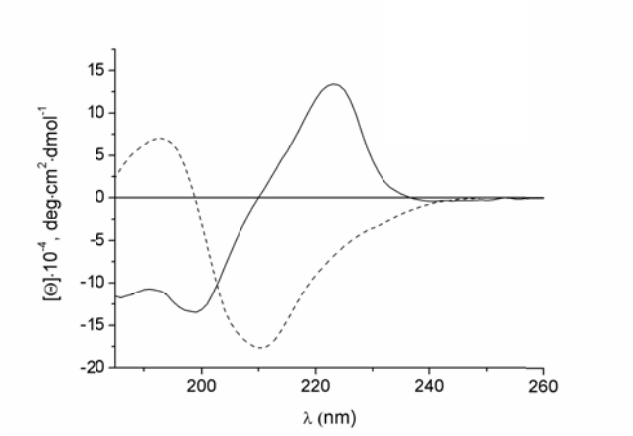

Fig. 5.6 CD spectra of (solid line) K_6-gA and (dashed line) K_6-LgA in TFE.

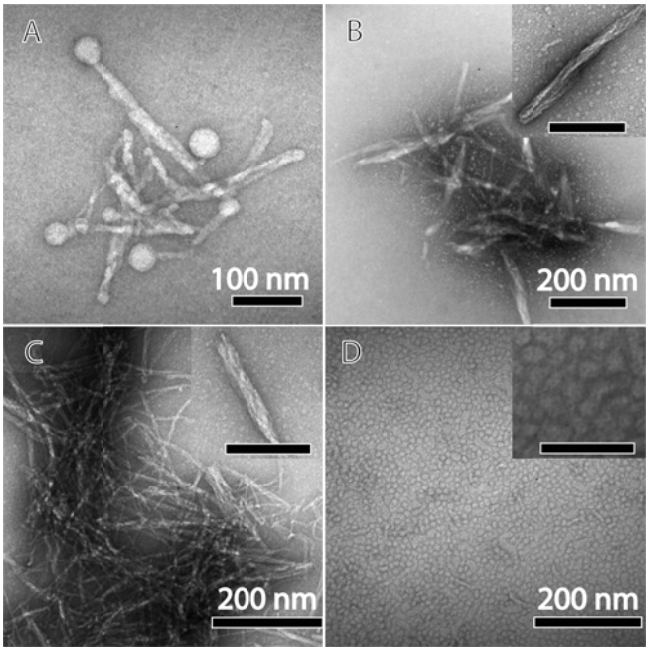

Fig. 5.7 TEM of various peptides in dd H_2O: A) X_8-gA B) K_1X_7-gA C) K_2X_6-gA D) K_3X_5-gA (inset scale bar 50 nm).

To observe the superstructures formed by the self-assembly of peptide series in solution we used TEM. Self-assembly was induced by changing the surrounding polarity during the exchange of the organic solvent to dd H_2O. TEM images show fibers as the main superstructure generated by peptides ranging from X_8-gA to K_2X_6-gA (Fig. 5.7A to C). Fibers have a length ranging from less than 30 nm up to 800 nm and can even self-assemble further into a 'helical superstructure', although in a rather disorderly manner (Fig. 5.7B/C).

Additionally, two other superstructures have been found for Ac-X_8-gA: triangles and nanospheres with a diameter of about 100 nm. Nanospheres resemble peptide beads as presented in chapter two,[18] while triangles represent an unexpected structure and experiments that should explain their formation are ongoing. The triangular superstructures have also been demonstrated for peptides ranging from Ac-X_8-gA to K_1X_7-gA (Fig. 5.8).

The analysis of TEM images for peptides with an α-helical character indicates the formation of suprastructures containing worm-like micelles and regular micelles (Fig. 5.7D). Micelles with a radius of 6 ± 1 nm were the major component observed for peptides ranging from K_4X_4-gA to K_8-gA. The excellent solubility of peptides K_3X_5-gA to X_8-gA in aqueous solution is therefore associated with the α-helical secondary structure,

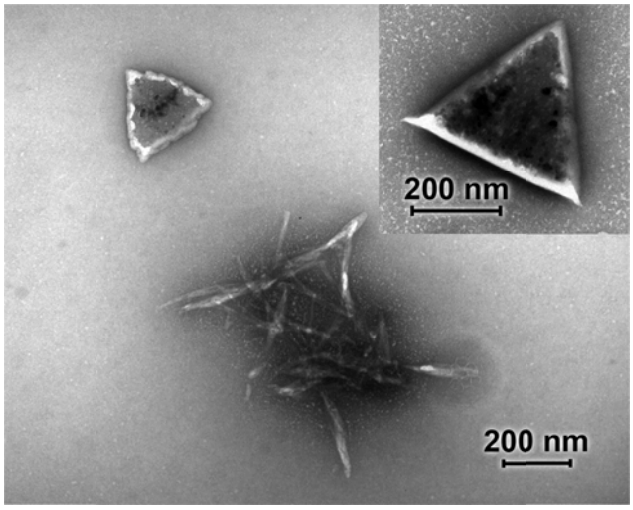

Fig. 5.8 TEM of triangular structures of K_1X_7-gA.

which prevents the creation of intermolecular hydrogen-bonds and therefore favors the formation of micelles. Peptide nanoparticles have also been observed for these peptides, but at a significantly lower fraction than that of the micellar.

5.2.3. Degree of acetylation influences micelle behavior

In order to gain greater insight into the behavior of micelles we used DLS in combination with ζ -potential, which provides information on the superstructures and their surface charges. DLS of K_3X_5-gA to K_8-gA revealed, in addition to micelles, another superstructure population. In combination with TEM images, we determined that micelles at a size of 7 ± 3 nm represent the major component, while the second population – assigned to peptide nanoparticles at a radius of 50 nm – represents only a minor component.

Peptide particles and micelles exhibit a hydrodynamic radius that does not depend on either the degree of acetylation (DA 3/9 to 9/9) or on the peptide concentration (0.1 – 1.28 mg mL^{-1}). Similarly, the ζ-potential did not change upon varying the DA and concentration. Because the peptide nanoparticle population is a minor component, we neglected its influence on the ζ-potential, and only the micelle population has been taken into account. As illustrated in Fig. 5.9, ζ -potential values lie between 52 and 64 mV and are comparable to values obtained for a saturated polylysine surface (60 to 80 mV).[27] Aggregation of the amphiphiles into micelles governs the surface charge, and likely limits the aggregation number and dissociation of the lysine-counter ions.

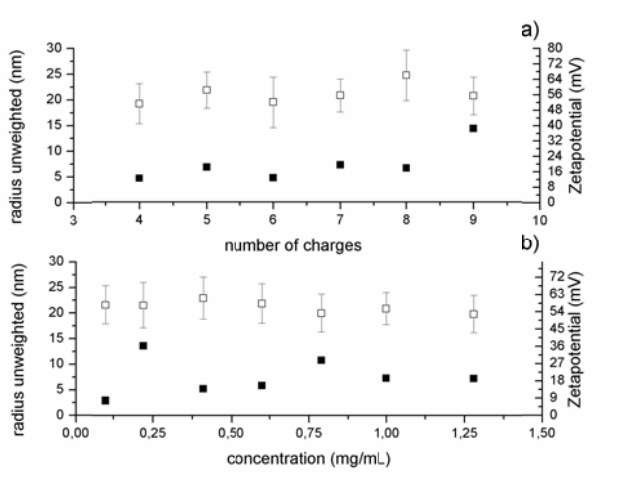

Fig. 5.9 Hydrodynamic radius obtained from DLS (■) and ζ-potential values (□) for micellar species of a) K_3X_5-gA to K_8-gA and of b) K_6X_2-gA for different concentrations.

Therefore, the surface charge and consequently the ζ-potential values were basically independent of the number of amine-groups and peptide concentration. However, it is known that micelle formation depends on the amphiphile concentration and environmental conditions that include pH, T, buffer and ionic strength.[28] In this respect we noted with interest that the impact of DA on micelle formation could hardly be detected by DLS and the ζ-potential and therefore we performed tensiometric measurements for peptides ranging from K_3X_5-gA to K_8-gA. Amphiphiles decrease the surface tension of water with increasing concentration until a critical micelle concentration (cmc) is reached and excess molecules are assembled mainly into micelles. The process of micelles formation for K_3X_5-gA to K_6X_2-gA can be followed in Fig. 5.10A-D. Cmc values calculated for these peptides both in H_2O and in buffer (pH = 7.4) indicate no difference related to the solvent for peptides ranging from K_3X_5-gA to K_5X_3-gA, while starting with K_6X_2-gA a different behavior was observed (Fig. 5.10D). In water, the cmc increased slightly with the number of charges/molecule for the whole series of peptides, and a plateau was obtained starting with K_6X_2-gA. In buffer, the cmc value for K_6X_2-gA represents a maximum, which is followed by a strong decrease of the cmc values upon increasing the number of charges/molecule. From K_3X_5-gA (DA 5/9) to K_6X_2-gA (DA 3/9) – with all peptides exhibiting the same hydrophobic gA part – the self-assembly was driven by the hydrophilic part, indicated by an equal rise in cmc per charge for both solvent media. The reason for the plateauing of the cmc for dd H_2O with decreasing DA might be

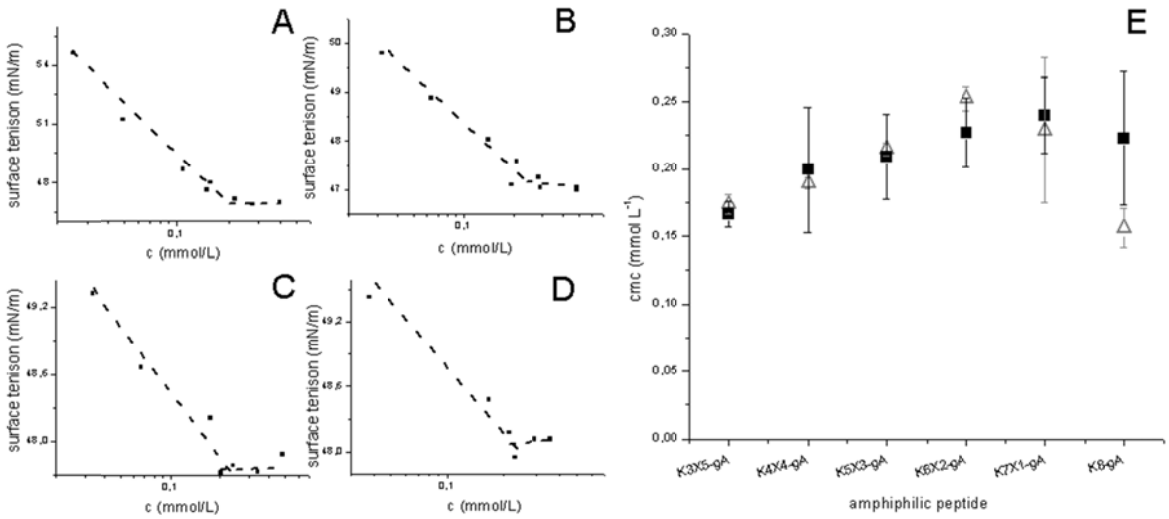

Fig. 5.10 Surface tension of aqueous peptide solutions of A) K_3X_5-gA B) K_4X_4-gA C) K_5X_3-gA D) K_6X_2-gA. E) Cmc of peptides in H_2O (■) and in buffer, pH = 7.4 (△).

due to incomplete dissociation of the amine functionalities – defining the surface charge of the micelles. It is known that increasing the salt concentration of the media induces a decrease in the cmc, as reported for sodium alkyl sulphates[29] or 1-oleoyl-lysophosphatidic acid.[30] The presence of ions serves to shield the negative charges of neighboring headgroups, and thus favors micelle formation, *i.e.* leads to decreasing cmcs. However, comparing measurements in dd H_2O and in buffer solution, the decrease in cmcs in buffer were only observed for K_7X_1-gA and K_8-gA and was coincident with the plateauing cmc values in dd H_2O. Therefore counter ion exchange, from hydroxide to multivalent ions and organic buffer ions (EDTA, TRIS) is likely to account for this decrease in cmc. Similar to other systems,[31] the presented responsiveness towards ionic strength may find usage in biomedical applications.

5.3. Conclusion

We designed a library of amphiphilic peptides (Ac-X_8-gA to K_8-gA) containing three parts: (a) a charged lysine part (b) an acetylated lysine part, and (c) a hydrophobic gA, whereby the overall amphiphilicity is reflected in and controlled by the degree of acetylation or number of charges, respectively.

A basic structural change was located between DA of 6/9 (K_2X_6-gA) and 5/9 (K_3X_5-gA). Variation of the primary sequence caused a transition in the secondary structure of the hydrophilic part from β-sheet to α-helix. This switch-over was found to be responsible for the change in morphology from fibres to micelles *i.e.* the secondary

structure was a function of the degree of acetylation. These morphological changes suggested based on solubility testing, and were confirmed by CD and TEM measurements.

An additional change in properties was observed with a DA of less than 2/9, beyond which a reduction in cmc in buffer took place. A lower DA of 2/9 obviously has a negligible impact on self-assembly but provides means to regulate the system, *e.g.* adjustment of the cmc by adding salt.

The peptide library can be divided into two main regions at high DA (9/9 to 6/9) we found β-sheet-like secondary structures that correlated with fiber formation on the macroscopic scale and, at moderate and high DA (5/9 to 0/9), the peptides possessed an α-helical-like secondary structure and assembled into micelles. A second, minor population was found in both regions, and was assigned to peptide nanoparticles. Point mutation allowed us to tune the hydrophilic part of an amphiphilic peptide and we were thereby able to localize the origin of differences in morphologies and behavior on a molecular level. We highlighted the importance of the secondary structure for the hydrophilic part (α -helix, β -sheet) as a crucial parameter for the self-assembly. Similarly, the alternating D, L configured gA-sequence is essential for the induction of self-assembly due to its hydrophobic contribution.

This study represents a first step towards the creation of molecular switches such as we find in nature, where proteins are converted into the active or inactive state by structural changes upon phosphorylation. Here – a proof of concept – acetylation of K_3X_5-gA to K_2X_6-gA converted water soluble micelles into water insoluble fibres. Creation of an *in situ* reversible acetylation should be the next logical step and could open the door to new biomimetic smart materials and biomedical applications.

5.4. References

[1] A. Carlsen and S. Lecommandoux, *Curr. Opin. Colloid Interface Sci.* **2009**, *14*, 329-339.
[2] A. Taubert, A. Napoli and W. Meier, *Curr. Opin. Chem. Biol.* **2004**, *8*, 598-603.
[3] S. Belegrinou, J. Dorn, M. Kreiter, K. Kita-Tokarczyk, E.-K. Sinner and W. Meier, *Soft Matter* **2009**, *6*, 179-186.
[4] a) A. Koide, A. Kishimura, K. Osada, W.-D. Jang, Y. Yamasaki and K. Kataoka, *J. Am. Chem. Soc.* **2006**, *128*, 5988-5989; b) V. Balasubramanian, O. Onaca, R. Enea, D. W. Hughes and C. G. Palivan, *Expert Opinion on Drug Delivery* **2010**, *7*, 63-78; c) K. Kita-Tokarczyk, J. Grumelard, T. Haefele and W. Meier, *Polymer* **2005**, *46*, 3540-3563.
[5] W. R. Veatch and E. R. Blout, *Biochemistry* **1974**, *13*, 5257-5264.

[6] E. P. Holowka, V. Z. Sun, D. T. Kamei and T. J. Deming, *Nat. Mater.* **2007**, *6*, 52-57.
[7] J. Rao, Z. Luo, Z. Ge, H. Liu and S. Liu, *Biomacromolecules* **2007**, *8*, 3871-3878.
[8] a) S. Ghosh, S. K. Singh and S. Verma, *Chem. Commun. (Cambridge, U. K.)* **2007**, 2296-2298; b) J. Lin, J. Zhu, T. Chen, S. Lin, C. Cai, L. Zhang, Y. Zhuang and X.-S. Wang, *Biomaterials* **2009**, *30*, 108-117.
[9] W. C. Chan, P. D. White and Editors, *Fmoc Solid Phase Peptide Synthesis: A Practical Approach*, **2000**, p. 346 pp.
[10] a) S. G. Zhang and X. J. Zhao, *J. Mater. Chem.* **2004**, *14*, 2082-2086; b) S. G. Zhang, *Nat. Biotechnol.* **2003**, *21*, 1171-1178.
[11] G. von Maltzahn, S. Vauthey, S. Santoso and S. Zhang, *Langmuir* **2003**, *19*, 4332-4337.
[12] D. J. Adams, K. Holtzmann, C. Schneider and M. F. Butler, *Langmuir* **2007**, *23*, 12729-12736.
[13] F. Qiu, Y. Chen and X. Zhao, *J. Colloid Interface Sci.* **2009**, *336*, 477-484.
[14] N. Wiradharma, Y. W. Tong and Y.-Y. Yang, *Macromol. Rapid Commun.* **2010**, *31*, 1212-1217.
[15] T. Hashimoto, R. Iwase, A. Murakami and T. Yamaoka, *Polym. Degrad. Stab.* **2009**, *94*, 1349-1353.
[16] M. Nakano, J.-R. Shen and K. Kamino, *Biomacromolecules* **2007**, *8*, 1830-1835.
[17] J. N. Shera and X. S. Sun, *Biomacromolecules* **2009**, *10*, 2446-2450.
[18] T. Schuster, D. de Bruyn Ouboter, E. Bordignon, G. Jeschke and W. Meier, *Soft Matter* **2010**, 6, (21), 5596-5604.
[19] B. A. Wallace, *Biophys. J* **1986**, *49*, 295-306.
[20] L. E. Townsley, W. A. Tucker, S. Sham and J. F. Hinton, *Biochemistry* **2001**, *40*, 11676-11686.
[21] a) A. K. Khandpur, S. Foerster, F. S. Bates, I. W. Hamley, A. J. Ryan, W. Bras, K. Almdal and K. Mortensen, *Macromolecules* **1995**, *28*, 8796-8806; b) A. Laschewsky, *Curr. Opin. Colloid Interface Sci.* **2003**, *8*, 274-281; c) N. S. Cameron, A. Eisenberg and G. R. Brown, *Biomacromolecules* **2002**, *3*, 124-132.
[22] a) N. Greenfield and G. D. Fasman, *Biochemistry* **1969**, *8*, 4108-4116; b) C. Toniolo, A. Polese, F. Formaggio, M. Crisma and J. Kamphuis, *J. Am. Chem. Soc.* **1996**, *118*, 2744-2745.
[23] a) J. D. Tovar, R. C. Claussen and S. I. Stupp, *J. Am. Chem. Soc.* **2005**, *127*, 7337-7345; b) A. M. Ruschak and A. D. Miranker, *J. Mol. Biol.* **2009**, *393*, 214-226; c) S. Gilead and E. Gazit, *Angew. Chem., Int. Ed.* **2004**, *43*, 4041-4044.
[24] A. V. Mikhonin, N. S. Myshakina, S. V. Bykov and S. A. Asher, *J. Am. Chem. Soc.* **2005**, *127*, 7712-7720.
[25] C. Dittrich and W. Meier, *Macromol. Biosci.* **2010**, *10*, 1406-1415.
[26] B. A. Wallace, *J. Struct. Biol.* **1998**, *121*, 123-141.
[27] S. Tanimoto, T. Iwata, H. Yamaoka, M. Yamada and K. Kobori, *Res. Lett. Mater. Sci.* **2009**, No pp. given.
[28] a) A. Ponta and Y. Bae, *Pharm. Res.* **2010**, *27*, 2330-2342; b) Y. Jin, X.-D. Xu, C.-S. Chen, S.-X. Cheng, X.-Z. Zhang and R.-X. Zhuo, *Macromol. Rapid Commun.* **2008**, *29*, 1726-1731; c) G. Gunnarsson, B. Joensson and H. Wennerstroem, *J. Phys. Chem.* **1980**, *84*, 3114-3121; d) M. R. Dreher, A. J. Simnick, K. Fischer, R. J. Smith, A. Patel, M. Schmidt and A. Chilkoti, *J. Am. Chem. Soc.* **2008**, *130*, 687-694.
[29] M. Venanzi, G. Pace, A. Palleschi, L. Stella, P. Castrucci, M. Scarselli, M. De Crescenzi, F. Formaggio, C. Toniolo and G. Marletta, *Surf. Sci.* **2006**, *600*, 409-416.
[30] Z. Li, E. Mintzer and R. Bittman, *Chem. Phys. Lipids* **2004**, *130*, 197-201.

[31] F. Checot, A. Brulet, J. Oberdisse, Y. Gnanou, O. Mondain-Monval and S. Lecommandoux, *Langmuir* **2005**, *21*, 4308-4315.

6. Exploiting dimerization of purely peptidic amphiphiles to form vesicles

Thomas B. Schuster, Dirk de Bruyn Ouboter, Nico Bruns, Wolfgang Meier

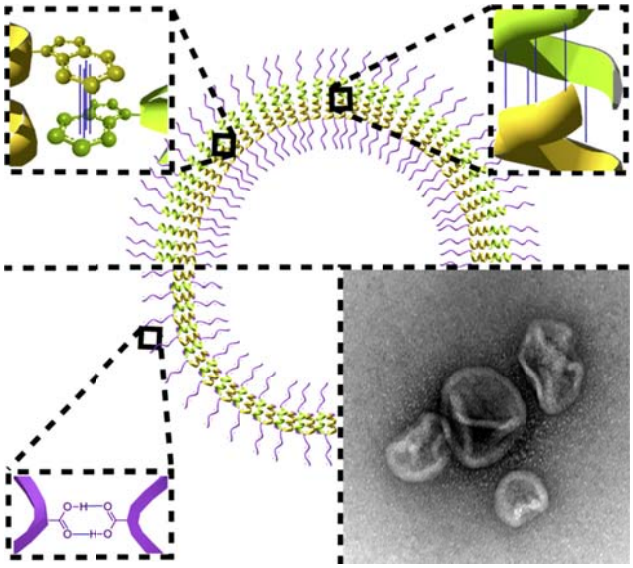

Scheme of peptide vesicle stabilization through Trp-Trp interactions (π-π-stacking), gA-OEt-dimerization, or carboxyl dimerization.

Reprinted in parts with permission from: *Small* **2011**, DOI: 10.1002/smll.201100701

6.1. Introduction

Medicine in the future will make use of drug delivery systems (DDSs) that transport drugs directly to a targeted tissue. To maximize drug efficacy and minimize side effects, the active substance should be segregated from physiological fluids during circulation, for example by cargo encapsulation. One morphology in focus for such an application are vesicles that self-assemble from amphiphilic building blocks, such as lipids,[1] block copolymers,[2] and block copolypeptides[3] – amino acid (AA) analogues of block copolymers. These vesicles can entrap a drug payload in their aqueous cavities or in the hydrophobic leaflet of their membranes and thus transport the payload through the blood stream. However, peptide vesicles are rarely reported in literature.[4][5] Here we present vesicles using responsive, purely peptidic amphiphiles, designed to interact specifically with one another. These vesicles showed pH responsiveness and ability to encapsulate different fluorophores.

Materials based on AAs are preferred for applications in the human body due to the fact that AAs are intrinsic body components and therefore generally considered biocompatible and biodegradable; therefore these peptide vesicles may find application as new advanced drug delivery systems. Peptide degradation pathways that are intrinsic to the body eliminate the problem of accumulation, especially for patients undergoing long-term therapy. Moreover, peptides can be designed to fold into well-ordered secondary structures, and AAs offer a diversity of functional groups that can be used as chemical handles to create selectively-labeled nanostructures.

Deming et al.[6] and Lecommandoux et al.[7] reported vesicles formation using peptide-based amphiphilic block copolymers synthesized by ring-opening polymerization of N-carboxy anhydrides (NCAs). This technique was also used to synthesize a variety of peptide-based polymers[8] and combine them with synthetic polymers to obtain block copolymer hybrids. A diversity of self-assembling bioconjugates exist which have been shown to be useful in the field of material science, e.g. bio-medical applications.[9] A drawback of such polymers is their synthesis via polymerization, which does not allow the creation of block copolypeptides with a defined sequence of amino acids.

On the other hand, peptides can be precisely synthesized by bioengineering techniques or solid-supported peptide synthesis (SPPS). Short peptides are well-suited to control and direct the self-assembly of amphiphiles into higher order structures such as

micelles and vesicles, e.g. by exchanging a single AA. The use of peptide-polymer hybrids can lead to the formation of superstructures such as vesicles,[10] also in coexistence with large compound micelles[11] and nanofibers.[12] Creating the necessary hydrophobic block using peptides, however, proved a difficult task, due to the hydrophilic character of the peptide backbone. Thus, not many suitable hydrophobic blocks exist.

Examples of amphiphilic short peptides that were successfully designed to assemble into membranes and vesicles have therefore rarely been reported: Zhang et al.[4] reported self-assembled superstructures which, however, proved to be highly sensitive to the purity of the peptide.[13] The driving force for membrane formation, the segregation in solvophobic blocks, is not strong enough due to insufficient, non-homogeneous hydrophilic and hydrophobic surfaces. Mastrobattista et al.[5] reported recombinatly produced amphiphilic peptides with an additional conical geometry of the hydrophobic part that directs the self-assembly towards nano-sized vesicles. However the polyproline II (PP II) secondary structure displays the hydrophilic backbone and therefore lacks a completely hydrophobic part.

We present an approach to limit the influence of the hydrophilic backbone. Additionally we used localized specific points of non-covalent binding, between the short peptides in order to stabilize a formed membrane. Another key parameter, besides $\pi-\pi$ stacking is intermolecular hydrogen bonding, involved in supramolecular assemblies [12][14] that include β-sheet[9d, 15] or cyclic peptides.[16] We investigate the

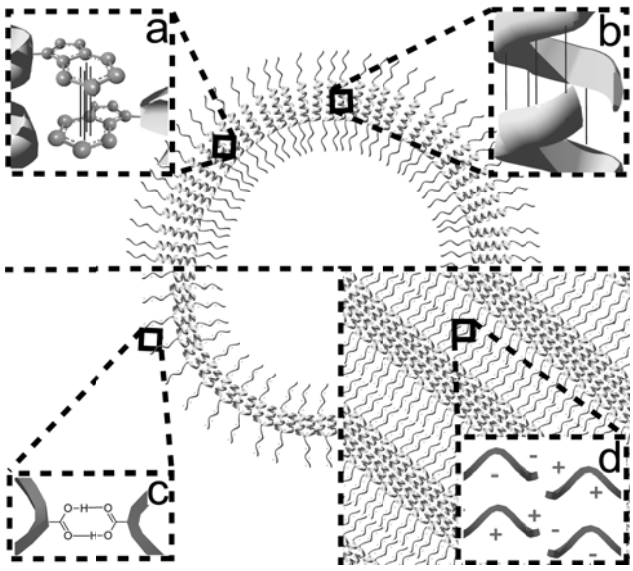

Scheme 6.1 Vesicle stabilization through: a) Trp-Trp interactions (π-π-stacking); b) gA-OEt-dimerization; c) carboxyl dimerization and d) charge compensation.

requirements posed in the formation of peptide vesicles. By providing different potential dimerization sites in addition to the intrinsic inter- and intramolecular π–π stacking of tryptophan-rich domains (Scheme 6.1a), we expected that additional interactions by such sites would induce and stabilize bilayer formation. The amphiphilic peptides in this work were designed to allow for dimerization perpendicular to the membrane via tail-to-tail dimerization (Scheme 6.1b), or by lateral association of two peptides, via carboxyl dimerization (Scheme 6.1c), or by charge compensation of oppositely charged hydrophilic components (Scheme 6.1d).

Amphiphilic design is fundamental to every supramolecular aggregation, whether in the form of micelles, tubes or vesicles. A hydrophilic to hydrophobic AA ratio of about 1:3 is comparable to lipids and appears to be favorable for membrane formation.[17]

Thus, we chose the hydrophilic to hydrophobic ratio in our amphiphilic peptides accordingly. The hydrophobic part was inspired by gramicidin A (gA). This pentadecapeptide, known as antibiotic for gram positive bacteria, features an alternating D, L configuration, leading to a α-helix from which all of the hydrophobic side chains project outwardly.[18] The surface of the helix, i.e. the rod, is therefore hydrophobic and the hydrophilic backbone is hidden within. Gramicidin A is a membrane peptide that can assemble and form patterns that are thought to stabilize both inter- and intra-molecularly by π–π stacking of the tryptophan-rich domains.[19] Gramicidin A is insoluble

Table 6.1 Code and sequence of the amphiphilic peptides.

Code	Sequence[a]
Ac-X_8-gA	*Ac*-[LK(Ac)]$_2$-G-[LK(Ac)]$_3$-G-[LK(Ac)]$_3$-LV-G-LA-DL-LA-DV-LV-DV-[LW-DL]$_3$-LW-*NH*$_2$
Ac-X_8-gA-OEt	*Ac*-[LK(Ac)]$_2$-G-[LK(Ac)]$_3$-G-[LK(Ac)]$_3$-LV-G-LA-DL-LA-DV-LV-DV-[LW-DL]$_3$-LW-*OEt*
Ac-E_6-gA	*Ac*-LE$_3$-G-LE$_3$-LV-G-LA-DL-LA-DV-LV-DV-[LW-DL]$_3$-LW-*NH*$_2$
Ac-K_6-gA	*Ac*-LK$_3$-G-LK$_3$-LV-G-LA-DL-LA-DV-LV-DV-[LW-DL]$_3$-LW-*NH*$_2$

[a] one letter code, X = LK(Ac)

Table 6.2 Peptide masses and purity.

Code[a]	Mass[b] (g mol^{-1})	Mass (MALDI-TOF-MS)	Purity[c]
Ac-X_8-gA	3328.1	3329.9	>99.5%*
Ac-X_8-gA-OEt	3358.1	3357.1	>99.5%*
Ac-E_6-gA	2684.0	2682.5	95%
Ac-K_6-gA	2678.3	2677.4	96%

[a] one letter code with abbreviations for gramicidin (gA), acetylated lysine (X) and acetylated N-terminus (Ac) [b] calculated with Pinsoft2 [c] Area % on an analytical RP-HPLC [*] HPLC purity from precursor K_8-gA.

in aqueous solution and forms dimers in lipid bilayers. A truncated version (gT) of gA was recently shown by our group to be effective as a hydrophobic contributor in an amphiphilic peptide, and led to self-assembled structures such as micelles and solid peptide particles.[20] However, these peptides did not form vesicles, presumably because they lacked the opportunity to form dimers.

For this work we synthesized new, short, amphiphilic peptides 22 and 25 AAs in length with a predefined sequence by means of SPPS. The produced amphiphilic peptides are shown in Table 6.1. They were examined in terms of whether they formed vesicles by using TEM, CryoTEM, and static- and dynamic light scattering techniques (SLS/DLS).

6.2. Results and discussion

6.2.1. Tail-to-tail dimerization

Tail-to-tail dimerization that results from the formation of hydrogen-bonds between corresponding amino acids in the final turn of the helix is known from wild-type gA (Scheme 1b).[18] Therefore GPC leads to a separation into a monomer and dimer peak. Ac-X_8-gA exhibits a C-terminal amide function on the hydrophobic end, which decreases the probability of tail-to-tail dimerization,[20] most probably due to non-matching hydrogen bond partners, accompanied by reduced hydrophobic interactions.

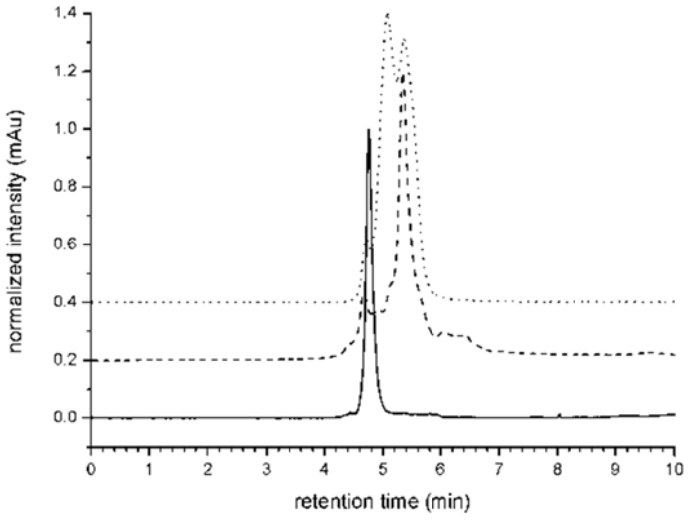

Fig. 6.1 GPC of monomeric Ac-X_8-gA (dashed line) and dimerized Ac-X_8-gA-OEt (solid line) compared with the dimer and monomer peaks of wild-type gramicidin A (dotted line).

Consequently, GPC showed only a single peak (Fig. 6.1). Similar Ac-X_8-gA-OEt dimers are eluted earlier compared to Ac-X_8-gA. Thereby, the mass difference of only 29 g mol^{-1} is negligible.

To increase hydrophobic interactions, an ethoxyl group (OEt) was used to mask the terminal amide function of the amphiphilic peptide. In this way, we eliminated the last remaining hydrophilic moiety on the hydrophobic end of Ac-X_8-gA-OEt, and thus expected the facilitation of tail-to-tail dimerization, which would be perpendicular to the membrane (Scheme 6.1b). Indeed, a decrease in retention time caused by dimerization was found in GPC for the esterified Ac-X_8-gA-OEt (Fig. 6.1). As a result of this modification, vesicle formation was observed for Ac-X_8-gA-OEt, which was not the case for Ac-X_8-gA.[21] Fig. 6.2a shows collapsed vesicles. These resulted from the drying effect on the TEM grid and thereby evidenced that the objects had a hollow structure. Perpendicular (relative to the membrane) dimerization is thought to initiate and lead to membrane association, most likely in a bilayer-type conformation.

6.2.2. Carboxyl dimerization

Another type of dimerization between amino acid residues can be caused by the formation of hydrogen bonds between two carboxylic acids (Scheme 6.1c). Glutamic acid, more precisely the carboxyl functionality thereof, forms dimers and poly(glutamic acids) consequently associate.[22] They can even form a β-structure in a condensed Langmuir-Blodgett film.[23] At neutral pH, oligo- and poly(glutamic acids) are charged and adopt an extended 2.5_1 helix, or polyproline II, conformation.[24] We aimed to exploit this type of

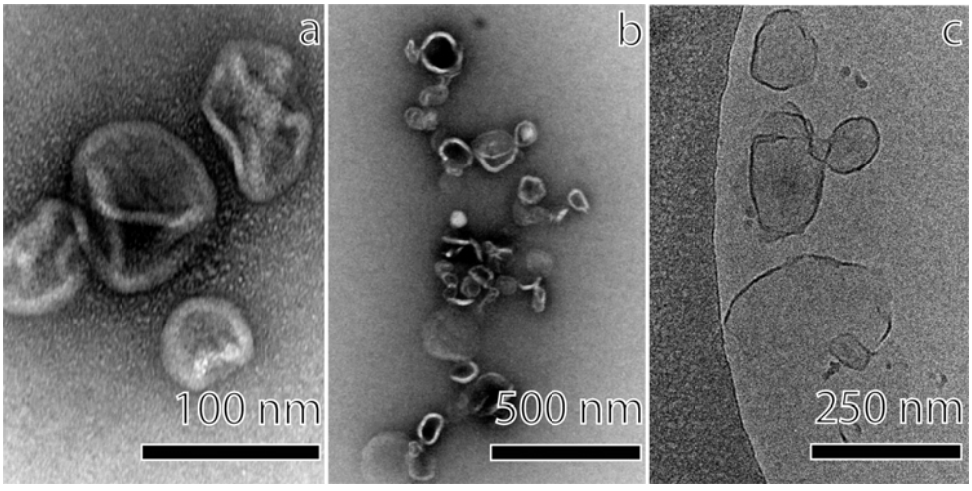

Fig. 6.2 TEM of self-assembled structures of a) Ac-X_8-gA-OEt b) Ac-E_6-gA and c) CryoTEM of Ac-E_6-gA.

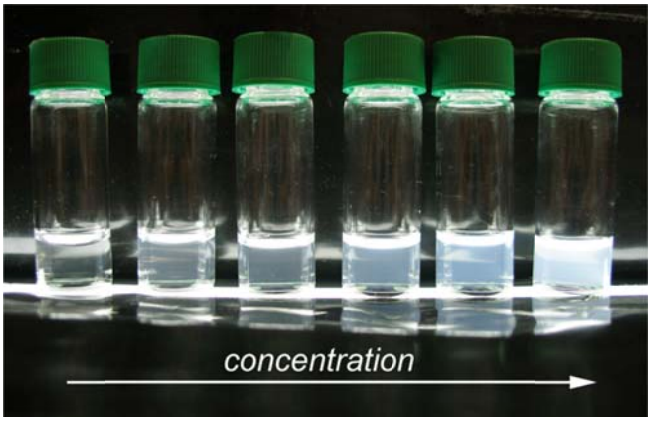

Fig. 6.3 Aqueous Ac-E_6-gA solution of different concentrations.

dimerization of the hydrophilic block by using negatively charged oligoglutamic acid (E, pKa of 4.7) as the hydrophilic component in an amphiphilic peptide Ac-E_6-gA. After allowing the peptide to self-assemble a translucent solution could be observed, a hint for a successful organization (Fig. 6.3).

Indeed, collapsed vesicles were observed when this peptide was allowed to self-assemble, as shown in the TEM micrograph in Fig. 6.2b. That implies that, in fact, a peptide membrane was formed. Crystallization plates usually are used to screen for best protein-crystallization conditions and only request small volumes of sample solution and therefore were used for the self-assembly process as an alternative to dialysis tubes. Dialysis in dialysis tubes is essentially similar, but the vesicles do not completely collapse on the TEM grid. This behavior can likely be attributed to a thicker or more stable membrane, or encapsulated micelles.

In CryoTEM, thin sheet fragments were observed, also illustrating the formation of thin peptide membrane. Its thickness, as deduced from the CryoTEM images, is 5 ± 1 nm. The membrane of the vesicles formed by Ac-E_6-gA cannot be stabilized by dimerization

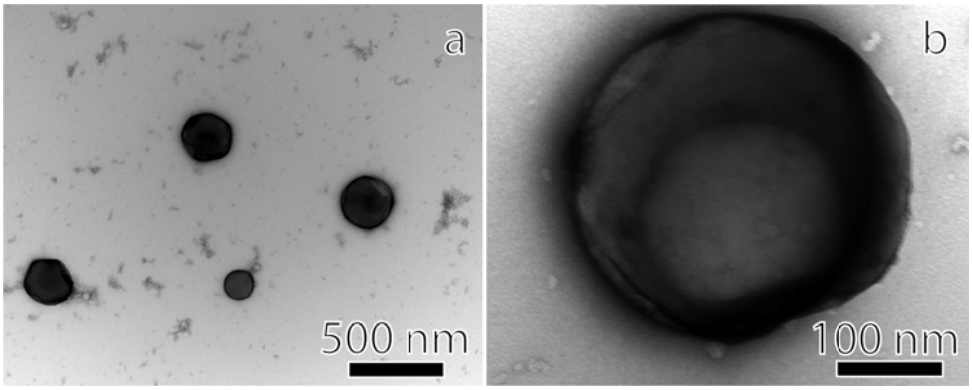

Fig. 6.4 TEM of Ac-E_6-gA self-assembled structures induced by dialysis in tubes.

through the hydrophobic chain ends, as in the case for Ac-X_8-gA-OEt. Thus, the association and dimerization of the hydrophilic blocks are the essential factors that allow the formation of stable Ac-E_6-gA vesicle membranes. Considering the length of an amphiphilic peptide of about 3.7 nm, the measured membrane thickness suggests that the hydrophobic parts of the amphiphiles share one layer instead of forming a bilayer, the expected morphology of membranes formed by Ac-X_8-gA-OEt (Scheme 6.1c).

Light scattering provided further evidence of vesicle formation (Fig. 6.5). Ac-E_6-gA exhibited a radius of gyration (R_g) of 194 nm and a molecular weight (M_w) of$3.3 \bullet 10^8$ g mol^{-1}. A Guinier plot for Ac-E_6-gA is shown in Fig. 6.5a. The measured M_w of the vesicle corresponds to 123,000 aggregated peptide molecules. Assuming the gA helix represents the group that requires the most space (r = 1.5 nm[18c], A = $(2r)^2 \sin 60°$), these values would either fit a peptide bilayer, or a single peptide layer where two gAs form a double helix, a structure also known from wild-type gA.[18] The latter arrangement would also allow two oligoglutamic parts to approach each other to a favorable distance for H-bonding.

R_g, together with the hydrodynamic radius (R_h) of 205 nm from DLS data analysis, permits the calculation of the ρ-parameter (R_g/R_h) – an indicator of the underlying structure – of 0.95. This value is close to the typical value for hollow spheres (1.0),[25] while variances might arise due to the presence of micelles in the system, which would lower the ρ-parameter towards that of micelles (0.75). We found that the dimensions of the vesicles did not depend on the concentration of amphiphilic peptides, as shown by DLS (2^{nd} cumulant fit, 90°), up to a concentration of 0.7 mg mL^{-1}. Above approx. 1 mg mL^{-1} aggregates that were also observed by TEM and CryoTEM were formed (Fig. 6.6).

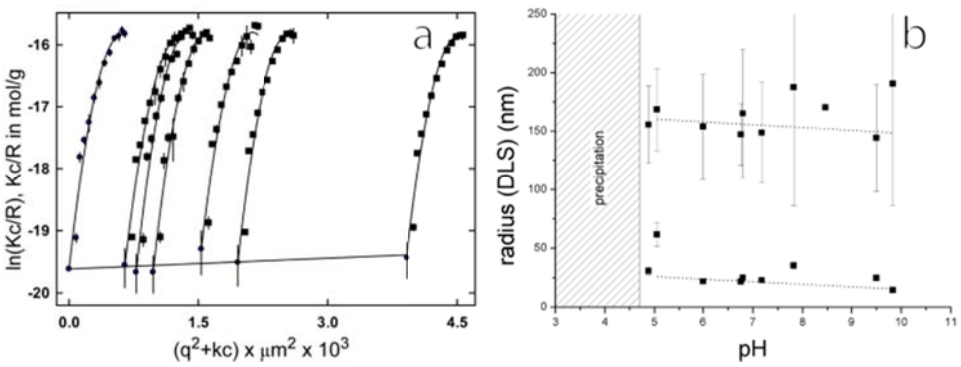

Fig. 6.5 a) Static light scattering analysis (Guinier plot) and b) pH response of Ac-E_6-gA (DLS).

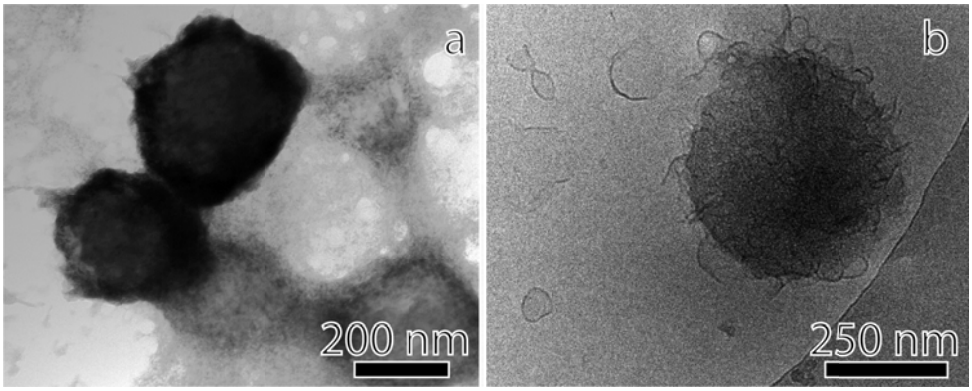

Fig. 6.6 Ac-E_6-gT aggregates formed beyond a concentration of 0.7 mg mL^{-1} in a) TEM and b) CryoTEM.

6.2.3. Charge compensation

We expected that charge compensation would also drive the association of oppositely charged moieties. Mixtures of poly(L-lysine) (PLL) and poly(glutamic acid) (PGA) are known to form a β-sheet-like structure[24a, 26] and to interact electrostatically (Scheme 6.1d).

The amphiphilic peptide Ac-K_6-gA (K = lysine, pKa 10.2), the positively charged analogue of Ac-E_6-gA, exhibits the same amphiphilic design and hydrophilic-to-hydrophobic ratio as Ac-E_6-gA but lacks carboxyl dimerization. Not surprisingly, we found that it assembles into micelles and solid spherical objects, but not into vesicles. However, when mixed with Ac-E_6-gA, it did generate multi-lamellar structures at molar ratios of Ac-K_6-gA between 0.3 to 0.8 (Fig. 6.8). However, even multilamellar vesicles were found near the point of complete charge compensation (0.5); an example is given in Fig. 6.8 j for a molar ratio of 0.6.

Electron micrographs showed a lamellar thickness of 8.3 ± 1.3 nm, which is around double the length of the amphiphiles. Thus, lateral association of neighboring, oppositely

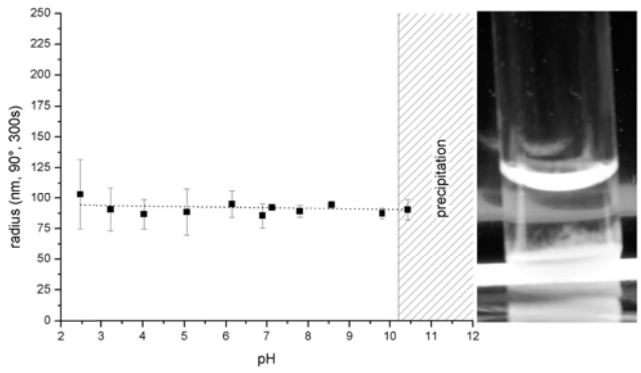

Fig. 6.7 pH response of Ac-K_6-gT (DLS) and a precipitated solution at high pH.

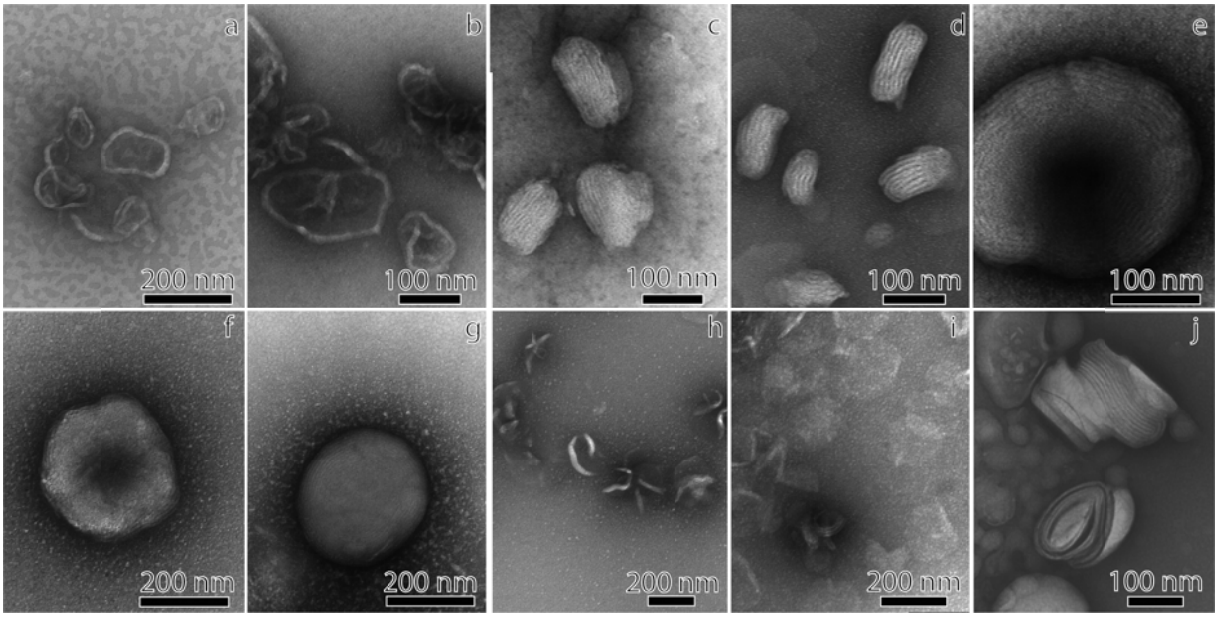

Fig. 6.8 TEM of Ac-E_6-gA and Ac-K_6-gA mixtures with molar ratios of a) 0.1 to i) 0.9 in 0.1 steps; j) multilamellar vesicle at ratio 0.6.

charged hydrophilic peptide blocks induced membrane formation. Moreover, perpendicular dimerization took place despite the hydrophilic chain end of the gA block. The interaction of both types of dimerization resulted in lamellar structures and not in vesicles.

Once vesicles were obtained from short amphiphilic peptides, these peptosomes were explored in preliminary experiments to investigate their use as functional, nano sized containers, *e.g.* for drug delivery. The introduction of pH-sensitive glutamic acid was expected to lead to a pH-responsive 'smart' material. Therefore, the response to a change in acidity was monitored by DLS. The self-assembled structures were stable over.

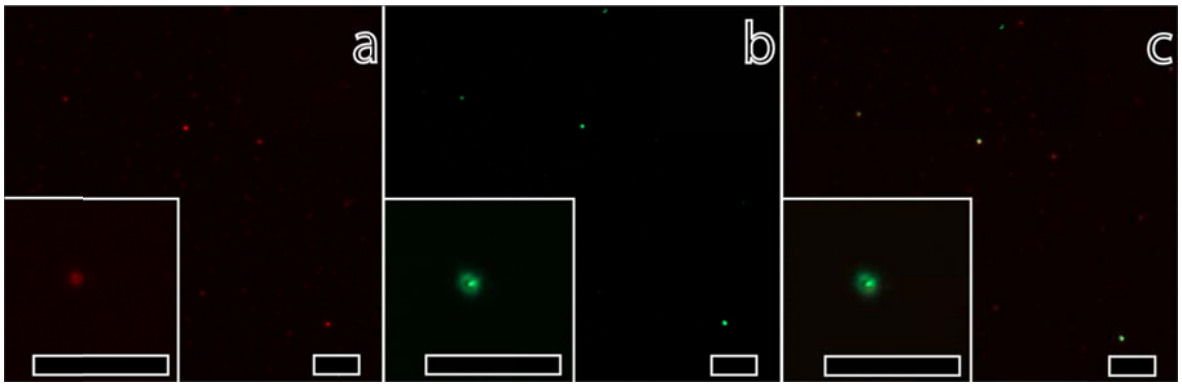

Fig. 6.9 Laser scanning microscopy images of Ac-E_6-gA-based vesicles and micelles loaded with BODIPY 650/665 and Alexa Fluor 488. a) Red fluorescence of the hydrophobic BODIPY, b) Green fluorescence of the hydrophilic Alexa Fluor, and c) overlay, co-localized fluorophores, which indicate vesicles. Scale bars = 10 μm.

a wide range of pH, but they precipitated when the pK_a was exceeded (Fig. 6.5b)

Vesicles possess the potential to encapsulate hydrophilic moieties within their aqueous cores and to integrate hydrophobic compounds within the hydrophobic membrane layers. In an initial trial, we successfully accomplished this, respectively, with hydrophilic Alexa Fluor 488 and hydrophobic BODIPY 650/665 within Ac-E_6-gA assemblies (Fig. 6.9). The co-localization of both fluorophores indicates the presence of vesicles. Not all fluorescent spots that showed fluorescence of the hydrophobic fluorophore showed fluorescence signal in the green channel. Therefore, micelles were also present next to vesicles, because the micelles are also able to accommodate the hydrophobic fluorophore in their cores only.

6.3. Conclusion

In conclusion, we found that additional intermolecular non-covalent bonds and interactions are necessary to stabilize vesicles formed from small amphiphilic peptides. A crucial requirement for the formation of stable peptide membranes appears to be the dimerization of peptides that were specifically designed as amphiphiles (Scheme 6.1). Dimerization in the lateral or perpendicular directions, and thus the formation of a stabilized membrane subunit, produced stable, purely peptidic vesicles and may well apply to other systems.

The novel systems presented here offer hydrophilic and hydrophobic compartments that could encapsulated different drugs and could be used *e.g.* for gene delivery, since the design includes charged moieties.[27] Furthermore, the peptidic vesicles are expected to be biodegradable and thus have great potential as a DDS.

In addition to diffusion, two release mechanisms that stem from intrinsic properties are possible. The first mechanism is natural degradation due to the fact that the materials consist of only 22 naturally occurring AAs; the drug will be released upon degradation of the peptide. Second, release is triggered by pH. Furthermore, multilamellar structures could also increase the loading efficiency of hydrophobic moieties due to increased hydrophobic volume. This behavior also qualifies the materials for an ideal candidate in self-assembly studies and further in application as biocompatible devices.

6.4. References

[1] J. A. Opsteen, J. J. L. M. Cornelissen and J. C. M. van Hest, *Pure Appl. Chem.* **2004**, *76*, 1309-1319.

[2] a) K. Kita-Tokarczyk and W. Meier, *Chimia* **2008**, *62*, 820-825; b) O. Onaca, R. Enea, D. W. Hughes and W. Meier, *Macromol. Biosci.* **2009**, *9*, 129-139; c) C. G. Palivan, C. Vebert, F. Axthelm and W. Meier, **2007**, pp. 32/31-32/26.

[3] A. Carlsen and S. Lecommandoux, *Curr. Opin. Colloid Interface Sci.* **2009**, *14*, 329-339.

[4] a) S. Santoso, W. Hwang, H. Hartman and S. G. Zhang, *Nano Lett.* **2002**, *2*, 687-691; b) S. Vauthey, S. Santoso, H. Gong, N. Watson and S. Zhang, *Proc. Natl. Acad. Sci. U. S. A.* **2002**, *99*, 5355-5360; c) Y.-R. Yoon, Y.-b. Lim, E. Lee and M. Lee, *Chem. Commun. (Cambridge, U. K.)* **2008**, 1892-1894.

[5] a) A. J. van Hell, C. I. C. A. Costa, F. M. Flesch, M. Sutter, W. Jiskoot, D. J. A. Crommelin, W. E. Hennink and E. Mastrobattista, *Biomacromolecules* **2007**, *8*, 2753-2761; b) A. J. van Hell, A. Klymchenko, P. P. Burgers, E. E. Moret, W. Jiskoot, W. E. Hennink, D. J. A. Crommelin and E. Mastrobattista, *J. Phys. Chem. B* **2010**, *114*, 11046-11052.

[6] a) E. G. Bellomo, M. D. Wyrsta, L. Pakstis, D. J. Pochan and T. J. Deming, *Nat. Mater.* **2004**, *3*, 244-248; b) E. P. Holowka, V. Z. Sun, D. T. Kamei and T. J. Deming, *Nat. Mater.* **2007**, *6*, 52-57.

[7] J. Rodriguez-Hernandez and S. Lecommandoux, *J. Am. Chem. Soc.* **2005**, *127*, 2026-2027.

[8] a) K. T. Kim, M. A. Winnik and I. Manners, *Soft Matter* **2006**, *2*, 957-965; b) C. Schatz, S. Louguet, J.-F. Le Meins and S. Lecommandoux, *Angew. Chem., Int. Ed.* **2009**, *48*, 2572-2575.

[9] a) F. Checot, S. Lecommandoux, Y. Gnanou and H.-A. Klok, *Angew. Chem., Int. Ed.* **2002**, *41*, 1339-1343; b) H. Kukula, H. Schlaad, M. Antonietti and S. Forster, *J. Am. Chem. Soc.* **2002**, *124*, 1658-1663; c) J. Lin, J. Zhu, T. Chen, S. Lin, C. Cai, L. Zhang, Y. Zhuang and X.-S. Wang, *Biomaterials* **2009**, *30*, 108-117; d) J.-F. Lutz and H. G. Boerner, *Prog. Polym. Sci.* **2008**, *33*, 1-39; e) J. Sun, C. Deng, X. Chen, H. Yu, H. Tian, J. Sun and X. Jing, *Biomacromolecules* **2007**, *8*, 1013-1017.

[10] S. Kimura, D.-H. Kim, J. Sugiyama and Y. Imanishi, *Langmuir* **1999**, *15*, 4461-4463.

[11] L. Ayres, P. Hans, J. Adams, D. W. P. M. Loewik and J. C. M. van Hest, *J. Polym. Sci., Part A Polym. Chem.* **2005**, *43*, 6355-6366.

[12] H. A. Behanna, J. J. J. M. Donners, A. C. Gordon and S. I. Stupp, *J. Am. Chem. Soc.* **2005**, *127*, 1193-1200.

[13] D. J. Adams, K. Holtzmann, C. Schneider and M. F. Butler, *Langmuir* **2007**, *23*, 12729-12736.

[14] E. Jahnke, I. Lieberwirth, N. Severin, J. P. Rabe and H. Frauenrath, *Angew. Chem., Int. Ed.* **2006**, *45*, 5383-5386.

[15] V. Castelletto, G. E. Newby, Z. Zhu, I. W. Hamley and L. Noirez, *Langmuir* **2010**, *26*, 9986-9996.

[16] a) R. Gokhale, J. Couet and M. Biesalski, *Phys. Status Solidi A* **2010**, *207*, 878-883; b) S. Loschonsky, J. Couet and M. Biesalski, *Macromol. Rapid Commun.* **2008**, *29*, 309-315.

[17] J. Yoon, M. Ree, Y. Hwang, S. W. Lee, B. Lee, J.-S. Kim, H. Kim and S. N. Magonov, *Langmuir* **2004**, *20*, 544-549.

[18] a) R. Sarges and B. Witkop, *J. Am. Chem. Soc.* **1965**, 2027-2030; b) D. W. Urry, *Proc. Natl. Acad. Sci. U. S. A.* **1971**, *68*, 672-676; c) B. A. Wallace, *Biophys. J* **1986**, *49*, 295-306.

[19] a) R. Brasseur, J. A. Killian, B. De Kruijff and J. M. Ruysschaert, *Biochim. Biophys. Acta, Biomembr.* **1987**, *903*, 11-17; b) M. Diociaiuti, F. Bordi, A. Motta, A. Carosi, A. Molinari, G. Arancia and C. Coluzza, *Biophys. J.* **2002**, *82*, 3198-3206.
[20] T. B. Schuster, D. de Bruyn Ouboter, E. Bordignon, G. Jeschke and W. Meier, *Soft Matter* **2010**, *6*, 5596-5604.
[21] T. Schuster, D. de Bruyn Ouboter, C. Palivan and W. Meier, *manuscript preparation* **2010**.
[22] a) T. Makovec, *Biochem. Mol. Biol. Educ.* **2000**, *28*, 244-247; b) E. J. Spek, Y. Gong and N. R. Kallenbach, *J. Am. Chem. Soc.* **1995**, *117*, 10773-10774.
[23] N. Higashi, M. Shimoguchi and M. Niwa, *Langmuir* **1992**, *8*, 1509-1510.
[24] a) A. V. Mikhonin, N. S. Myshakina, S. V. Bykov and S. A. Asher, *J. Am. Chem. Soc.* **2005**, *127*, 7712-7720; b) A. L. Rucker and T. P. Creamer, *Protein Sci.* **2002**, *11*, 980-985.
[25] O. Stauch, R. Schubert, G. Savin and W. Burchard, *Biomacromolecules* **2002**, *3*, 565-578.
[26] F. Boulmedais, M. Bozonnet, P. Schwinte, J. C. Voegel and P. Schaaf, *Langmuir* **2003**, *19*, 9873-9882.
[27] J. H. Jeong and T. G. Park, *J. Controlled Release* **2002**, *82*, 159-166.

7. Experimental part

7.1. Materials

Materials and reagents were of the highest commercially available grade and were used without further purification, unless indicated. HCTU, Rink Amide AM resin (0.61 mmol g^{-1}) and Fmoc-Trp(Boc)-OH were purchased from IRIS Biotech GmbH. All other amino acids and succinimidyl ester activated dyes were obtained from Novabiochem. Dichloromethane and ethanol (96%) F15 were provided by Brenntag Schweizerhall AG, DMF by J. T. Baker and acetonitrile (ACN) by Fischer Scientific. DMF was treated with aluminum oxide to reduce free amines prior to use in peptide synthesis. Solvent exchange was carried out in 24-well sitting-drop crystallization plates (HR3-158, Hampton Research) or by dialysis (Spectrum, cellulose esther (CE), MWCO = 500 - 1000 Da) against double-distilled water (dd H_2O). Remaining chemicals were purchased from Sigma-Aldrich. Dppc was purchased from Avanti-Lipids Inc. Template stripped gold (TSG) substrates were prepared as described elsewhere.[1]

7.2. Amphiphilic peptides design and synthesis

All *peptides* were synthesized on a Syro I Peptide Synthesizer (MultiSynTech GmbH, Witten, Germany) on solid-phase using Fmoc-strategy. 2-(6-chloro-1H-benzotriazole-1-yl)-1,1,3,3-tetramethylaminium hexafluorophosphate (HCTU) as the coupling reagent and N-ethyldiisopropylamine (DIPEA) dissolved in N-methyl-2-pyrrolidone (NMP) as the base were used to couple α-N-Fmoc-protected amino acids to the resins (220 mg). For elongation, Fmoc-Xxx-OH (0.5 mol L^{-1}, 4 equiv.), HCTU (0.5 mol L^{-1}, 4 equiv.) dissolved in dimethylformamide (DMF), and DIPEA (12 equiv.) were added to the resin. The mixture was agitated for 1 h and washed with DMF (3x3 mL). Fmoc deprotection was performed with 20% piperidine in DMF followed by 3 min agitation, draining, and repetition of deprotection for 10 min. Resin was subsequently washed with DMF (5x3 mL). Acetylation of unreacted amine groups was performed following each coupling using acetic anhydride/DIPEA (3 mol L^{-1}, 5 equiv.) in DMF. After synthesis, the peptide resin was washed alternating with DMF (3x6 mL), isopropanol (3x6 mL), and dichloromethane (3x6 mL), and dried under vacuum.

Cleavage from the resin and removal of protective groups was performed with a

mixtures of 95% trifluoroacetic acid (TFA), 2.5% triisopropylsilane, and 2.5% H_2O and of 94% trifluoroacetic acid (TFA), 2.5% triisopropylsilane, 2.5% ethandithiol and 1% H_2O for cysteine containing peptides. The cleavage cocktail was filtered and resin was washed additional two times with cold cleavage cocktail (2 mL) and precipitated in 40 mL cold diisopropylether (IPE). The precipitated crude peptide was washed with cold IPE three times by centrifugation and decantation, before being dried under vacuum.

Hydrophobicity was calculated with Pinsoft32 (Chiron Technologies Pty Ltd., Australia) which uses the hydrophobicity algorithm from Fauchere & Pliska[2] (for X = Lys (Ac) a value of - 0.55 was used[3]).

7.3. Peptide purification, post-modification and characterization

Purification and analysis of the peptides were carried out by HPLC (Shimadzu Prominence 20A, Japan) on reverse phase (RP) columns (Merck Chromolith, RP-18e, 100 mm x 10 mm and 100 mm x 4.6 mm) by dissolving the peptide crude product in DMF and keeping it at its solubility limit by adding the corresponding buffer (solvent B) and ACN (solvent A). Two runs were necessary to yield sample purities higher than 95% as detected by absorption at 280 nm and 488 nm in case of fluorescently labeled peptides. Linear gradients of solvent A (ACN) and solvent B (0.1% TFA, 2 % AcOH or 0.23% formic acid in dd H_20) (example given in Fig. 2.13) were used.

AcC-X_3-gT and C-K_3-gT disulfides were reduced with 1,3-propanedithiol (5 equiv.) in methanol or tris(2-carboxyethyl)phospine (5 equiv.) in water/ACN solution before the second run. The eluted sample was collected in fixed volume fractions which were subsequently analyzed for purity and molecular weight. Fractions exceeding 95% purity were pooled before neutralization with ammonia and lyophilized.

N-terminal acetylation was performed after the completed reaction of Ac-E_6-gA/Ac-K_6-gA with 30 equiv. of Ac_2O/DIPEA for one hour. Ac-X_8-gA, the precursor for Ac-X_8-gA-OEt, was synthesized by post purification acetylation from K_8-gA.

Purification of Ac-E_6-gA was carried out by HPLC on a PRP-3 column (10 µm 300 Å, 4.1 x 250 mm, Hamilton) for peptide/protein/DNA purification. Two runs were necessary to reach a purity of > 95% detected at 280 nm. Conditions used were ACN/0.5% aqueous TRIS·HCl solution (pH 7) and ACN/50 mM NH_4OAc/HOAc (pH 7). Final fractions with confirmed masses and purities of at least 95% were unified, neutralized with ammonia and lyophilized, yielding a white, fluffy powder. Ac-X_8-gA-OEt was prepared by

transesterification of the Ac-X_8-gA amide in ethanol/0.1 M HCl at 70°C for 3 x 10 min and intermediate ultrasonic treatment for 3 x 30 s at 70 °C. Table 6.2 presents mass confirmation by MALDI-TOF-MS.

Post-functionalization ***i.e.*** biotinylation was performed after SPPS of K_6-gA with three fold excess with HCTU/DIPEA for 12 h, followed by cleavage (cleavage cocktail for thiols with additional 0.025% phenol) and purification already described.[4] Dye coupling to the N-terminus of K_8-gA was performed on the still to solid-phase bound peptide using a carboxylic acid succinimidyl ester activated dye (Oregon Green® 488 carboxylic acid succinimidyl ester) dissolved in DMF. Uncoupled dye was washed away alternating with DMF (3x6 mL), isopropanol (3 x 6 mL), and dichlormethane (3 x 6 mL), and dried under vacuum. Completeness of the reactions was controlled by Kaiser-test, TNBS-test and MALDI-TOF-MS. The reaction mixture was re-purified.

Post-purification acetylation of the free N-terminal and lysine amines of C-K_3-gT was performed on the purified peptide dissolved in DMF using a 40-fold excess of acetic anhydride and DIPEA. Completeness of the reaction was controlled by matrix-assisted laser desorption/ionization time-of-flight mass spectroscopy (MALDI-TOF-MS). The reaction mixture was re-purified according to the procedure described above. Due to acetylation the retention time shifted from 1.9 min to 3.2 min (*cf.* Fig. 2.14A and C). Products were stored under argon at -18 °C.

MALDI-TOF-MS was performed on Voyager-DE™ System (Applied Biosystems, USA) with α-cyano-4-hydroxycinnamic acid as the matrix in positive ion reflector mode for lysine-rich peptides and negative ion reflector mode for glutamate-rich peptides, respectively, an accelerating voltage of 25 kV, grid voltage of 75% and 300 ns extraction delay time. These standard values were optimized according to the sample. A 100-well stainless steel plate was used.

Gel permeation chromatography (GPC) measurements of wild-type gramicidin A and Ac-X_3-gT (c = 1 mg mL^{-1}) were performed on a Shimadzu Prominence HPLC, using an Agilent PLgel column (5 μm, 10^3 Å, 2 x 250 mm) and isocratic elution with THF/10% H_2O. Stabilizer-free solvent improved detection at the tryptophan adsorption maximum at 280 nm. GPC measurements for wild-type gA, Ac-X_8-gA and dimerized Ac-X_8-gA-OEt were carried out by mounting two GPC-columns in series (1. CATSEC-100, 5 μm, 250 x 4.6 mm 2. GPCPEP 5 μm, 250 x 4.6 mm, Eprogen Inc.) on HPLC and isocratic elution (1 mL min^{-1})

with 95% THF (without stabilizer for UV detection at 220 nm, T = 295 K) and 5% dd H_2O.

Surface tension was measured on a Sigma 703D Tensiometer (KSV Inst., Finland) with a platinum Wilhelmy plate, pre-cleaned with ethanol and water, followed by flame annealing. Solutions were prepared 24 h prior to measurements, which were performed at room temperature.

7.4. Peptide particle formation

For *peptide bead formation* either the peptide or the corresponding mixtures (*e.g.* AcC-X_3-gT/AcC(sl)-X_3-gT) were dissolved in ethanol at the appropriate concentration and filtered through a 0.2 µm or 0.45 µm hydrophilic PTFE filter. The self-assembly process was initiated by solvent exchange from the organic solvent to dd H_2O or the corresponding dd H_2O/ethanol mixture. A change in polarity was usually accompanied by opalescence. Solvent exchange (in dialysis tubes or on crystallization plates) was performed within 24 h with dd H_2O exchanged three times. The self-assembly process for the peptide library K_mX_{8-m}-gA was initiated by solvent exchange from the organic solvent to dd H_2O or buffer (NaCl (140 mM), EDTA (0.5 mM), TRIS (10 mM), NaN_3 (0.003 mM) adjusted to pH 7.4 with HCl (2 M) and filtered through a 0.22 µm filter)). Solvent exchange (in dialysis tubes or crystallization plates) was performed within 24 hours with 3x exchange of water. Since K_3X_5-gA to K_8-gA are water soluble, they were dissolved directly in water or buffer for the surface tension and light scattering measurements.

7.5. Peptide particle characterization

Transmission electron microscopy (TEM) images were taken on an FEI Morgani 268D operated at 80 keV. Samples were deposited on carbon-coated, parlodion (2% in n-butyl acetate)-covered copper grids, stained (when necessary) with uranyl acetate (2%) and dried in air.

Cryogenic-transmission electron microscopy (CryoTEM). A holey carbon-coated grid (Quantifol, Germany) was used to adsorb 4 mL of an aqueous Ac-E_6-gA solution (~5 mg mL^{-1}) which was blotted with Whatman 1 filter paper and vitrified in liquid ethane at -178 °C using a Vitrobot (FEI Company, Netherlands). After transferring the frozen grids onto a Philips CM200-FEG electron microscope using a Gatan 626 cryo-holder, measurements were performed at an acceleration voltage of 200 kV and a 20k magnification. Micrographs were recorded on a 2K x 2K CCD camera (Gatan, USA) using a

low-dose system (10 $e^-/Å^2$) while keeping the sample at -172 °C.

Scanning Electron Microscopy (SEM) was done on a Philips XL 30 ESEM operating between 2 and 5 kV. The aqueous peptide samples were frozen with liquid nitrogen and lyophilized directly on the SEM grid, or lyophilized powder was put on a double-sided carbon sticker before being sputtered with gold or platinum.

Energy dispersive X-ray spectroscopy (EDXS) was performed with an EDAX spectrometer form 0 to 10 keV after sputtering the sample with silver.

Dynamic and static light scattering (DLS and SLS) experiments were performed with an ALV/CGS-8F platform-based goniometer system equipped with an ALV/-5000/E correlator and a HeNe laser with a wavelength λ_0 of 633 nm (35 mW). Measurements were made at 20 °C and at a scattering angle θ from 30° − 150° in steps of 10°. DLS correlation functions were fitted with the 2nd cumulant function and the CONTIN algorithm. The resulting hydrodynamic radii (mass weighted) were extrapolated to zero wave vector ($q = (4\pi n_0/\lambda_0) \sin(\Theta/2)$). 2nd cumulant fit analysis at 90° was used to determine size dependency of the peptide particle. 2nd cumulant function (90°, 300 s) was also used for pH dependent size evolution of Ac-K_6-gA and Ac-E_6-gA. Aliquots of 2-10 μL of corresponding molarities (10^{-3} to 1 mol L^{-1}) NaOH or HCl were used to adjust the pH of the 800 μL peptide solution.

The following parameters were used to calculate micelle rotational time so as to compare DLS with EPR: R = 5.65 nm, T = 293 K and n = 1.3583, η = 2.84 10^3 $kgs^{-1}m^{-1}$ for 40 weight % (wt %) ethanol.

SLS provides useful information on the size and shape of the particle under investigation. Data analysis was done with ALVStat 4.31 software (ALV, Langen, Germany) by constructing a Guinier plot (second order in q and linear concentration dependency)

$$\ln\left(\frac{K \cdot c}{R_\Theta}\right) = \ln\left(\frac{1}{M_W \cdot e^{-\frac{1}{3}R_g \cdot q^2}} + 2A_2 \cdot c\right) \quad (1)$$

with the optical constant (K), concentration (c), Rayleigh ratio (R_θ), molar mass (M_W), radius of gyration (R_g) and 2nd virial coefficient (A_2). The refractive increment (dn/dc) was set to 0.185 mL/g (commonly used for peptides [5]). The deviation in dn/dc, caused by the different ethanol concentrations,[6] provided negligibly different results.

The scattering intensity $i(\theta)$ can be normalized to zero angle, yielding the particle scattering factor P.

$$P(\theta) = \frac{i(\theta)}{i(\theta = 0)} \tag{2}$$

This provides information on the shape and internal structure of the particle in solution. Structural differences become apparent by plotting P versus $u = q \cdot R_g$. For analysis, the experimental data from the present system were compared to well-known particle scattering factors for hard spheres and monodispersed coils, given in eq. 3 and 4 respectively.

$$P(\theta) = \left(\frac{3}{x^2} (\sin(x) - x\cos(x)) \right)^2 \tag{3}$$

$$x = \sqrt{\frac{5}{3} u}$$

$$P(\theta) = \left(\frac{2}{u^4} \left(e^{-u^2} - 1 + u^2 \right) \right)^2 \tag{4}$$

More detail on theoretical background and data analysis can be found in the literature.[7]

For *fluorescence spectroscopy*, carried out at room temperature (293 K), a Perkin Elmer LS55 Luminescence Spectrometer with a 1 mm QS cuvette in a 90° arrangement was used. The quencher acrylamide (c = 2.26 mol L^{-1}) was added stepwise to the peptide solutions (c = 0.04 to 0.31 mol L^{-1}) in 2 to 40 μL quantities and intensity was corrected for dilution. High tryptophan and peptide concentrations required the use of a built-in 1% filter to prevent detector saturation. Data analysis was performed by plotting F_0/F (fluorescence intensities without and with the presence of quencher) *vs.* the concentration of the quencher [Q] according to the modified Stern-Volmer law[8]. It can be divided into collisional and static components characterized by K_{SV} (Stern-Volmer constant) and V (active volume).[9]

For UV-VIS a Perkin Elmer Lambda 35 UV/VIS Spectrometer, equipped with a Peltier temperature control element and a 1 mm cuvette, was used to detect (280 nm) the onset of scattering due to particle formation.

Atomic force microscopy (AFM) measurements were carried out using a 5100 Agilent system (formerly PicoLE Molecular Imaging) equipped with a multi-purpose scanner. Images were acquired using a silicon cantilever (type-NCHR PointProbe® Plus, force

constant 42 N/m) as indicated by the manufacturer for acoustic mode images. Samples were prepared by exposing aqueous peptide solution to a freshly cleaved mica surface for 2 min, removing the supernatant solution, and drying. The free AFM analysis software Gwyddion was used.

EPR measurements. A spin label (sl) was attached to the amphiphilic peptide by dissolving AcC-X_3-gT and 3-(2-iodoacetamido)-2,2,5,5-tetramethyl-1-pyrrolidinyloxy in a mixture of 58% ethanol in TRIS buffer (25 mM) and incubated for 12 h. The spin labeled peptide was separated from the reaction mixture by using solid-phase extraction cartridges (Whatman Inc., ODS-5 Octadecyl; 18%; EC) with a purity of 97% (HPLC).

All continuous wave (cw) EPR experiments were performed at X-band frequencies (9.3 – 9.4 GHz) with a Bruker Elexsys 500 spectrometer equipped with a Bruker Elexsys Super High Sensitive probe head equipped with a continuous flow N_2 cryostat controlled by a Bruker Er 4111 VT temperature controller. Samples were loaded into EPR glass capillaries (0.9 mm inner diameter, sample volume 15 µL) and recorded with 100-kHz field modulation, 2 mW microwave power, 0.15 mT modulation amplitude. For low temperature (160 K) cw EPR spectra, samples were loaded into EPR quartz capillaries (3.8 mm inner diameter, sample volume 30 µL) and recorded with 100-kHz field modulation, 0.08 mW microwave power, 0.2 mT modulation amplitude.

Pulse EPR experiments were performed at X-band frequencies (9.3 – 9.4 GHz) at 50 K with a Bruker Elexsys 580 spectrometer equipped with a Bruker Flexline split-ring resonator ER 4118X-MS3 that included a continuous flow He cryostat (ESR900; Oxford Instruments) controlled by an Oxford Instruments temperature controller ITC 503S.

Dipolar time evolution data were recorded using a four-pulse DEER (double electron-electron resonance) experiment.[10] The measurements were performed at 50 K with observer pulse lengths of 32 ns for $\pi/2$ and π pulses, with the ELDOR π pulse set to 12 ns. Deuterium nuclear modulations were averaged (50 volume % (v %) of deuterated glycerol was added to the ethanol sample to increase the signal to noise ratio). Traces were accumulated for 24 hours. Data analysis of the DEER traces was performed with DeerAnalysis 2009 software.[11]

Circular Dichroism (CD) was measured on a Chirascan (Applied Biophysiscs Ltd., Leatherhead, UK) using 1 mm path length QS cuvettes. The solvent concentration was adjusted according to an HT voltage between 300 and 600 V in the far UV range.

Surface tension was measured on a Sigma 703D (KSV Inst., Finland) tensiometer with a platinum-Wilhelmy plate, precleaned with ethanol and water, followed by flame annealing. Solutions were prepared 24 h prior to measurements by dissolving the products in dd H_2O or buffer and subsequent dilution.

Confocal laser scanning microscopy (CLSM). BODIPY 650/665 and Alexa488 solutions were added to an ethanol solution with Ac-E_6-gA (0.5 mg mL^{-1}) to reach a concentration of 0.2 μmol L^{-1} and 0.5 μmol L^{-1} respectively before vesicle formation and dialysis (MWCO = 100 kDa). Measurements were performed with Zeiss Confocor 2 LSM equipment (sequential, trace 1: excitation: 633 nm, 3%, long pass (LP) 650 filter and trace 2: excitation: 488 nm, 10%, LP 505 filter, 100x/1.4 oil objective).

Sonication and *freeze-thaw cycles* have been used for the destabilization of micelle and removal from peptide beads, which included 5 min sonication in a water bath at 20 °C followed by ten freezing – in liquid nitrogen – and thaw – in a water bath at 40 °C – cycles.

7.6. Gold nanoparticle – peptide composite formation

The peptides AcX_3-gT-C (0.17 mg mL^{-1}), K_3-gT-C (0.22 mg mL^{-1}) and K_3-gT (0.13 mg mL^{-1}) have be mixed (1:2) with filtered $AgNO_3$ solution (40 mM and 4 mM) and 5 nm Au NP (48 mg mL^{-1} and 4.8 mg mL^{-1}) in a crystallization plate. A lag time of 2 and 6 h was given for the formation of the metal gold bond, after which self-assembly was induced. TEM was used to analyze the assemblies in the manner mentioned above but without negative staining.

7.7. Film preparation and characterization

Film preparation. Aliquots ranging from 50 to 120 mL of mixed peptide/lipid solutions with different molar ratios ($x = n_{peptide}/n_{total}$) in $CHCl_3$:EtOH (90:10 v%/v%), were spread with a Hamilton syringe on dd H_2O, 4-(2-hydroxyethyl)-1-piperazineethanesulfonic acid (HEPES/KCl, 1 mM/10 mM, pH 7), phosphate buffer (Na_2HPO_4, 25 mM, pH 10) or carbonate buffer (Na_2CO_3/$NaHCO_3$, 25mM, pH 10) held in a Langmuir–Blodgett (LB) trough (total area 420 cm^2) from KSV, placed on an anti-vibration table in a dust-free room or for LB film transfer on a mini deposition trough (total area 242 cm^2) equipped with a dipper. After spreading, 10 min were allowed for the solvent to evaporate, followed by compression of the film at 8 mm min^{-1}. The surface pressure (π) of the monolayers was measured to ± 0.1 mN m^{-1} with a Wilhelmy plate

(chromatography paper, ashless Whatman Chr 1) connected to an electrobalance. Monolayers were compressed at 20 °C. LB-films were deposited onto Si-wafers (prior cleaned in piranha solution for 10 min and rinsed in dd H_2O), freshly cleaved mica or TSG by pulling the substrate out of the subphase through the interface at a constant rate of 0.5 mm min^{-1} while keeping π at 28 or 35 mN m^{-1}, if not mentioned differently. Immersion took place over night (12 h) with freshly cleaved TSG in the corresponding solutions, followed by generous washing with ethanol. Samples were either dried in vacuum or have been covered with buffer solution.

EP^3 system (Brewster angle microscope) (Nanofilm, Göttingen, Germany) was used to visualize monolayer morphology, with a 50 mW Nd:YAG laser at the wavelength of 532 nm and a 20 × Nikon long-distance objective lens; recorded images correspond to 220 μm in width.

Monolayer characterization. The free energy of mixing binary monolayers ΔG was calculated according to equation 1 and 2,

$$A^{exc} = A_{12} - (A_1 X_1 + A_2 X_2) \quad (1)$$

$$\Delta G^{exc} = \int_0^{\pi} A^{exc} \quad (2)$$

where A^{exc} is the excess molecular area, A_{12} is the MmA in the mixed film, $A_{1,2}$ are the MmA and $X_{1,2}$ the molar ratios of the components 1 and 2, respectively.[12]

The intensity of light (I) reflected from an optically isotropic molecular film at the Brewster angle of the subphase depends on the film thickness (d) as $I = Cd^2$, with the instrument constant (C), it is possible to estimate the relative thickness of the investigated monolayer. The gray level of the camera was converted into absolute intensity values as described elsewhere.[12a]

For *mineralization* an amphiphilic peptide C-K_3-gT (0.5 mg mL^{-1}) in chloroform ethanol mixture (9:1) was spread on phosphate buffer (c(NaH_2PO_4) = 2 mM, pH was adjusted with NaOH to 7.4) in a Langmuir trough. After evaporation of the solvent the film was compressed to π = 8 mN m^{-1} before $CaCl_2$ solution was injected into the subphase using a Hamilton syringe. For analysis (TEM, SEM, EDXS) films were directly transferred onto TEM grids from the trough.

For *quartz crystal microbalance (QCM)* frequency and dissipation shifts were monitored using the QSense D300 Quartz Crystal Microbalance (QSense, Gothenburg,

Sweden). The QCM sensors consist of a disc-shaped, AT-cut piezoelectric quartz crystal coated with metallic electrodes on both sides. The QCM sensor crystal (1.4 cm diameter crystal, 1.2 cm diameter gold area, 0.2 cm^2 active area, approximately 0.3 mm thickness, roughness of the electrode <3 nm (rms)) operates at a resonance frequency of 4.95 MHz (50 kHz). The flow cell had an 80 μL working volume.

Polarization-modulation infrared reflection-absorption spectra (PM-IRRAS) were recorded on a Bruker IFS 66v IR equipped with a PMA 37 polarization-modulation accessory. The incoming beam from the external beam port of the spectrometer, polarized by a KRS-5 wire-grid polarizer and modulated by a ZnSe photoelastic modulator, was reflected off the sample surface and detected with a liquid nitrogen-cooled MCT detector. The maximum in polarization retardation was set at 2000 cm^{-1}, and the polarization was modulated with a frequency of 50 kHz. Spectra were acquired with a resolution of 4 cm^{-1} using 1024 scans of multiplexed interferograms. The data was processed with OPUS software (Bruker Optics, Germany) and background corrected with a polynomial.[13]

7.8. Micro-contact printing and immobilization procedure

The structured poly(dimethylsiloxane) (PDMS) mask was cleaned with ethanol and dried with nitrogen flow. BSA-biotin solution was cast onto the mask (0.1 mg ml^{-1} BSA-biotin, sodium acetate buffer, pH 5.5), incubated for 10 min and dried with nitrogen flow forming protein film. The BSA-biotin covered mask was than pressed to the surface of dried clean microscopy glass slides (cleaned by multiple sonication in 2% Hellmanex detergent, water and methanol) and incubated for 10 min resulting in patterning of the surface with BSA-biotin. The glass slide was than mounted into the chamber of the flow cell and sealed. The surface was passivated by incubation with BSA solution (1 mg ml^{-1}, sodium acetate pH 5.5), washed with buffer and incubated with streptavidin solution (0.1 mg ml^{-1}, dd H_2O) resulting in its immobilization in structured manner followed by washing steps. Biotinylated K_6-gA in dd H_2O was than immobilized on the streptavidin stripes resulting in formation of BSA-biotin-streptavidin-biotin-K_6-gA.[14] The hydrophobic gA part was probed by OG488-K_8-gA or saturated and blocked by K_8-gA.

7.9. References

[1] A. Weiss Emily, K. Kaufman George, K. Kriebel Jennah, Z. Li, R. Schalek and M. Whitesides George, *Langmuir* **2007**, *23*, 9686-9694.
[2] J. L. Fauchere and V. Pliska, *Eur. J. Med. Chem.* **1983**, *18*, 369-375.
[3] E. Casero, M. Darder, D. J. Diaz, F. Pariente, J. A. Martin-Gago, H. Abruna and E. Lorenzo, *Langmuir* **2003**, *19*, 6230-6235.
[4] T. Schuster, D. de Bruyn Ouboter, E. Bordignon, G. Jeschke and W. Meier, *Soft Matter* **2010**, 6, (21), 5596-5604.
[5] a) K. Kitagawa, T. Morita and S. Kimura, *J. Phys. Chem. B* **2004**, *108*, 15090-15095; b) C. Nogues and M. Wanunu, *Surf. Sci.* **2004**, *573*, L383-L389.
[6] M. Wanunu, A. Vaskevich and I. Rubinstein, *J. Am. Chem. Soc.* **2004**, *126*, 5569-5576.
[7] a) E. Bayer and M. Mutter, *Nature (London, U. K.)* **1972**, *237*, 512-513; b) O. Stauch, R. Schubert, G. Savin and W. Burchard, *Biomacromolecules* **2002**, *3*, 565-578; c) W. Burchard, *Adv. Polym. Sci.* **1983**, *48*, 1-124.
[8] D. de Bruyn Ouboter, T. Schuster, A. Mantion and W. Meier, *J. Phy. Chem. C* **2011**, accepted.
[9] M. Hegner, P. Wagner and G. Semenza, *Surf. Sci.* **1993**, *291*, 39-46.
[10] S. M. Schiller, R. Naumann, K. Lovejoy, H. Kunz and W. Knoll, *Angew. Chem., Int. Ed.* **2003**, *42*, 208-211.
[11] D. I. Chan, E. J. Prenner and H. J. Vogel, *Biochim. Biophys. Acta, Biomembr.* **2006**, *1758*, 1184-1202.
[12] a) J. M. Rodriguez Patino, C. Carrera Sanchez and M. R. Rodriguez Nino, *Langmuir* **1999**, *15*, 4777-4788; b) K. Kita-Tokarczyk, F. Itel, M. Grzelakowski, S. Egli, P. Rossbach and W. Meier, *Langmuir* **2009**, *25*, 9847-9856.
[13] E. Beurer, N. V. Venkataraman, A. Rossi, F. Bachmann, R. Engeli and N. D. Spencer, *Langmuir* **2010**, *26*, 8392-8399.
[14] M. Grzelakowski, O. Onaca, P. Rigler, M. Kumar and W. Meier, *Small* **2009**, *5*, 2545-2548.

8. General conclusion and outlook

This thesis describes the synthesis and characterization of short, amphiphilic peptides as well as the characterization of their self-assembled structures in solution and on surface to get a better understanding of the underlying mechanism and driving forces and finally control and direct hierarchical self-organization towards desirable properties and functions. The main findings of this work were:

- ✓ A reversible self-assembly process from the molecular dissolved amphiphilic peptide AcC-X_3-gT, via its micellization and subsequently formation of peptide nanoparticles, termed peptide beads with decreasing ethanol concentration and decreasing temperature.
- ✓ Peptide beads using uncharged C-K_3-gT likely undergo an identical formation process by the addition of counter ions, leading to charge compensation and aggregation.
- ✓ The nature of these peptide beads were revealed to be aggregated micelles, so called 'multicompartment micelles' by the detected species in solution, broken peptide beads structure due to modification - revealing their inner structure of small spherical aggregates. Furthermore the micellar core of peptide beads was visualized by gold nanoparticle - peptide composites.
- ✓ Formation of stable molecular thin peptide layers on the air-water interface as well as self-assembled monolayers on template stripped gold.
- ✓ Within a partially acetylated oligolysine chain attached to gA the crucial acetylated lysine was determined to cause a conformational change form β-sheet to α-helix which switches the formation of fibers to micelles.
- ✓ For the first time dimerization and predefinition of membrane subunits leads to the formation of stable pure peptide membranes.

On the basis of the synthesized purely peptidic amphiphiles, their properties and self-assembling behavior the following outlooks are suggested:

- ✓ The presented systems exhibit, due to their biodegradability, biocompatibility and stable, self-assembled nanostructures (~ 200 nm) combined with the ability to encapsulate or integrate payload within, a high potential in any medical application such as a drug or gene delivery systems, sensor and implants interface.
- ✓ Creating targeted nanostructures by presenting respective groups on their surface would accumulate them in a specific tissue *e.g.* cancer tissue over receptor-ligand binding, which therefore reduces side effects. Peptides respond to environmental stimuli and release the embedded payload, which consequently reduces also the needed drug concentrations, due to the high functionality of their AAs.
- ✓ Peptide-based material similar can be used as a template for mineralization and protein crystallization.
- ✓ The created peptide membranes are unique and the question arises if they could be used besides lipid and block copolymer membranes to insert membrane proteins in an active state. Combined with the encapsulation of enzymes within the peptide vesicle it would open the door towards totally peptidic nanoreactors.

9. Acknowledgments

First of all, I am thankful to thank *Prof. Wolfgang Meier* for the possibility to perform the Ph.D. thesis under his supervision and most of all for the trust and freedom he offered me. I thank my co-referee, *Prof. Dr. Corinne Vebert (University Geneva)* and *Prof. Thomas Pfohl* for their interest in my research work. This work would not be possible without people who helped me with measurements and techniques outside the group and therefore I am very thankful. Especially *Dr. Daniel Häussinger*, *Dr. Michael Kümin* and *Roman Erdman* (Prof. H. Wennemers, University of Basel), *Dr. Enrica Bordignon* (*Prof. G. Jeschke,* ETH Zürich), *Prof. Andreas Taubert* (University of Potsdam), *Mathias Junginger* (University of Potsdam), *Dr. Mohammed Chami* (C-CINA, Basel), *Eva Beurer* (DMATL, ETH Zürich), *Prof. Markus Meuwly* (University of Basel), *Dr. Franziska Schmid* (University of Basel), and *Ursula Sanders, Vesna Oliveri* and *Evi Bieler* (ZMB). I also want to thank *Helmut Fally* (FHNW) for access to the Zetasizer and my 'Nanostudents' *Chaim*, *Cornelia*, *Daniela*, *David*, and *Joachim*.

There are so many people to thank for this period of time so it is difficult where to continue. I want to thank here my previous office mates*, Smahan, Philipp, Diana* ('Cailler' is still the best!) and *Christian*. For revision of manuscript(s) I specially thank *Nico*.

Furthermore I thank *Dr. Katarzyna Kita* for her time spent explaining me surface science. I am also very thankful to *Cornelia* for advice and guidelines and to *Ozana* for motivation issues and appreciate the fascination for dialysis that we share! Many thanks also, *Mark* to setting up the 'assemblers', for discussions and for 'pimping my English' and to *Gabi* for all those TEM images. I am also thankful to *Vimal* and *Karolina* for practical course issues and discussions and to *Agnieszka* for mineralization experiments.

I am also grateful to the former group members *Fabian A., Carolina F., Alessandro* and *Susana*. I would like to thank *Lucy*, *Mariusz* and *Harry* and their way of dealing with problems. Similar I am thankful to *Sylvia, Per, Rainer, Kate, Julia, Alex* and *Francisco.* I would also like to thank The Flying Monkey/The Green Horse (*Bernhard, Sandro* and *Lukas*) and of course their fans *Ramona, Olivier, Sindhu, Agnieszka* for their support and the good concerts. I also want to thank *Jörg, Etienne, Patric, Pascal, Nicolas, Yves and Martin* and all the other people in the group, for help and the time we spent together. Thanks also to the workshop, secretary office especially *Danni* and *Esthi*, *Urs* and *Jean-*

Pierre Ramseyer.

Great thanks to *Dirk* for his expertise, help and knowledge but also for the funny times at conferences & in the office. Special thanks to *Serena,* my bavarian backup! Ps.: No drinking in the lab, Himmeherrgott…..! Equally I would like to thank the 9 o'clock coffee group especially *Stefan* and *Sven*, furthermore the jogging, swimming and 'free time activity' team *Stefan* and *Sven*.

Finally, friends & family from good old Germany, *Bernhard, Martin, Florian, Kathrin, Michi* and *Kathi* and my parents *Peter* and *Sieglinde Schuster*, my brother *Peter* and his girlfriend *Sarah*, my sister *Regina* and my girlfriend *Elisa* are acknowledged for support and an 'open ear'.

10. Curriculum vitae, references and lists of contributions

PERSONAL INFORMATION

Date of Birth	August 21th, 1979
Place	Moosburg a. d. Isar
Nationality	Germany
Contact	Thomas.Schuster@unibas.ch

EDUCATION

2006-2011	Doctorate (Chemistry), University of Basel, Switzerland, Prof. W. Meier Purely Peptidic Amphiphiles: Understanding and Controlling their Self-Assembly Structures
2001-2006	Diploma (Chemistry), University of Regensburg, Germany Colloidal & formulation concepts, bio-analytical methods; diploma work: "Fluorescent Nanoparticles and their Use as Specific Sensors for Metal Ion" performed at the University of Versailles (UVSQ), France, Prof. Ch. Larpent
2000-2001	Civil service, BRK Moosburg
1991-2000	High-school diploma, Karl-Ritter-von-Frisch Gymnasium, Moosburg

ORAL PRESENTATIONS

Schuster T., De Bruyn Ouboter D., Bordignon E., Dittrich C., Jeschke G. and Meier W., Reversible Peptide Particle Formation of a Mini Amino Acid Sequence, EUPOC - HIERACHRICALLY STRUCTURED POLYMERS, Gargnano, Italy, 2010

Schuster T., De Bruyn Ouboter D., Meier W., From Fibers to Micelles Using Point Mutated Amphiphilic Peptides, SCS Fall Meeting, ETH Zürich,, Switzerland, 2010

de Bruyn Ouboter, D.; Schuster, T.; Mantion, A.; Meier, W., Hierarchical organization of purely amphiphilic peptides into peptide microspheres. *J. Phys. Chem. C,* **2011**, accepted.

Schuster, T.; de Bruyn Ouboter, D.; Bruns, N.; Meier, W., Exploiting dimerization of purely peptidic amphiphiles to form vesicles. *Small* **2011**, DOI: 10.1002/smll.201100701.

Schuster, T.; de Bruyn Ouboter, D.; Palivan, C.; Meier, W., From Fibers to micelles using point-mutated amphiphilic peptides. *Langmuir* **2011**, *27*, 4578-4584.

Schuster, T.; de Bruyn Ouboter, D.; Bordignon, E.; Jeschke, G.; Meier, W., Reversible peptide particle formation using a mini amino acid sequence. *Soft Matter* **2010**, 5596-5604.

Schuster, T.; de Bruyn Ouboter, D.; Meier, W., Access to controlled self-assembly from fibers to micelles of a lysine rich amphiphilic peptide via point mutation. *Chimia* **2010,** 64, (7/8), 954

Schuster, T.; de Bruyn Ouboter, D.; Meier, W., Vesicular structures using short amphiphilic peptides. *European Cells and Materials* **2010**, 20, 232.

de Bruyn Ouboter, D.; Schuster, T.; Dittrich Ch., Meier, W., Self-assembled peptide microspheres. *European Cells and Materials* **2010,** 20, 51

Junginger, M.; Kita-Tokarczyk, K.; Schuster, T.; Reiche, J.; Schacher, F.; Mueller, A. H. E.; Coelfen, H.; Taubert, A., Calcium phosphate mineralization beneath a polycationic monolayer at the air-water interface. *Macromolecular Bioscience* **2010,** 10, (9), 1084-1092.

Schweizer, S.; Schuster, T.; Junginger, M.; Siekmeyer, G.; Taubert, A., Surface modification of nickel/titanium alloy and titanium surfaces via a polyelectrolyte multilayer/calcium phosphate hybrid coating. *Macromolecular Materials and Engineering* **2010,** 295, (6), 535-543.

Montenegro, J.; Hennig, A.; Geotti-Bianchini, P.; Eggimann, G. A.; Jeannerat, D.; Matile, S.; Misek, J.; Schuster, T.; Uhlich, N. A.; Vargas, A., Functional biosupramolecular systems: 40th CUSO Summer School, Aug. 23-27, 2009. *Chimia* **2009,** 63, (12), 881-884.

Gouanve, F.; Schuster, T.; Allard, E.; Meallet-Renault, R.; Larpent, C., Fluorescence quenching upon binding of copper ions in dye-doped and ligand-capped polymer nanoparticles: a simple way to probe the dye accessibility in nano-sized templates. *Advanced Functional Materials* **2007,** 17, (15), 2746-2756.

LIST OF POSTER PRESENTATIONS

Mathias Junginger, Katarzyna Kita-Tokarczyk, Thomas Schuster, Juergen Reiche, Felix Schacher, Axel H.E. Müller, Andreas Taubert, Calcium phosphate mineralization beneath a positively charged block copolymer monolayer at the air-water interface, LB13, 13th International Conference on Organized Films, Quebec, Canada, **2010**

Th. Schuster, D. de Bruyn Ouboter, W. Meier: Vesicular structures from short amphiphilic peptides; 3rd International NanoBio Conference, ETH Zürich, Switzerland, **2010**

Th. Schuster, D. de Bruyn Ouboter, W. Meier; Reversible peptide particle formation of a mini amino acid sequence, SPS Annual Meeting, Basel, Switzerland, **2010**

D. de Bruyn Ouboter, T. Schuster, Ch. Dittrich, W. Meier, Applications for self-assembled peptide beads, NCCR Nanoscience Annual Meeting, Basel, Switzerland, **2010**

D. de Bruyn Ouboter, Th. Schuster, Ch. Dittrich, W. Meier: Suitable applications of self-assembled peptide beads; 40th CUSO Summer School, Villars, Switzerland, **2009**

T. Schuster, D. de Bruyn Ouboter, Ch. Dittrich, W. Meier, Insights in the self-assembly of helical peptides, 40th CUSO Summer School, Villars, Switzerland, **2009**

T. Schuster, D. de Bruyn Ouboter, Ch. Dittrich, W. Meier, Controlling the assembly of short helical D, L- peptides, Swiss Chemical Society, Swiss Federal Institute of Technology Zürich, Switzerland, **2009**

T. Schuster, D. de Bruyn Ouboter, Ch. Dittrich, W. Meier, Controlling the assembly of short helical D, L- peptides, Swiss Chemical Society, Workshop on Nanoscience and the NCCR Nanoscience Annual Meeting, Basel, Switzerland, **2009**

T. Schuster, Ch. Dittrich, D. de Bruyn Ouboter, W. Meier, Short helical D, L - peptides in solution and on surfaces, Polymers in Life Science, Basel, Switzerland, **2008**

T. Schuster, Ch. Dittrich, D. de Bruyn Ouboter, W. Meier, Solid supported membranes based on short helical peptides, 11th European Conference on Organized Films, Potsdam, Germany, **2008**

T. Schuster, Ch. Dittrich, D. de Bruyn Ouboter, W. Meier, Solid supported membranes based on amphiphilic gramicidin derivatives, Biosurf VII, Zürich, Switzerland, **2007**

11. Abbreviations

AA	amino acid
ACN	acetonitrile
AFM	atom force microscope
Alox	aluminium oxide
CLSM	confocal laser scanning microscope
Da	Dalton, molecular weight
DA	degree of acetylation
dd H_2O	double distilled water
DDS(s)	drug delivery system(s)
DIPEA	N-ethyldiisopropylamine
DLS	dynamic light scattering
DMF	dimethylformamide
Dppc	dipalmitoylphosphatidylcholine
Dmpc	dimyristoylphosphatidylcholine
EDT	ethandithiol
EPR	electron paramagnetic resonance
EtOH	ethanol
HCTU	2-(6-chloro-1H-benzotriazole-1-yl)-1,1,3,3-tetramethylaminium hexafluorophosphate
IR	infrared spectroscopy
LCM	large compound micelle
LCST	low critical solution temperature
MALDI-TOF-MS	matrix assisted laser desorption/ionization - time of flight – mass spectroscopy
MCM	multicompartment micelle
NMP	N-methyl-2-pyrrolidone
PAA	poly(acrylic acid)
PD.I.	polydispersity index
PDMS	poly(dimethylsiloxane)
PEO	poly(ethylenoxid)
PLGA	poly(L glutamic acid)
PM IRRAS	Polarization modulation infrared reflection absorption spectroscopy
PMOXA	poly(2-methyloxazoline)
PNIPAM	poly (N-isopropylacrylamide)
PS	polystyrene
R_g	radius of gyration

R_h	hydrodynamic radius
SEM	scanning electron microscope
SLS	static light scattering
SPPS	solid-phase peptide synthesis
TEAP	triethylammoniumphosphate
TEM	transmission electron microscope
TES	triethylsilane
TFA	trifluoroacetic acid
TIS	triisopropylsilane
Tris	tris-(hydroxymethyl)aminomethan

Amino acids (one letter code) and sequences

DL	D-leucine
LC	L-cysteine
LK	L-lysine
LW	L-tryptophan
LX	acetylated L-lysine
-gA	gramicidin A inspired hydrophobic part of the amphiphile
-gT	truncated version of gA